Theoretical Study of Thermal Diode

LAN JINGHUA
(*M.Sc, Lanzhou Univ, China*)

A THESIS SUBMITTED FOR THE DEGREE OF DOCTOR OF PHILOSOPHY

DEPARTMENT OF PHYSICS

NATIONAL UNIVERSITY OF SINGAPORE

2007

Acknowledgements

Firstly, I would like to devote my deepest thanks and gratitude to my supervisor, Prof. Li Baowen. Thanks a lot for his valuable guidance and continuous encouragement throughout my research. I have benefited much from his profound experiences and deep insights in many problems. His encouragement has driven me to develop positive attitude towards my research and life. Many thanks to Prof. Li for his valuable instruction, special concern, encouragement and support!

Warm thanks to my collaborators, Prof. Giulio. Casati, who have influenced me by his precise work style, as well as earnest scientist research attitude. Under his guidance, I learned the proper way to formulate and solve a problem.

I would also like to express my sincere gratitude to Mr. Li Nian bei and Dr. Wang Lei for valuable discussion during this PhD research.

My thanks to Dr. Wu Chunfeng for giving me her thesis templates and Mr. Dario for helping to solve latex problem when writing the thesis.

My warmest thanks to my parents and my husband for their love, care and encouragement.

Finally, I would like to thank the National University of Singapore for the scholarship during my study in NUS.

Contents

Summary

Thermal diode or thermal rectifier is a new concept in classical systems. It is a device which has a high/infinite thermal resistance in one direction whereas it has a low resistance when the temperature gradient is reversed. In this PhD project, we built up an efficient thermal diode by coupling two dissimilar anharmonic lattices from 1D to 2D and 3D successfully. This thesis is completed based on the following three works.

1. Baowen Li, Jinghua Lan, and Lei Wang, "Interface Thermal Resistance between Dissimilar Anharmonic Lattices", Phys. Rev. Lett. 95, 104302 (2005). Main work in this part is the successful building up an efficient thermal rectifier by connecting two dissimilar lattices. And the rectifying effect is connected with asymmetric properties in the interface.

2 Jinghua Lan and Baowen Li, "Thermal Rectifying Effect in two-dimensional Anharmonic Lattices", Phys. Rev. B 74, 214305 (2006). In this work, we extend the thermal rectifier to the 2D model. The dependence of rectifying efficiency on the temperature and temperature gradient is studied in this work.

3. Jinghua Lan and Baowen Li, "Vibrational Spectra and Thermal Rectification in Three-dimensional Anharmonic Lattices", accepted for publication in Phys. Rev. B. (2007). A further extension to a 3D model is studied. We provide both theoretical and numerical analysis of spectra for two representative nonlinear lattices in the 3D model, the Frenkel−Kontorova and the Fermi−Pasta−Ulam lattices. Analytic suggestion of suitable parameter settings for an efficient thermal rectifier is given and numerical confirmation is demonstrated.

The success for a thermal rectifier lies on two factors: The first one is the asymmetry

of the system; The second one is nonlinearity of the system. The broken of the spatial symmetry is necessary to make the heat flow asymmetric, while the introduction of the nonlinearity allows us to adjust the parameters to get the vibrational spectra match or mismatch by reversing the temperature gradient.

We show that because of anharmonic terms, the width and position of an "effective" phonon band depend on temperature. By tuning the anharmonicities of two different coupled chains it is possible to control the effective overlap between the phonon bands of the two chains. In particular, the extent of this overlap can be made to depend on the sign of the imposed thermal gradient, thus leading to thermal rectification.

Controlling heat current is not only a problem of scientific curiosity but also a practical application problem. It might have potential applications in energy saving materials. It may also promise to explain certain important fundamental questions in biophysics, such as controlled energy transport in living organisms on a cellular level. Our study on thermal rectifying effect in dissimilar anharmonic lattices is general meaningful since the two anharmonic lattices we investigated are two representative ones widely studied in different field of physics. Most physical system can be divided into these two representative models: one with on-site potential and another without on-site potential. We believe our systematical study on thermal rectifier based on these two representative models can provide useful guidance and meaningful suggestion when designing thermal rectifiers with other different materials or different structures.

List of Tables

List of Figures

Chapter 1

Introduction

Heat, like gravity, penetrates every substance of the universe, its ray occupies all parts of space. There are many kinds of description about heat from thousands years ago. As early as 460 BC Hippocrates, the father of medicine, postulated that:

" **Heat**, a quantity which functions to animate, derives from an internal fire located in the left ventricle."

The hypothesis that heat is a form of motion was proposed initially in the 12th century. Around 1600, the English philosopher and scientist Francis Bacon surmised that:

"**Heat** itself, its essence and quiddity is motion and nothing else."

In the mid-17th century English scientist Robert Hooke stated:

" ...**heat** being nothing else but a brisk and vehement agitation of the parts of a body."

.....

Other important historical postulates of heat include the phlogiston (1733), fire air (1775), and the caloric (1787).

The modern history of heat, however, begins in 1797 when cannon manufacturer Benjamin Thompson, otherwise known as Count Rumford, methodically first set out to quantify the well-known phenomenon of frictional heat, i.e. to find out how much heat is produced by metal rubbing against metal [1].

In 1824, French engineer Sadi Carnot set forth the second law of thermodynamics: "production of motive power is due not to an actual consumption of caloric, but to its transportation form a warm body to a cold body, i.e. to its re-establishment of equilibrium." According to Carnot, this principle applies to any machine set in motion by heat [2].

In 1850, Rudolf Clausius firstly gave an explicit statement of the first law of thermodynamics and first formulated the second law in this form: heat does not spontaneously flow from cold to hot bodies.

In physics, heat is defined as energy in transit. Generally, heat is a form of energy associated with the motion of atoms, molecules and other particles which comprise matter. Heat can be created by chemical reactions (such as burning), nuclear reactions (such as fusion taking place inside the Sun), electromagnetic dissipation (as in electric stoves), or mechanical dissipation (such as friction). Temperature, defined as the measure of an object to spontaneously give up energy, is used to indicate the level of elementary motion associated with heat. Heat can only be transferred between objects, or areas within an object, with different temperatures, and then only in the direction of the colder body (as the Second Law of Thermodynamics).

Heat can be transferred between objects by radiation, conduction and convection. Conduction is the most common means of heat transfer in a solid. It is the transfer of energy through matter from particle to particle. It is the transfer and distribution of heat energy from atom to atom within a substance. Convection is usually the dominant form of heat transfer in liquids and gases. This is a term used to characterize the combined effects of conduction and fluid flow. In convection, enthalpy transfer occurs by the movement of hot or cold portions of the fluid together with heat transfer by conduction. For example, when water is heated on a stove, hot water from the bottom of the pan rises, heating the water at the top of the pan.

Radiation is the only form of heat transfer that can occur in the absence of any form of medium and as such is the only means of heat transfer through a vacuum. Thermal radiation is a direct result of the movements of atoms and molecules in a material. Since these atoms and molecules are composed of charged particles (protons and electrons), their movements result in the emission of electromagnetic radiation, which carries energy away from the surface. At the same time, the surface is constantly bombarded by radiation from the surroundings, resulting in the transfer of energy to the surface. Since the amount of emitted radiation increases with

increasing temperature, a net transfer of energy from higher temperatures to lower temperatures results.

Other heat transfer mechanisms includes the followings:

Latent heat: Transfer of heat through a physical change in the medium such as water-to-ice or water-to-steam involves significant energy and is exploited in many ways: steam engine, refrigerator etc.

Heat pipe: Using latent heat and capillary action to move heat, it can carry many times as much heat as a similar sized copper rod. Originally invented for use in satellites, they are starting to have applications in personal computers.

Here we are only interested in the mechanism of heat conduction in solid.

1.1 History Background of Heat Conduction

From above introduction, we know heat conduction is the transmission of heat across matter. Heat transfer is always directed from a higher to a lower temperature. On a microscopic scale, conduction occurs as hot, rapidly moving or vibrating atoms and molecules interact with neighboring atoms and molecules, transferring some of their energy (heat) to these neighboring atoms. So when there exists a temperature gradient within a body, heat energy will flow from the region of high temperature to the region of low temperature. This phenomenon is known as heat conduction, and is described by Fourier's Law.

Fourier's Law describes the macroscopic transport properties of heat, i.e., energy, in non-equilibrium systems. Similar laws are valid for the transport of other locally conserved quantities, e.g., charge, particle density, momentum, and etc. We will not discuss these laws. However we'd like to point out that in none of these cases, macroscopic transport laws have been derived rigorously from microscopic dynamics.

1.1.1 Fourier's Law

As pointed out above, Fourier's law is not a theoretical derivation from microscopic dynamic. Actually, it is an empirical observation. But under the hypothesis of being

close enough to global equilibrium, this can be accomplished by postulating that the fluxes is proportional to the thermodynamic forces [3].

Consider a macroscopic system characterized at some initial time, say $t = 0$, by a nonuniform temperature profile $T_0(r)$. This temperature profile will generate a heat, i.e., energy, current $J(r)$. Due to energy conservation and basic thermodynamics:

$$\frac{\partial}{\partial t}\varrho(r,t) = -\nabla \cdot J, \tag{1.1}$$

where $\varrho(r,t) = C_v(T)T(r,t)$ is the energy density. This is assuming that energy and temperature are linearly dependent. $C_v(T)$ is the specific heat per unit volume. On the other side we know that if the temperature profile is uniform, *i.e.*, $T_0(r) \equiv T_0$ there is no current in the system. It is then natural to assume that, for small temperature gradients, the current is given by:

$$J(r) = -k(T)\nabla T(r), \tag{1.2}$$

where $k(T)$ is the thermal conductivity. The heat flux $J(r)$ is the amount of heat transported through the unit surface per unit time and $\nabla T(r)$ is the local temperature gradient. Here we have assumed that there is no mass flow or other mode of energy transport beside heat conduction (we also ignore for simplicity any variations in density or pressure). Equation (1.2) is normally called Fourier's Law. It is an empirical law based on observation.

Such a phenomenological relation was first proposed in 1808 by J.B.J. Fourier as an attempt to explain the thermal gradient present inside the Earth - a problem that had raised a long and controversial debate inside the scientific community at that time. The Eq. (1.2) is assumed to be valid close to equilibrium. Actually, the very definition of local energy flux $J(r)$ and of temperature field $\nabla T(r,t)$ relies on the local equilibrium hypothesis, i.e., on the possibility of defining a local temperature for a macroscopically small but microscopically large volume at each location r for each time t.

Neither phenomenological nor fundamental transport theory can predict whether or not a given classical many-body Hamiltonian system yields an energy transport

governed by the Fourier's heat law. Indeed, transport theory circumvents this quite deep dynamical problem by explicitly postulating that the many-body problem is analytically unsolvable and that dynamics can be replaced by suitably chosen probability assumptions which are, by definition, unverifiable in terms of first principles [16]. In this respect, simple mathematical models are an invaluable theoretical playground to provide a more firm foundation to heat conductivity and to understand more deeply the hypotheses underlying Eq. (1.2). Admittedly, this program is still nowadays far from being accomplished, at least from a mathematically rigorous point of view [4]. On the other hand, even in the absence of solvable examples, one can rely on numerical simulations as a tool to investigate heat transport properties.

1.1.2 Heat Transport in Lattice Models

The ultimate goal of a complete theory would be to derive an equation like (1.2) from some statistical-mechanics calculation, a task which may be formidably difficult. So far, only integrable system (harmonic oscillator [5–9] and Toda model [10–12]) was exactly solved in theoretical framework. In 1967, Z. Rieder *et al.* studied homogenous harmonic chain contacted with two heat bathes and found there is no well-defined temperature gradient in the stationary state [13]. Heat flux was found, as expected, to be proportional to the temperature difference $T_1 - T_N$ rather than to the temperature gradient $(T_1 - T_N)/N$, i.e, the thermal conductivity is proportional to system size. For insulating crystals where heat is transported by lattice vibrations, the first and most elementary attempt to give a microscopic foundation to Fourier's law dates back to Debye. By rephrasing the results of the kinetic theory for the (diluted) phonon gas, he found that the thermal conductivity should be proportional to Cvl. where C is the heat capacity and v,l are the phonon mean velocity and free path, respectively. In 1929, R. Peierls further extended this idea and formulated a Boltzmann equation [14] that shows how anharmonicity is necessary to obtain genuine diffusion of the energy through the so-called Umklapp processes. Since then, the Boltzmann-Peierls approach became the cornerstones in the theory of lattice thermal conductivity. Standard methods, like the relaxation-time approximation,

allow to compute, say, the temperature dependence of κ. As Peierls once put it: *"It seems there is no problem in modern physics for which there are on record as many false starts, and as many theories which overlook some essential feature, as in the problem of the thermal conductivity of [electrically] non-conducting crystals"*. Because a direct mathematical derivation about heat conduction in nonequilibrium system has been proved to be very difficult, and in only a very simple model can such an approach be established, many works about heat conduction have to rely on massive numerical simulations.

The first simulation dates back to the pioneering work of recurrence phenomenon in the model devised originally by Fermi, Pasta and Ulam (FPU) [15]. Their purpose was to check numerically that a generic, but very simple, nonlinear many-particle dynamical system would indeed behave for a long period of time as a statistical mechanical system, that is, it would approach equilibrium if not initially in equilibrium. In particular their purpose was to obtain the usual equipartition of energy over all the degrees of freedom of a system, for generic initial conditions. To their surprise, for the FPU system considered a one-dimensional anharmonic chain of 32 or 64 particles with fixed ends and in addition to harmonic, cubic (α model) or quartic (β model) anharmonic forces between nearest neighbors equipartition was not observed. A variety of manifestly nonequilibrium and non-equipartition behaviors was seen, including quasiperiodic recurrences to the initial state. Beyond these "FPU recurrences", later studies showed the existence of "Super-recurrences" in which the return to the initial state was still more precise. The pursuit of the understanding of the FPU recurrences leads to a rich vein of profound and subtle problems in mathematics and physics. Numerous attempts to resolve the FPU paradox have resulted in a burst of analytical and numerical studies of nonlinear effects in physical systems. One branch is to study the transport properties of heat in anharmonic lattices with the aim of clarifying the necessary and sufficient conditions for various type of conductivity-normal (Fourier's law, with a finite coefficient of thermal conductivity) or anomalous (e.g., divergent coefficient of thermal conductivity).

The first convincing result of Fourier's law in a classical system was given by Casati *et al* [16]. They studied the so-called ding-a-ling model, which is a 1D chain consisting of the fixed equidistant hard-point particle harmonic oscillators, and in between two fixed particles there is a free particle. Classically, this system can be changed from integrable to fully chaotic by adjusting the system parameter. They found that the key ingredient for the normal thermal conductivity is chaos. Later on, Prosen and Robnik [17] studied the ding-dong model by three different numerical methods and verified Fourier's law. After these two works, there have been a large number of numerical works on Fourier's law of heat conduction of different systems and the connection between Fourier's law and the underlaying dynamic mechanisms which determines that the microscopic laws of heat conduction is an important task of non-equilibrium statistical mechanics [4, 18–28, 30, 33–39].

Generally,we can classify 1D uniform lattice systems into two categories: momentum conserving one (referring integrable model and non-integrable model without interaction with substrate), and momentum non-conserving one (non-integrable model with interaction with substrate).

Numerous numerical [22, 24–26, 29, 30, 41–45] and analytic studies [5–9, 13, 46, 47] of heat conduction for 1D anharmonic lattices with conserving momentum allow us safely to claim that the momentum conservation leads, in general, to anomalous heat conduction (see Ref. [4] and [48] for review). The thermal conductivity κ is observed to be anomalous, i.e., dependent on the system size and divergent in the thermodynamic limit.

$$\kappa(N) \sim N^{\alpha}. \tag{1.3}$$

A modeling theory analysis by S. Lepri [22] for the 1D FPU model gives a divergent exponent 2/5, which is supported by numerics from different groups and confirmed recently by Pereverzev from Peierls equation. S. Lepri also gave the following prediction of thermal conductivity for a 2D and a 3D lattice system [48].

$$\begin{aligned} \kappa(N) &\sim \ln N \quad (two \;\; dimension) \\ \kappa(N) &\sim finite \quad (three \;\; dimension) \end{aligned} \tag{1.4}$$

System	Macroscopic thermal behavior	mechanism	Examples
IS	$\kappa \sim L^1$	ballistic motion	Harmonic Toda
HNIS	$\kappa \sim L^\alpha$ $0 < \alpha < 1$ (at high temperature) $\alpha \to 1$ (at low temperature)	superdiffusion	FPU diatomic Toda
UHNIS	$\kappa \sim L^{-\alpha}$ $0 < \alpha$	subdiffusion	disorder FPU
HNISS	$\kappa \sim constant$	normal diffusion	FK ϕ^4 ding-a-ling ding-a-dong

Table 1.1: Thermal conductivity and the underlying main transport process of different systems. IS: Integrable system; HNIS: Homogeneous nonintegrable system without on-site potential; UHNIS: Unhomogeneous nonintegrable system without on-site potential; HNISS: Homogeneous nonintegrable system with on-site potential.

This prediction was confirmed recently by G. Basile *et at.* [49]. They introduced a model whose thermal conductivity diverges in dimensions 1 and 2 if momentum is conserved, while it remains finite in dimension $d = 3$. They considered a system of harmonic oscillators perturbed by a nonlinear stochastic dynamics conserving momentum and energy. $\kappa(N) \sim \ln N$ has been observed numerically and experimentally in two-dimensional systems; while other three works gave a prediction with $\alpha = 1/3$ for 1D chain with 2D motions [45, 47, 53]. This prediction was confirmed recently by T. Mai and O. Narayan [54]. These results are general accepted for 1D chains.

Secondly, when momentum conservation is broken such as the one with on-site potential (representing interaction with substrate), the heat conduction can become normal again like the Frenkel-Kontorova model [25, 50] and the ϕ^4 model [4, 20].

The on-site potential plays a very important role in heat transport process. In non-integrable lattices without on-site potential, the existence of solitary waves is responsible for the divergent heat conduction. On-site potential destroys the

momentum conservation, produces a diffusive energy transport, and thus leads to a finite thermal conductivity.

We can use concepts of kinetic theory to explain the observed thermal conductivities in harmonic lattice, anharmonic lattice without on-site potential, and anharmonic lattice with on-site potential. In (electrically) insulators the heat flux is carried almost entirely by phonon vibrations. It is useful to picture a solid as a gas of phonons which can store and transmit heat. A perfectly harmonic crystal, due to the fact that phonons do not interact, has an infinite thermal conductivity (no temperature gradient): in the language of kinetic theory the mean free path is infinite. In anharmonic lattice, the anharmonic forces produce interactions between the phonons and therefore a finite mean free path. Another source of finite thermal conductivity may be the lattice imperfections and impurities which scatter the phonons.

In order to understand the underlying microscopic dynamical mechanism of Fourier's law, a different class of models − billiard channels − have been introduced and studied in recent years [33–35, 37, 38, 51]. Various exponent values are found in such systems. Thus, it is believed that a universal constant does not exist at all. Instead, the divergent (convergent) exponent of the thermal conductivity is found related to the power of super (sub) diffusion [37]. A connection between the anomalous heat conduction and anomalous diffusion has been established with

$$\alpha = 2 - 2/\beta, \tag{1.5}$$

where β is the exponent of the diffusion ($\triangle x^2 \sim t^\beta, 0 < \beta \leq 2$). The main conclusion from their study is that an anomalous diffusion indicates an anomalous heat conduction with a divergent (convergent) thermal conductivity. More precisely, they tells us that: a ballistic motion means thermal conductivity proportional to the system size L; a normal diffusion means a normal heat conduction obeying the Fourier law; a superdiffusion means a divergent thermal conductivity; and a subdiffusion means a zero thermal conductivity in the thermodynamic limit.

It states that a subdiffusive system is an insulator in the thermodynamic limit and a ballistic system is a perfect conductor, Fourier's law being therefore valid only when phonons undergo a normal diffusive motion. Based on the Levy walk assumption, another relation $\alpha = \beta - 1$ is suggested in several gas systems [52, 53] and supported by recent work [55]. These two relations converge [37, 52, 53, 55] in normal diffusion and ballistic systems.

The effect of nonlinearity and chaos on heat conduction is also clear now. One can safely say that nonlinearity is a necessary condition for the valid of Fourier's law and exponential local instability is neither a necessary condition nor a sufficient condition for normal heat conduction. As shown in the Table. 1.1, 1D nonlinear lattices with momentum conservation, such as Fermi-Pasta-Ulam and alike lattices, exhibit abnormal heat conduction; whereas in 1D nonlinear lattices without momentum conservation, such as Frenkel-kontorova and ϕ^4 lattices, obey Fourier's law. The relationship between the heat conduction and nonlinearity was study systematically recently by N.-B Li and B Li [40]. They found that the heat conductivity depends on temperature via the strength of nonlinearity. We will show later that nonlinearity has been found very useful in controlling heat flow.

These basic studies about heat conduction not only enrich our knowledge of the fundamental transport laws in statistical mechanics, but also open the way for applications such as designing novel thermal materials or devices such as thermal rectifiers [60–63, 65–67, 69] and the thermal transistors [68].

1.2 Methodology for General Computation of Thermal Conductivity

In this section, we will introduce general methodology for studying the phenomenon in heat conduction in low-dimensional lattice system. Since most work about the phenomenon of heat conduction is numerical or theoretical approximation, how to define variables related to heat conduction becomes an important problem. So in this section, we will give an introduction about the background related with

numerical calculation and theoretical analysis [48] about heat conduction in separate subsections. For the sake of simplicity, we discuss the problem with reference to 1D systems with nearest-neighbor interactions, the extension to the more general case being more technically involved but conceptually equivalent.

The general procedure to treat issues of thermalization, transport, and heat conduction in a 1D classical lattice can be divided into several steps which are presented in the following sections.

1.2.1 Model

The class of models is described by quite general 1D classical lattice Hamiltonian of the form

$$H = \sum_{i=1}^{N} [\frac{p_i^2}{2m_i} + V(x_{i+1} - x_i) + U(x_i)]. \tag{1.6}$$

N atoms are sited one by one along 1D chain. x_i, p_i are the displacement and momentum of the ith particle. Usually, only nearest interaction, which is included in $V(x_{i+1,i})$, is considered for simplicity. $U(x_i)$ is the imposed potential of the ith particle from substrate. Boundary conditions need to be specified by defining x_0 and x_{N+1}. Typical choices are periodic, fixed or free boundaries.

When only internal forces ($V(x_i, x_{i+1}) \neq 0$, $U(x_i)$=0), that depend on relative positions, are present, the total momentum is conserved and thus a zero (Goldstone) mode exists. In the harmonic limit, Hamiltonian system with $U = 0$ in Eq. (1.6) admits at least a phonon branch whose frequency vanishes for vanishing wave number. Long-wavelength waves move at the sound velocity and for this reason one sometimes refer to this kind of system as acoustic models. An important example of Eq. (1.6) is the well-known Lennard-Jones potential

$$V(r) = \epsilon[(\frac{a}{r})^{12} - 2(\frac{a}{r})^{6}]. \tag{1.7}$$

In this formula a is the equilibrium distance and ϵ is the well depth. The other example we will often consider is the celebrated Fermi-Pasta-Ulam (FPU) potential [15]

$$V(z) = \frac{k_2}{2}(z-a)^2 + \frac{\alpha}{3}(z-a)^3 + \frac{\beta}{4}(z-a)^4. \tag{1.8}$$

This model can be regarded as a result from an expansion of V close to its equilibrium position $z = a$. Due to its simple algebraic form, the model is computationally very convenient. Two important particular cases are worth mentioning: the quadratic plus cubic ($\beta = 0$) and quadratic plus quartic ($\alpha = 0$) potentials that, for historical reasons, are referred to as the FPU-α and FPU-β models, respectively. In the former one, sufficiently small coupling constant α and (or) energies must be considered to avoid runaway instability of trajectories. Models in Eq. (1.6) with $U = 0$ are a very drastic idealization of a real crystal. Natural low-dimensional lattice structures are usually embedded in three-dimensional matrices that couple them to the environment. At the simplest level of modelization, this can be described by adding an external, on-site , potential ($U(x_i) \neq 0$) as in Eq. (1.6).

The substrate potential U in Eq. (1.6) breaks the invariance $x_i \rightarrow x_i + const.$ of system without on-site potential in Eq. (1.6) and the total momentum is no longer a constant of the motion. Accordingly, all branches of the dispersion relation have a gap at zero wave number. We therefore refer to models with on-site potential as optical ones. Dimensionless variables will be used throughout whenever possible, especially when reporting simulation data. The choice of the most natural units is usually dictated by the particular model at hand.

1.2.2 Heat bathes

Here we will introduced two most popular heat bathes in numerical calculations. One is a stochastic bath and another one is a deterministic heat bath.

A . Stochastic Baths

A traditional way to implement the interaction with reservoirs amounts to introducing simultaneously random forces and dissipation according to the general prescription of fluctuation dissipation theorem. Let us consider the finite N-particle chain exposed to on-site potential as in Eq. (1.6) with end regions connected to

the Langevin thermostats [4, 73–77] with temperature T_+ and T_-. The Newton equations of the particles coupled with heat baths take a form

$$\begin{aligned} m_i\ddot{q}_1 &= -F(q_2-q_1)+F(q_1-q_0)-F(q_i)-\gamma\dot{q}_1+\xi_1^+ \\ m_n\ddot{q}_n &= -F(q_{n+1}-q_n)+F(q_n-q_{n-1})-F(q_n)-\gamma\dot{q}_n+\xi_n^- \end{aligned} \tag{1.9}$$

where function $F(q) = dU(q)/dt$; $1, n$ are indexes of the particles coupled with thermostats at the two ends; γ is a relaxation coefficient and $\xi_i^{\pm}$ $(i = 1, n)$ is white Gaussian noise modelling the interaction with the thermostats

$$\begin{aligned} &\langle\xi_i^{\pm}(t)\rangle = \langle\xi_i^{\pm}(t_1)\xi_i^{\mp}(t_2)\rangle = 0 \quad (i=1,n) \\ &\langle\xi_n^{\pm}(t_1)\xi_1^{\pm}(t_2)\rangle = 2\gamma T_{\pm}\delta_{n1}\delta(t_2-t_1). \end{aligned} \tag{1.10}$$

In the case of stochastic reservoirs, the heat flux vanishes both in the weak- ($\gamma \to 0$) and strong-coupling ($\gamma \to \infty$) limits. The opposite regime is less trivial. For $\gamma \to \infty$ the temperature of the extremal particles converges to the temperature of the reservoir. In other words the temperature-drop is observed between the boundary particle coupled in stochastic reservoir and its neighbor.

B. Deterministic Baths

In the attempt of providing a self-consistent description of out-of-equilibrium processes, various types of deterministic heat baths have been introduced [78]. This was also motivated by the need to overcome the difficulties of dealing with stochastic processes. The scheme that has received the largest support within molecular-dynamics community is perhaps the so-called Nośe-Hoover thermostat [79]. More precisely, the evolution of the particles in thermal contact with the bath is ruled by the equation

$$\begin{aligned} m\ddot{q}_1 &= F(q_1-q_0)-F(q_2-q_1)-\zeta_+\dot{q}_1 \\ m\ddot{q}_n &= F(q_n-q_{n-1})-F(q_{n+1}-q_n)-\zeta_-\dot{q}_n, \end{aligned} \tag{1.11}$$

where $\zeta_{\pm}$ are two auxiliary variables modeling the microscopic action of the thermostat, and $1, n$ denote the indexes of the two-end particles in contact with the

reservoirs. The dynamics of $\zeta_\pm$ is governed by the equation

$$\begin{aligned}\dot{\zeta}_+ &= \frac{1}{\Theta_+^2}(\frac{m\dot{q_1}^2}{k_B T_+} - 1) \\ \dot{\zeta}_- &= \frac{1}{\Theta_+^2}(\frac{m\dot{q_n}^2}{k_B T_-} - 1),\end{aligned} \tag{1.12}$$

where $\Theta_\pm$ are the thermostat response times.

The heat flux vanishes in the week coupling limit (the response time Θ goes to 0) for deterministic reservoirs. In the opposite limit $\Theta \to \infty$ the heat flux does not go to 0 but reaches asymptotically a constant. When increasing Θ the distribution of ζ becomes narrower and narrower. So in order to reach the asymptotical value, longer and longer computational time is required when Θ becomes larger and larger. As a result of this analysis we can conclude that values of Θ of order 1 (in the chosen dimensionless units) are the optimal choices for numerical simulations, since smaller values imply smaller heat fluxes, while larger ones would require longer simulation times.

1.2.3 Statistical properties

After the system contact with thermal reservoirs for sufficient time, a stationary state can be reached, thus the statistical variables which are concerned can be computed. The most concerned variables in molecular dynamics simulation of thermal conductivity are the temperature profile and heat flux along the chain.

A. Temperature

In molecular-dynamics simulations, averages are more conveniently computed by following single trajectories over time

$$\frac{1}{2}k_B T = \frac{1}{2}m\langle v^2 \rangle. \tag{1.13}$$

That is to regard the time average as ensemble average in numerical computation. This is not a problem whenever the system is ergodic. In this case, the system can experience each state after sufficient long time. So ensemble and time averages are equivalent. However, time averages of quantities corresponding to thermodynamic

observables have been found to converge to the expected ensemble averages even in systems that are known not to be ergodic in a strictly mathematical sense (as e.g. the FPU-β model at sufficiently small energy values) and even when fluctuations around the mean value are not consistent with equilibrium predictions. This suggests that a weaker condition than ergodicity might suffice to ensure the equivalence of time and ensemble averages of the physically relevant observables.

Eq. (1.13) can be obtained from the virial theorem (see details in Ref. [48]). The identification of an optimal definition of temperature to be adopted in numerical studies is strictly related to the convergence properties of time-averages. In this sense, it has been observed that definitions like the above ones involving only momenta converge always quite rapidly, also when the dynamics is weakly chaotic, while definitions involving an explicit dependence on space coordinates may converge over much longer time scales [27].

In a dimensionless unit which is popular in molecular dynamical simulations, the real temperature T_r is related to the effective dimensionless temperature T through the following relation [25],

$$T_r = \frac{m\omega_0^2 b^2}{k_B} T, \tag{1.14}$$

where m is the mass of the particle and b is the period of external potential. ω_0 is the vibration frequency. k_B is the Boltzman constant. It is helpful to establish the above relationship (1.14). It can give us very useful information about the corresponding real temperature and enable us to gain some physical insights. For instance, for the typical values of atoms, we have $T_r \sim (10^2 - 10^3)$ [25], which means that the room temperature corresponds to the dimensionless temperature T about the order of $0.01 \sim 1$.

B. Flux

The heat flux $j(x,t)$ at time t in the spatial position x is nothing but the energy current, implicitly defined by the continuity equation

$$\frac{d\varepsilon(x,t)}{dt} + \frac{\partial j(x,t)}{\partial x} = 0, \tag{1.15}$$

where $\varepsilon(x,t)$ is the energy density. With reference to an ensemble of interacting particles, we can write the microscopic energy density as the sum of the isolated contributions located in the instantaneous position of each particle

$$\varepsilon(x,t) = \sum_i \varepsilon_i \delta(x_i - x), \tag{1.16}$$

where ε_i is the energy density in the instantaneous position of i and

$$\varepsilon_i = \frac{p_i^2}{2m_i} + U(x_i) + \frac{1}{2}[V(x_{i+1} - x_i) + V(x_i - x_{i-1})], \tag{1.17}$$

is the energy contribution of the ith particle. In a similar way, we can write the heat flux as the sum of localized contributions,

$$j(x,t) = \sum_i j_i(x). \tag{1.18}$$

The problem amounts therefore to give a definition of the local heat flux j_i. The time derivative of ε_i

$$\frac{d\varepsilon_i}{dt} = m_i \dot{x}_i \ddot{x}_i + \dot{x}_n U'(x_i) - \frac{1}{2}[(\dot{x}_{i+1} - \dot{x}_i)F(x_{i+1} - x_i) + (\dot{x}_i - \dot{x}_(i-1))F(x_i - x_(i-1))], \tag{1.19}$$

where the prime is the time derivative and $F(x) = -V'(x)$ can be rewritten by the equations of motion derived from model in Eq. (1.6)

$$m_i \ddot{x}_i = -U'(x_i) - F(x_{i+1} - xi) + F(x_i - x_{i-1}) \tag{1.20}$$

as

$$\frac{d\varepsilon_i}{dt} = -\frac{1}{2}[(\dot{x}_{i+1} + \dot{x}_i)F(x_{i+1} - x_i) - (\dot{x}_i + \dot{x}_{i-1})F(x_i - x_{i-1})]. \tag{1.21}$$

This equation can, in turn, be rewritten as

$$\frac{d\varepsilon_i}{dt} + \frac{j_i - j_{i-1}}{a} = 0, \tag{1.22}$$

where

$$j_i = \frac{1}{2}a(\dot{x}_{i+1} + \dot{x}_i)F(x_{i+1} - x_i) \tag{1.23}$$

which can thus be interpreted as the local heat flux. The average local heat flux is

$$\langle j_i \rangle = a\langle \dot{x}_{i+1} F(x_{i+1} - x_i) \rangle \tag{1.24}$$

since in a stationary state $\langle \dot{x}_{i+1} F(x_{i+1} - x_i) \rangle = \langle \dot{x}_i F(x_{i+1} - x_i) \rangle$. Accordingly, the average local heat flux is constant along the chain as it should be.

After temperature and heat flux are known, thermal conductivity can be known through the Eq. (1.2). Also there are other tools to calculate thermal conductivity k, such as Green-Kubo formula. In Green-Kubo formula [31], the thermal conductivity in the classical case is defined as

$$k = \lim_{\tau \longrightarrow \infty} \lim_{L \longrightarrow \infty} \frac{1}{LT^2} \int_0^\tau dt \langle J(t) J(0) \rangle, \tag{1.25}$$

where $J(t)$ is the total energy current. However, in this formular the same observable has different time-correlations in the different ensembles. So in order to obtain a converged value, one needs to do the average over different ensembles.

The formula Eq. (1.25) provides a well defined prescription for determining the thermal conductivity from the current-current correlation function at equilibrium. Mode-coupling theory [32,45,48] and renormalization group [47] are two alternatives for estimating this correlation function. More details about these methods can be found in the report by S. Lepri *et al.* [48] and an application about mode-coupling theory is referred in the work by J.-S. Wang and B Li [45].

1.3 Thermal Diode

The understanding of heat conduction mechanism and the existing method to study heat conduction made it possible for physicists to seek the possibility to control and manipulate heat current, and eventually to design novel thermal devices with certain function. An intriguing mode of behavior often addressed in recent studies of heat transport devices is current rectification, allowing larger conduction in one direction than in the opposite one when driven far enough from equilibrium [60, 61]. Such phenomena were extensively studied for electronic conduction in molecular junctions,

but much less so for thermal nano-conductors. For example, the electronic transistor has been invented for more than 50 years, and it has revolutionized our daily life in many aspects, but there are still no similar devices to control heat current.

Although electrical rectifiers are commonplace, thermal rectification has received attention in only relatively few cases. For example, the absorption with shorter wavelengths and re-radiation with longer wavelengths of thermal radiation from the sun through a glass window with internal walls was caught attention in 1968 by Markus. Another thermal rectifier consists of a closed tube containing a vapour in contact with its own liquid [57]. Unfortunately, neither of these physical processes possesses the versatility necessary for a commercially viable thermal rectification device. However the asymmetrical behavior of certain contacts between solid offers a potential method for thermal rectification. In 1966 Williams [56] and in 1970 Thomas and Probert [58] found that the directional effect can occur between similar solids with different surface histories. In 1970 P. W. O'callaghan, S. D. Probert and A. Jones designed a thermal rectifier experimentally [59]. It consists of a multilayer stack of thin disks, each having one roughened and one smooth surface. When assembled in the stack, the layers are so arranged that all the rough surfaces are facing in the same direction like shown in the Fig. 1.1. By changing the applied pressure and fixed temperatures at the two ends, they found that the directional effect (R_T/R_A) of thermal resistances from two directions can be up to 1.5. Also there are other experimental investigations of thermal rectification between dissimilar metals [56–58].

However, the possible theoretical explanation of thermal rectification from microscopic point of view is available only recently [60]. Terraneo *et al* [60] introduced a one dimensional (1D) model consisting of three segments of nonlinear lattices with on-site Morse potential. By adjusting the nonlinear parameters appropriately, one can achieve a rectification between 1 and 2. Later on, a complete new model, a two-segment model has been proposed by our group [61]. The two-segment model consists of two dissimilar anharmonic lattices, namely the Frenkel-Kontorova (FK) lattice with different parameters in different parts. The nonlinearity of the lattice comes from the substrate interaction, or called on-site potential. By adjusting the

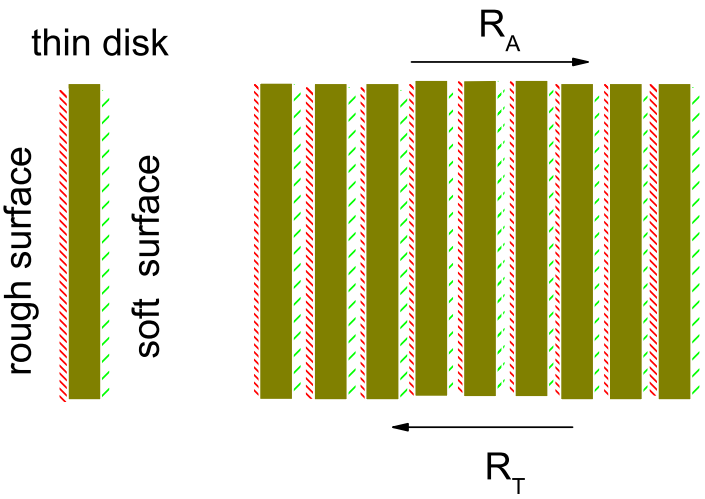

Figure 1.1: Schematic picture of thermal resistance along a multilayer stack of thin disks, each having one roughened and one smooth surface. R_A is when heat flows from smooth surface to rough surface and R_T is when heat flows from rough surface to smooth surface

parameters in two segments, one can achieve a rectification as high as 200, which is two orders of magnitude better than the three segment model.

Since a nonlinear lattice has many parameters to adjust, there are different possibilities to achieve the rectification, such as a change of potential periodicity. [63]

The above works show the possibility to control heat flux in lattice model and eventually to design novel thermal materials and/or devices. They opens a new sight to control and manipulate heat current, and eventually to design novel thermal devices with certain function.

1.4 Motivation and Goals

Controlling heat current is not only a problem of scientific curiosity but also a practical application problem. It might have potential application in energy saving materials or unidirectional processes. It may also promise to explain certain im-

portant fundamental questions in biophysics, such as controlled energy transport in living organisms on a cellular level.

Theoretical study of thermal rectification is important not only from the fundamental point of view but also from the application point of view. The understanding of thermal rectification will give reliable guidance to control and manipulate heat current in practical applications.

1.4.1 Motivation

So far, there is no unique theoretical framework to explain the phenomenon of thermal rectification. Previous theoretical works about thermal rectifier focused on realization of thermal rectifying effect in different models and effort of seeking the optimum set-up for rectifying performance. In this thesis, we will try to realize thermal rectifying effect in more general models. Based on the two-segment prototype, we will use two representative lattices to construct an efficient thermal diode. One is the Frenkel-Kontorova (FK) lattice, another one is the Fermi-Pasta-Ulam model (FPU). The FPU model is a representative anharmonic lattice without on-site potential and the FK model is the one with on-site potential. Most physical system can be divided into the two representative models: one with on-site potential and another without on-site potential. We expect that our study on thermal rectifying effect based on these two representative lattices has general meaning.

Also we should point out that almost all works about heat transport and control of heat current are focused on 1D systems of finite sizes. Obviously, much progress was acchieved, but the final purpose is to put these ideas to application. To this end, it is necessary to extend the study to higher dimension and more realistic system. In this PhD project, we will try to extend the study of thermal rectifier from 1D lattice [62] to a two dimensional (2D) lattice [65] or even to a bulk (3D) [66].

The microscopic properties depending on different parameters controlling and response to environment changes will be investigated and explored systematically.

General mechanism for rectifying effect in different models is only discussed qualitatively based on energy band theory or roughly explained based on numerical

methodology. The determinant factor for rectifying effect was found to be the match or mismatch of vibrational bands from different parts [60, 61]. But what is the underlying physics that results in the match or mismatch of bands and how to control the extent of overlap of bands are still not clear. This project is proposed to explore the underlying mechanism in both numerical and analytic approaches. We are trying to provide useful guidance and meaningful suggestion for a general set-up of thermal rectifiers in a theoretical framework or experiments.

We will demonstrate in this thesis that because of anharmonic terms, the width and position of an "effective" phonon band depend on temperature. By tuning the anharmonicities of different coupled chains it is possible to control the effective overlap between the effective phonon bands of the two parts. In particular, the extent of this overlap can be made to depend on the sign of the imposed temperature gradient, thus leading to thermal rectification. By coupling two representative dissimilar lattices, we will show that the rectification can be improved to several hundreds or few thousands, namely several times or one order of magnitude better than the two-segment FK model [61]. Moreover, a connection between the rectification or asymmetric flows, asymmetric thermal interface resistance - Kapitza resistance [62] and the extent of overlap of bands will be established.

1.4.2 Objectives and Significance

The main aim of this project was to establish a theoretical frame work for constructing an efficient thermal diode in lattice systems, and to give reliable guidance and reasonable suggestions for realizing thermal rectification and for controlling it in a general asymmetric model. To reach this aim, we proposed to do the following works.

1) To construct a thermal diode in a 1D chain which consists of two dissimilar lattices. Much better thermal rectification will be demonstrated in our model, which is one order of magnitude larger than that in the previous two-segment model [61].

2) To study the main mechanism for a good thermal diode. The rectification, or

asymmetric heat flow is related with an asymmetric thermal interface resistance - Kapitza resistance. A physical explanation will be connected with the thermal rectification in the view of energy band theory.

3) To extend the work to thin films or nanotubes and eventually to realize thermal rectification in a bulk.

4) To investigate different possibilities to control rectifying effect and possible response of a thermal rectifier to environment changes.

5) To bring forward an analytic framework about thermal rectification with general validity in anharmonic models.

The present research may provide some insights in understanding thermal rectification from a general view. Moreover the study on effective phonon bands (or vibrational bands) of anharmonic lattices may provide both numerical and theoretical approaches for a general anharmonic lattice. The connection of the extent of match of vibrational bands from different parts with the thermal rectification may give a possible explanation of energy transport between different materials.

The asymmetric property might be useful in heat control and management. The significant feature of thermal diode is to allow energy to dissipate directionally. This feature will be quite helpful in energy saving materials. For example, if we substitute glass windows with some thermal diode materials, when inside is hotter than outside, heat can flow out. However, if outside is hotter than inside, heat can not flow in. It would help to keep the inside at a comfortable temperature with very little energy consuming whether it is snowing or sun shining outside. It may help to solve many heat problems and may have wide applications in real life, like the fabrication of hi-tech items, drugs treatments in biological body, and so on.

1.5 Orgnization of the Thesis

In order to fulfill the basic purpose of the study, depth was chosen over breadth, that is, the study focuses on the area of constructing a general efficient thermal rectifier and generalize it from a low-dimensional model to higher-dimensional models rather than to realize rectifying effect in different 1D models. So to construct the efficient thermal diode from 1D to 3D is the central to this study. The underlying mechanics is investigated in both numerical and analytic ways. The thesis is organized as the follows. In Chapter 2, we establish an efficient thermal rectifier in a system consisting of two dissimilar anharmonic lattices exemplified by the Fermi-Pasta-Ulam (FPU) and Frenkel-Kontorova (FK) models. The directional effect is found to be related with asymmetric interface thermal resistance (ITR). The dependence of the ITR on the coupling constant, temperature, temperature difference, and system size is studied. Possible applications in nanoscale heat management and control are discussed. In Chapter 3, we do a direct extension from the 1D model to a 2D model. The dependence of rectifying efficiency on the temperature and temperature gradient is studied. Similar behaviors in the 2D thermal rectifier under similar parameters' control with that in the 1D model are founded. In Chapter 4, we do a further extension. We extend our model to a 3D model consisting of two segments of anharmonic lattices. One segment is layers of harmonic oscillators arrays coupled to a substrate potential, which is a 3D Frenkel-Kontorova model (3D FK), and the other segment is a three dimensional Fermi-Pasta-Ulam model (3D FPU). We study the lattice vibrational bands of the two models analytically and numerically. We make it clear that different nonlinearities will induce different temperature dependence for vibrational bands. The possible guidance and suggestion to increase thermal rectification is given. All problems investigated in this thesis are summarized in Chapter 5. Possible connection with a recent experiment in a heterostructure nanotube is discussed.

Chapter 2

1D Efficient Thermal Diode and Kapitza Resistance

Previous basic studies about heat conduction in low-dimensional systems [4, 14, 16–28, 30, 33–37, 39, 52, 55, 83], not only have enriched our knowledge of the fundamental transport laws in statistical mechanics, but also have made it possible to seek the practical application of heat control and management. An example is to design thermal rectifier [60, 61, 63] in solid in nanoscale.

A thermal rectifier or thermal diode is a device which has a high resistance to heat flow in one direction across it, which has a low resistance for the reversed direction of heat flow. Such devices are useful in maintaining constant temperatures within systems which are intermittently exposed or isolated from a source or sink for heat, or are continuously exposed to a fluctuating source or sink for heat. Various passive or active devices are possible which inhibit or enhance heat flows depending upon their magnitudes and directions. These include heat pipes, solar collectors, special cavities, distorting contacts and thermomechanically-switched arrangements. The greenhouse effect is a thermal rectification phenomenon, as are the body regulatory processes against heat and cold.

In quantum mechanics, for a harmonic thermal conductor connecting (by linear coupling) two (left (L), right (R)) harmonic thermal reservoirs that are maintained at equilibrium with the temperatures T_L and T_R, respectively, heat transfer is a ballistic

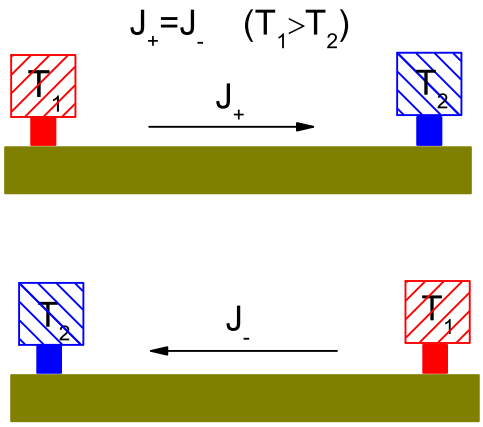

Figure 2.1: Schematic picture of heat fluxes along a symmetric chain when swapping the heat bathes on the two ends. In the upper chain, J_+ is flowing from the left to the right. In the bottom chain, J_- is flowing from the right to the left. $|J_+| = |J_-|$.

process and the heat current J can be recast into a Landauer type expression [69,70]

$$J(\omega) = \int \mathcal{T}(\omega)[n_L(\omega) - n_R(\omega)]\omega d\omega, \tag{2.1}$$

where $\mathcal{T}(\omega)$ is the transmission coefficient for phonons of frequency ω and $n_K(\omega) = (\exp^{\beta_K \omega} - 1)^{-1}$; $\beta_K = (k_B T)^{-1}$; $K = L, R(\hbar \equiv 1)$ are Bose-Einstein distribution functions characterizing the reservoirs. Obviously, this expression is symmetric to interchanging the reservoir temperatures and cannot show rectifying behavior irrespective of any asymmetry in the system structure.

Correspondingly, for a classical symmetric system, the fluxes from two directions are same when swapping the heat baths at the two ends. This is shown in Fig. 2.1. J_+ should be exact equal J_- with the a sign difference "$-$" when reversing the heat bathes on the two ends .

However what will happen if we break the symmetry of the system? Will J_+ still equals J_-? The study of this PhD project is focused on this problem. We will show that the phenomenon, directional effect or rectifying effect, is generally observed in asymmetric systems.

2.1 Mechanism of Thermal Rectifier

The first theoretical model of thermal rectification was a sandwich model [60] proposed by Terraneo, Peyard and Casati in 2002. They found that the model can rectify the heat fluxes through it when reversing the temperature at the two ends by acting on the Morse on-site potential strengths of three segments. The left and right segments are identical and connected to thermal baths in different temperatures, while the middle segment has different nonlinear parameter. By changing the difference between the nonlinear parameters of the middle and two-end segments, the sandwich model demonstrates a unidirectional heat flow as shown in Fig. 2.2. They approximated the nonlinear model by a fully harmonic Hamiltonian and used effective-phonon analysis to explain rectifying effect phenomenon like shown in Fig. 2.2. In the presence of a thermal gradient, the effective phonon frequencies of the central part evolve in space in a way that depends on the orientation of the gradient. This can provide either a good matching of the bands at the interfaces, leading to a thermal conduction across the system, or a complete mismatch leading to poor conduction. As a first trial in classical systems to control heat current along it, the thermal rectification from two directions is only about 2. But their ideas are general valid. The match of effective phonon bands, or the shift of frequency is associated to nonlinearity, so that one can expect that various physical systems could exhibit similar behaviors. And it is the first time to give a theoretical explanation for the possible mechanism of the thermal rectification phenomenon in solid.

Based on the idea of match or mismatch of effective phonon bands, B Li. *et al.* [61] constructed a new device by coupling two nonlinear one-dimensional(1D) lattices. The model comprised two Frenkel-Kontorova (FK) chains with different nonlinear strengths and the two chains were connected by a weak harmonic spring. In this new thermal device, they found a very good rectifying effect. And they demonstrated the thermal diode works in a wide range of system parameters. In their model, heat flow is allowed from one end to the other, but the flow is inhibited in the opposite direction. The underlying microscopic mechanism shown in Fig. 2.3

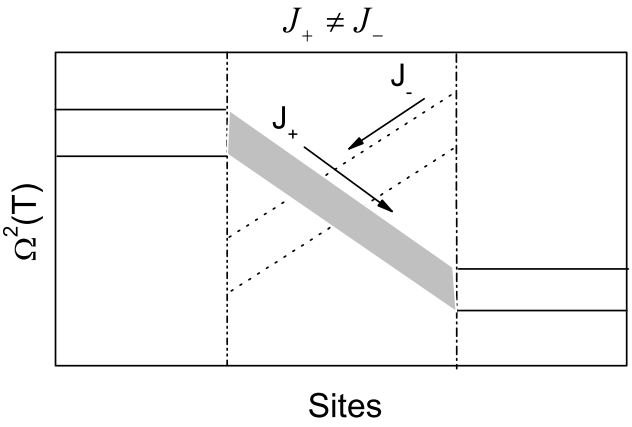

Figure 2.2: Schematic picture of the phonon bands in a "thermal rectifier" for two directions of the temperature gradient. The bands in the left and right weakly anharmonic regions do not change significantly with the orientation of the gradient. In the central part, when the high temperature side is on the right, the band evolves in space as shown by the shaded region, while, if the high temperature side is on the left, the band evolves according to the dashed lines.

is different from the one in the work by Terraneo *et al.* [60]. In this model the bands of the left part and the right part are both temperature dependent. The nonlinearity of this model results in the expansion of bands from high frequency region to low frequency region when increasing temperature. Different nonlinearities of the two parts result in different concentrating regions of the two bands. As shown in Fig. 2.3, the part with stronger nonlinearity (the left part) has a broad band, while the part with weak nonlinearity (the right part) has a narrow band when they are in the same temperature. So when the high temperature is added at the left part (with strong nonlinearity) and low temperature is added at the right part, the broad band of the left part matches the narrow band of the right part as shown in Fig. 2.3(a). In this situation, heat flux can go through the system fluently with a large value. However when reversing the temperature at the two parts, the band of the left band will shrink to the high-frequency region and the band of the right band will expand to a low-frequency region. So the total effect is the separation of the two bands as shown Fig. 2.3(b). In this situation, heat flux was inhibited by the mismatched

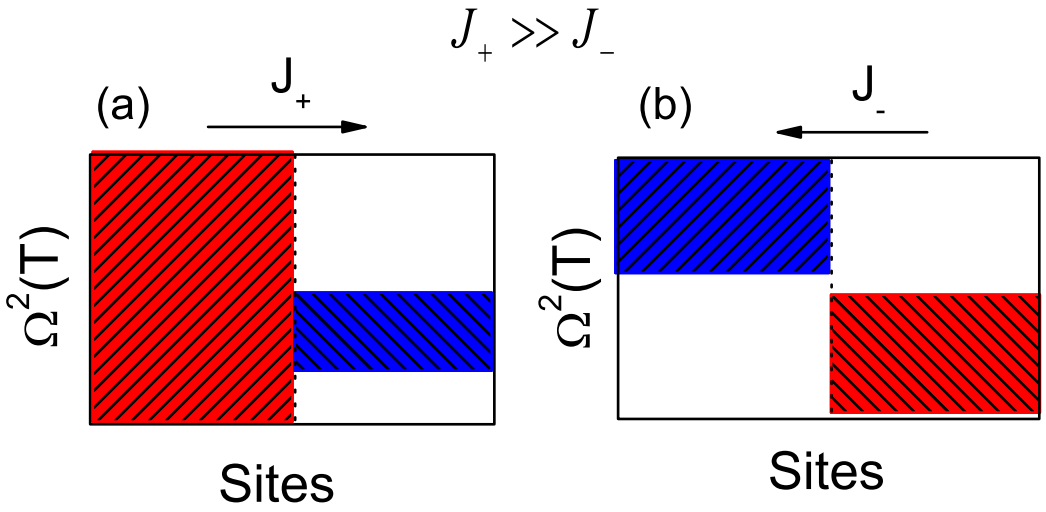

Figure 2.3: Schematic picture of the phonon bands in the work by B Li *et al.* The bands in the left and right anharmonic regions change significantly with temperature and concentrate on different region depending on the strength of nonlinearity. (a)When high temperature is added on the left end, the spectra of the two regions matched with each other. (b) when high temperature is added on the right end, the spectra of the regions separate with each other.

bands with a very small value.

The most successful improvement of the model by Li *et al.* [61] lies in three facts: First, the configuration is simple, it consists of only two different segments; Second, the ratio of heat current from two different directions is increased drastically about 100 times, which is much more effective, comparing with the three-segment device by Terraneo *et al.*; Third, the underlying mechanism of thermal rectifying effect is explained visually by illustrating the phonon bands of the particles in different segments.

2.2 1D FK-FPU Rectifier

From the above two trials to control heat current, we know that the success for a thermal rectifier should lie on two factors. The first one is the asymmetry of the

system. The second one is nonlinearity of the system. Out of question, asymmetry is the prerequisite to realize rectifying effect. Nonlinearity is necessary for a thermal rectifier.

Phonons are the normal modes of the elementary vibrations of a lattice under linear force driving; while vibrational modes of any arbitrary anharmonic lattice vibrating at some temperature can be regarded as effective phonons. The phonon band of a harmonic (or linear) system will not change with temperature. The increase of temperature will only result in the increase of the amplitude of the band in a harmonic system. However, the nonlinearity will induce the dependence of the effective phonon bands or vibrational bands on temperature. The increase of temperature will not only result in the increase of amplitude of bands of the nonlinear system, but also induce the change of concentrating region of bands. Consequently, asymmetric nonlinearity of the system will induce asymmetry dependence of spectra on temperature. This make it possible to realize rectifying effect by setting suitable strengthes of nonlinearity in different parts or by connecting two or three similar anharmonic segments. In this thesis, we will show the possibility to construct a thermal diode by coupling two dissimilar arharmonic lattices. It works efficiently not only in 1D lattice but also in two-dimensional (2D) film even in three-dimensional (3D) bulk by manipulating the structure and parameters properly. In this Chapter, we will firstly introduce our thermal rectifier or thermal diode in a 1D lattice. In the following two Chapters, we will talk about thermal diodes on higher dimensional models.

2.2.1 Model and Methodology

Our 1D model comprises two dissimilar anharmonic lattices. We choose two popular lattices as the components: the FK lattice and the FPU lattice. The FK model is a representative anharmonic lattice with on-site potential and the FPU model is the one without on-site potential. Both models have been widely used to study different problems in condensed matter physics and nonlinear dynamics. The FK model was first proposed by Frenkel and Kontorova in 1938 [50] to study surface phenomenon.

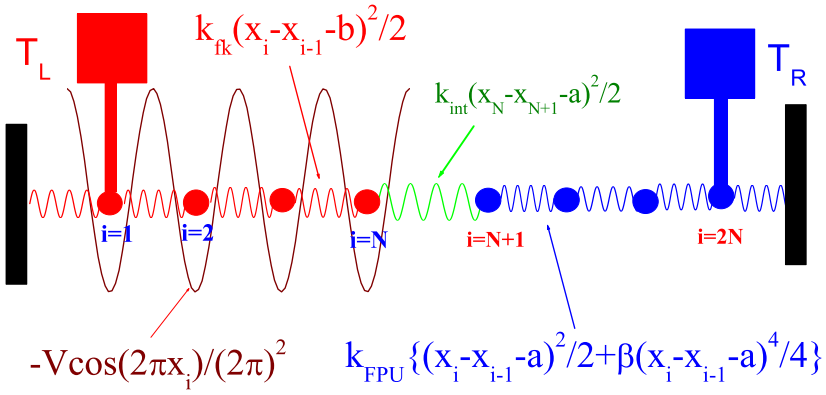

Figure 2.4: Configuration of the system. The left part is a Frenkel-Kontorova model and the right one is a Fermi-Pasta-Ulam model. The two parts are connected by a spring of constant k_{int}. The two particles on the left and right ends are put into contact with heat baths with temperature T_L and T_R, respectively.

Since then it has found applications in a wide variety of physical systems, such as adsorbed mono-layers, Josephson junctions, charge density waves, magnetic spirals, tribology, DNA denaturation, and so on. Despite its simple form, the FK model exhibits very rich and complex behaviors. The celebrated Fermi-Pasta- Ulam (FPU) model was introduced fifty years ago in order to study the process of equilibration of energy among normal modes due to mode-mode interactions. The FPU model has played an important role in the development of computational physics and nonlinear dynamics. Here we cite some words from the paper on the Focus Issue of the journal "Chaos" to commemorate the 50th anniversary of the May 1955 publication of the Los Alamos report about "Fermi-Pasta-Ulam" problem. *The "FPU problem", as it is universally known, marked a true sea change in modern science, both ushering in the age of computational science and marking the birth of our own field of "nonlinear science" [84].* These words show the importance of FPU model in computational physics and nonlinear dynamics.

Recent years have witnessed increasing interests in the study of heat conduction with these two models in low-dimensional systems [15, 25, 26, 50].

In our thermal diode, a weak harmonic spring connects a FK lattice and a FPU

lattice. For a 1D thermal rectifier, we denote it as a 1D FK-FPU model. In 2D and 3D cases, our thermal diode will be denoted as 2D FK-FPU and 3D FK-FPU models, respectively.

The system, illustrated in Fig. 2.4, consists of two chains of N oscillators. The left part is a FK chain of N harmonic oscillators on a substrate whose interaction is represented by a sinusoidal on-site potential. The right part is a FPU chain of N anharmonic oscillators. All oscillators are aligned along the chain stationarily with equal distances a. The two parts are connected by a spring of constant k_{int}, and the Hamiltonian of the system is,

$$H = H_{FK} + H_{FPU} + \frac{1}{2}k_{int}(x_{N+1} - x_N - a)^2, \tag{2.2}$$

where H_{FK} is the Hamiltonian of the left part which is in fact the Frenkel Kontorova (FK) model,

$$\begin{aligned} H_{FK} &= \sum_i H_i = \sum_i \frac{p_i^2}{2m} + V_{FK}(x_{i-1}, x_i) + U_{FK}(x_i) \\ &= \sum_{i=1}^{N} \frac{p_i^2}{2m} + \frac{1}{2}k_{FK}(x_i - x_{i-1} - a)^2 - \frac{A}{(2\pi)^2}\cos 2\pi x_i. \end{aligned} \tag{2.3}$$

H_{FPU} is the Hamiltonian of right part which is the Fermi-Pasta-Ulam (FPU) model,

$$\begin{aligned} H_{FPU} &= \sum_i H_i = \sum_i \frac{p_i^2}{2m} + V_{FPU}(x_{i-1}, x_i) \\ &= \sum_{i=N+1}^{2N} \frac{p_i^2}{2m} + k_{FPU}\left[\frac{1}{2}(x_i - x_{i-1} - a)^2 + \frac{\beta}{4}(x_i - x_{i-1} - a)^4\right], \end{aligned} \tag{2.4}$$

where inside EQs. (2.2),(2.3),(2.4),x_i is the position of the ith particle along the chain, m is the uniform mass of each particle, and a is the equilibrium distance among nearest neighbors. So $x_i - x_{i-1} - a$ is the deviation from the equilibrium distance between nearest neighbors; $V(x_i, x_{i-1})$ is the interaction potential of nearest-neighbor particles; $U(x_i)$ is a periodic external potential from the substrate added

to the harmonic oscillators. Each harmonic oscillator is put in the valley of the substrate potential in our simulation.

For convenience of numerical calculations, we use dimensionless unit in the Hamiltonian. We set the mass of particles and the lattice constant $m = a = 1$, the fourth-order interaction constant in the FPU lattice as a typical value $\beta = 1$, interaction constant in the FK lattice as dimensionless one $k_{FK} = 1$ and the effect from the FK substrate as a typical value $A = 5$.

2.2.2 Asymmetric Feature in the System

In order to establish a temperature gradient, we put the two-end particles of the chain into contact with two Nośe-Hoover heat bathes with temperature T_L and T_R for the left and the right end, respectively. We denote the system temperature in the following way

$$T_L = T_0(1 + \Delta), \quad T_R = T_0(1 - \Delta). \tag{2.5}$$

In this way, we can simply record the system temperature as T_0 and the normalized temperature difference between T_L and T_R as 2Δ. Notice that when $\Delta > 0$, the left end is at high temperature and corresponding heat flux is denoted as J_+. Vice versa when $\Delta < 0$, the right end is at high temperature and corresponding heat flux is denoted as J_-. The dynamics of the $2N - 2$ particles between two heat bathes is governed by the equation of motion

$$\ddot{x}_i = -\frac{\partial H}{\partial x_i} = f_i - f_{i+1}, i = 2, ..., 2N - 1, \tag{2.6}$$

where

$$f_i = -V'(x_{i-1}, x_i) - U'(x_i) \tag{2.7}$$

is the force acting on the particle. For the FPU part, $U(x_i) = 0$. The equations of motion of the two particles in Nośe-Hoover bathes are determined by

$$\begin{aligned} \ddot{x}_1 &= -\zeta_L + f_1 - f_2, \\ \ddot{x}_{2N} &= -\zeta_R + f_{2N} - f_{2N+1}, \end{aligned} \tag{2.8}$$

Here, $x_0 = 0$ and $x_{2N+1} = 2N$. In the Nośe-Hoover heat bath, the dynamics of ζ is governed by the equation $\dot{\zeta} = \frac{1}{\mathcal{Q}}(\dot{x}^2/k_BT - 1)$. T is the temperature of the heat bath (T_L orT_R), and $\mathcal{Q}$ is the parameter of coupling between the thermal bath and the system. In this study, we set $\mathcal{Q} = 1$ so that the response time of the thermostats, $\frac{1}{\sqrt{\mathcal{Q}}}$, becomes of the same order as the original time scale of the lattice. Here, we also set k_B as dimensionless one. So the dynamics of ζ_L and ζ_R is governed by

$$\begin{aligned} \dot{\zeta}_L &= \frac{\dot{x}_1^2}{T_L} - 1, \\ \dot{\zeta}_R &= \frac{\dot{x}_{2N}^2}{T_R} - 1. \end{aligned} \tag{2.9}$$

We checked that our result does not depend on the particular heat bath realization. A fixed boundary condition is used along the chain.

In our investigation we try to find suitable k_{int} and k_{FPU} to realize the rectifying effect in the 1D model. We find that when k_{int} is much smaller than k_{FK},k_{FPU}, there is obvious difference between heat fluxes from two directions. This indicates that our model also shows rectifying effect on heat fluxes. If we decrease k_{FPU} from the same value of k_{FK}, the difference of heat fluxes from two directions will increase drastically until it is about 0.2. Since the width of effective phonon band of the FPU model should be proportional to interaction strength, small k_{FPU} indicates small heat energy transferring along the chain in unit time. So continuous decrease of k_{FPU} will induce a big difficulty in numerical calculations since the heat flux is too small in both directions. The most important fact is that continuous decrease of k_{FPU} will not increase the rectifying effect significantly. So in our simulations, we keep $k_{FPU} = 0.2$ which we checked it is the best one when we fix $k_{FK} = 1$, $A = 5$ and $\beta = 1$.

We calculate the physical quantities after a time that is long enough to allow the system to reach a non-equilibrium steady state where the local heat flux is constant along the chain. We then integrate the differential equations of motion by using the seventh- or eight-order Runge-Kutta algorithm which provides very stable and more accurate results than those of the usual forth-order Runge-Kutta method as

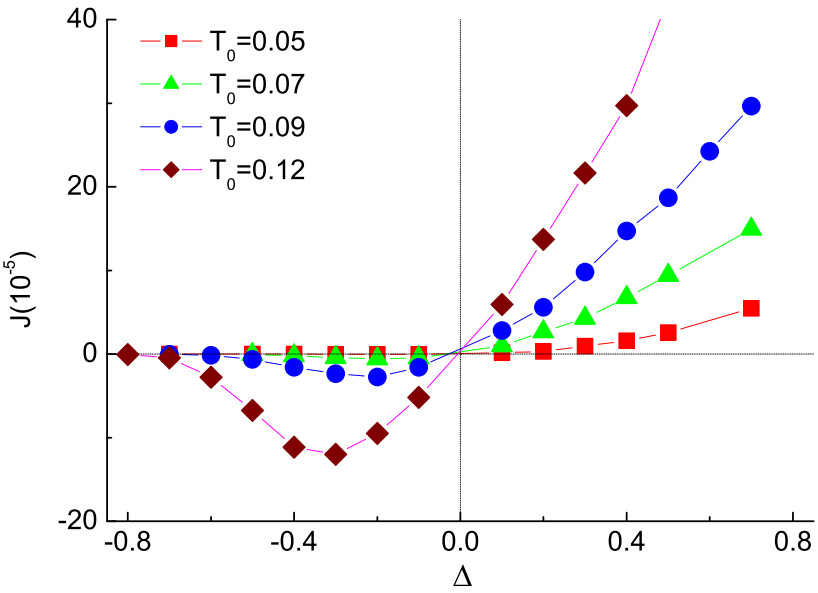

Figure 2.5: (a) Heat current J versus the dimensionless temperature difference δ for different values of temperature $T_0 = 0.05, 0.07, 0.09, 0.12$. Here total number of particles $2N = 100$, $k_{int} = 0.05$, $k_{FPU} = 0.2$. The dotted lines are drawn to guide the eye.

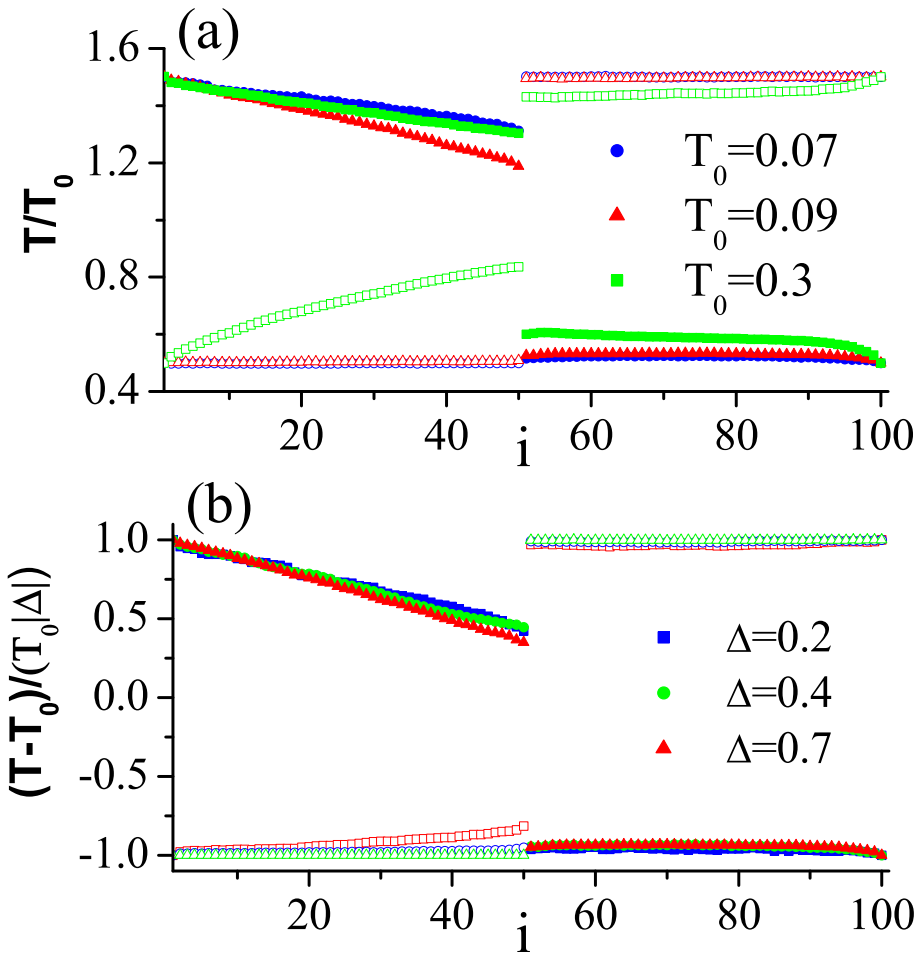

Figure 2.6: (a) T/T_0 versus lattice site for $T_0 = 0.07, 0.09, 0.3$. $|\Delta| = 0.5$. (b) $(T - T_0)/(T_0|\Delta|)$ versus lattice site, for different $|\Delta| = 0.2, 0.4$, and 0.7 with fixed $T_0 = 0.09$. The solid symbols are for the cases of $\Delta > 0$, and the empty symbols are for the cases of $\Delta < 0$. In both (a) and (b), $k_{FPU} = 0.2$ and $N = 50$.

described in Ref. [86]. The local temperature at site i is defined as $T_i = \langle \dot{x_i}^2 \rangle$, where $\langle\ \rangle$ stands for temporal average.

The local heat flux J_i is defined as

$$J_i = \dot{x}_i f(x_{i+1} - x_i) \tag{2.10}$$

same as in the equation(1.18). Then the temporal average heat flux becomes

$$J = \langle J_i \rangle = \langle \dot{x}_x f(x_{i+1} - x_i) \rangle. \tag{2.11}$$

Numerically, the time average $J = \langle J_i \rangle$ is independent of the index i for long enough time.

In Fig. 2.5 we plot the heat current (flux)J versus Δ for different temperature T_0. It is clearly seen that obvious difference exists between J_+ ($\Delta > 0$) and J_- ($\Delta < 0$). When $\Delta > 0$ the heat current increases with Δ monotonously, while in the region $\Delta < 0$ heat current is very small. The results in Fig. 2.5 show that our model has the rectifying effect in a wide range of temperatures. Or we can say the heat fluxes from two directions are asymmetric in the asymmetric system. This asymmetric feature also can be seen from the temperature profile in Fig. 2.6.

In Fig. 2.6(a), we show the normalized temperature profile, T/T_0, along the lattice site for three different temperatures, T_0=0.07, 0.09, and 0.3, with fixed $|\Delta| = 0.5$. Fig. 2.6(b), we draw $(T - T_0)/(T_0|\Delta|)$ versus lattice site for $|\Delta|$=0.2, 0.4, and 0.7 with fixed $T_0 = 0.09$. It is obvious that, in all cases, there exists a temperature jump (discontinuity) at the interface. The jump depends on different factors: (1) temperature T_0, and (2) temperature difference, Δ. The most interesting thing is that, *the temperature jump is asymmetric, namely, it depends on whether* Δ *is negative or positive.*

As we stated previously, the interface elastic constant k_{int} is a very important parameter to realize rectifying effect in our model. We find that we can control heat flow by adjusting this parameter. Obviously, when other parameters of the two segments are fixed, the smaller coupling constant k_{int}, the smaller heat fluxes from both directions through the system. Here we can introduce a quantity $|J_+/J_-|$

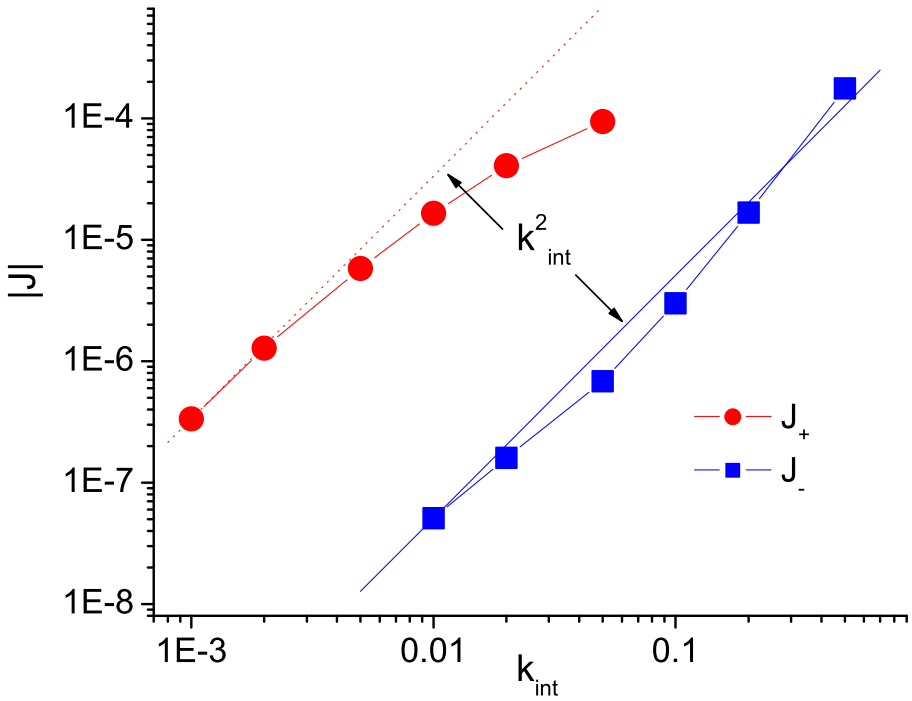

Figure 2.7: Heat current $|J_{\pm}|$ versus the interface elastic constant k_{int} for $2N = 100, T_0 = 0.07, \Delta = 0.5$. Square objects are J_+ and circle objects are J_-.

to measure the performance of rectifying effect of the system. It can be used to describe quantitatively the rectifier efficiency. We found that if we change k_{int} from the same value of k_{FPU}, the ratio $|J_+/J_-|$ will increase with decrease of k_{int} as shown in Fig. (2.7). From the figure, we also can see obvious difference between J_+ and J_-. Both of J_+ and J_- truly increase with increase of k_{int}. More importantly, this figure shows that the rectifying effect is very significant in a wide range of k_{int}. It also can be seen that, for small k_{int}, numerical data show this kind of relationship between heat fluxes and interface elastic constant: $J_{\pm} \propto k_{int}^2$. Therefore the ratio $|J_+/J_-|$ is a constant independent of k_{int} for small k_{int}.

2.3 Kapitza Resistance

In the above section, we introduced our model and our methodology to construct the 1D thermal rectifier. Our numerical results in the section indicate that our model really shows very good rectifying effect on heat fluxes. Or we can say the heat fluxes from two directions are asymmetric. Moreover, we found that the temperature jump (discontinuity) at the interface between two segments is also asymmetric. That is let us think about that the asymmetric properties of the system may be associated with intrinsic properties in the interface. As we found in the previous section, interface elastic constant k_{int} plays important role in the rectifying effect of the model on heat fluxes and big temperature jump is found in the interface. Asymmetric phenomenons we observed may be related with the properties in the interface. And as a common sense, heat current is reciprocal to the thermal resistance of the chain. That let us think about that all this asymmetric feature we observed maybe depend on the intrinsic property of thermal resistance at the interface. So continuous work focus on the investigation of interface thermal resistance(ITR) R.

$$R \equiv \frac{\Delta T}{J}, \tag{2.12}$$

where J is the heat flux density, namely, the heat flow across a unit area in unit time, ΔT is the temperature difference between two sides of the interface.

2.3.1 History of Kapitza Resistance

Thermal resistance between two different materials or between twin or twist boundaries of the same material has been extensively studied both experimentally and theoretically [90–92]. Thermal resistance at the interface was firstly found as early as 1936 between liquid helium and a solid by Kiirti, Rollin, and Simon. But they assumed such a thermal resistance to be small and ignored it. Only a few months later, Keesom and Keesom (1936) recognized that the thermal resistance at the interface was “relatively very considerable,” but they too allowed the idea to pass without further elaboration. In 1941, Kapitza reported his measurements of the

temperature drop near the boundary between helium and a solid when heat flows across the boundary [92]. More than ten years later, Khalatnikov (1952) presented a model, an approximation to what is now known as the acoustic mismatch model [93], to explain that a thermal resistance, the thermal boundary resistance, occurs at boundaries to helium. In the presence of a heat flux across the boundary, this thermal resistance causes a temperature discontinuity at the boundary. This thermal boundary resistance (often called Kapitza resistance) is defined as the ratio of the temperature discontinuity at the interface to the power per unit area flowing across that interface. Continuous efforts have been devoted to the thermal interface(or boundary)resistance at solid-liquid interface and solid-solid interface (see Review article [94], and the reference therein) since then. In 1987, Swartz and Pohl explored the effect of phonon scattering on the thermal boundary resistance and proposed the diffuse mismatch model to explain it [95].

So till now, there are two popular theories trying to explain or predict Kapitza resistance: diffuse mismatch theory [95] and acoustic mismatch theory [96]. The acoustic mismatch theory regards the two media as two elastic continua and phonons are governed by continuum acoustics and the interface is treated as a plane. That is, phonons are treated as plane waves, and materials in which the phonons propagate are treated as continua. In the diffuse mismatch theory the assumption is replaced with the opposite extreme: all the phonons are diffusively scattered at the interface. In the diffuse mismatch model, acoustic correlations at interface are assumed to be completely destroyed by diffuse scattering, so that the only determinants of the transmission probability are densities of phonon states and the principle of detailed balance. For phonons with wavelength much greater than typical interatomic spacings, the continuum approximations in acoustic mismatch model might be expected to be accurate. So the prediction of Kapitza resistance between helium and copper by acoustic mismatch model gave the upper limit of Kapitza resistance between helium and copper, which is usually 2 orders larger than the experimentally observed value; while the prediction of diffuse mismatch model gave the lower limit of Kapitza resistance at helium-copper interface.

However, the two theories are both based on the assumption that both sides of the interface are isotropic and the transmission probability is independent of temperature. That means in both theories nonlinearity are neglected. They close eyes to the possibility of anharmonic interactions. Unfortunately, our model is strong nonlinear and as discussed before nonlinearity of our model plays an important role in the realization of rectifying effect on heat fluxes. When anharmonic interaction is taken into account, superposition theorem fails, thus no analytic theory can be worked out. As we shall show in the following that, if the *anharmonic* interaction is taken into account, more interesting phenomena arise, the problem becomes theoretically more challenging, and of course it is closer to reality because harmonic is just a first order approximation. On the other hand, as the rapid development of nanotechnology, low dimensional nano-scale systems such as nanowires and nanotubes can be easily fabricated in the lab. At the nano-scale, the systems are of finite size, more precisely, they are discrete. Therefore, the continuous theory such as the acoustic mismatch theory will definitely not be suitable for such systems. The interface resistance in such nano systems becomes more and more important and has potential applications in nanoscale heat control and management [83].

2.3.2 Kapitza Resistance Between Two Dissimilar Lattices

In this section, we will show our numerical study on the ITR in the 1D FK-FPU model.

The asymmetric feature of the system is also well captured by ITR which is shown in Fig. 2.8. R_+ denotes the ITR when $\Delta > 0$, and R_- denotes the ITR when $\Delta < 0$. Fig. 2.8(a) shows that, at intermediate temperature, $T_0 \in (0.02, 0.1)$, the ratio, R_-/R_+, changes from about 10 to 1000. Both R_+ and R_- decrease with T_0 until $T_0 \approx 0.2$ and then become approximately constants. The dependence of $R_\pm$ can be explained from the temperature dependence of the phonon spectra, as we shall discuss fully later on. In the inset of Fig. 2.8(a), we show the heat currents $J_\pm$ versus temperature T_0. $J_\pm$ stands for the heat flux for $\Delta > 0$ and $\Delta < 0$,

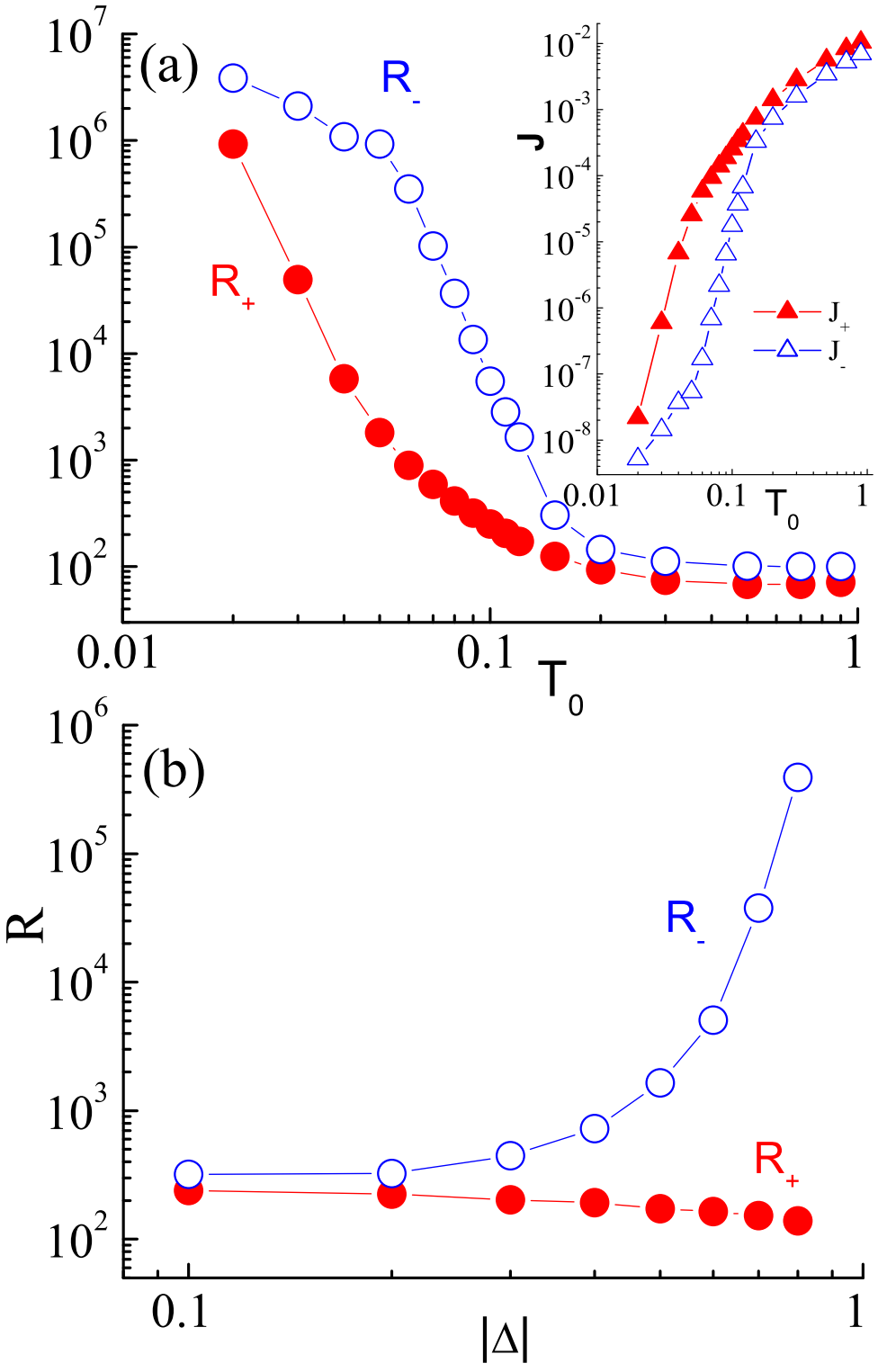

Figure 2.8: (a) $R_{\pm}$ versus T_0. $|\Delta| = 0.5$. Inset is heat current $J_{\pm}$ versus T_0. (b) $R_{\pm}$ versus $|\Delta|$ for $T_0 = 0.12$. In both (a) and (b), $N = 50$.

respectively. As it is clearly seen that the heat currents increase very fast (in several orders of magnitude) as T_0 is increased over two orders of magnitude.

In Fig. 2.8(b), we draw R_+ and R_- versus $|\Delta|$ for $T_0 = 0.12$. It shows that as $|\Delta|$ increases, R_+ does not change too much, it is always in the order of 200, whereas R_- increases more than three orders of magnitude. In the case of $|\Delta| = 0.8$, R_-/R_+ can be larger than 1,000 and $|J_+| \approx 2,000|J_-|$.

An obvious conclusion which can be drawn from above results is that the interface thermal resistance between dissimilar *anharmonic* lattices is *asymmetric*. Since the ITR has a major contribution to the totally thermal resistance along the system, we can say that the thermal rectifying effect observed in our model is mainly determined by the asymmetric ITR.

2.4 Vibrational Bands of Interface Particles

From the above investigation, we know that the asymmetric interface thermal resistance determines the asymmetry of heat current when reversing temperature gradient on the system, but what causes the asymmetrical behavior of the ITR?

To understand the physical mechanism of this asymmetric phenomenon observed in our model, we need to invoke the energy band theory. However, we should point out that an analytic approach seems impossible due to the presence of anharmonicity. We shall rather take a qualitative approach, which can also give us useful information in two extreme cases, namely, low-temperature limit (regime) and high-temperature limit (regime).

(a) FK model. At very low temperature, the particles are confined in the valleys of the on-site potential. Let us consider a linearized version of FK model (2.3), which is obtained by linearizing the substrate potential around $x_i^0 = ia$.

$$\begin{aligned} \mathbb{U}_{FK}(x_i) &= (x_i - ia)\frac{\partial U_{FK}(x_i^0)}{\partial x_i} + \frac{(x_i - ia)^2}{2}\frac{\partial^2 U_{FK}(x_i^0)}{\partial^2 x_i} \\ &= \frac{A(x_i - ia)^2}{2}. \end{aligned} \tag{2.13}$$

Substituting $\mathbb{U}_{FK}(x_i)$ into the motion equation, we have

$$\frac{d^2\delta x_i}{dt^2} = k_{FK}(\delta x_{i+1} + \delta x_{i-1} - 2\delta x_i) - A\delta x_i \tag{2.14}$$

We look for solutions with all displacements having the time dependence $e^{-i\omega t}$. Then the equations of motion become

$$-(\omega_{FK}^L)^2\delta x_i = k_{FK}(\delta x_{i+1} + \delta x_{i-1} - 2\delta x_i) - A\delta x_i. \tag{2.15}$$

This equations are familiar to us. We can get dispersion relation connecting the frequency ω and momentum K:

$$(\omega_{FK}^L)^2 = 2k_{FK} - 2k_{FK}cosKa + A \tag{2.16}$$

So we can find that the phonon band of the FK part is $\sqrt{A} < \omega_{FK}^L < \sqrt{A + 4k_{FK}}$. On the other hand, in the high-temperature limit, the particles have large enough kinetic energies to jump out the valleys of the on-site potential. The on-site potential becomes negligible, the FK model degenerates to an harmonic one, and the phonon band is, $0 < \omega_{FK}^H < 2\sqrt{k_{FK}}$.

(b) FPU model. For the FPU model, there exists a threshold temperature $T_{th}(\approx 0.1)$ [26], below which the FPU model is like a harmonic one, one thus has $0 < \omega_{FPU}^L < 2\sqrt{k_{FPU}}$. At the temperature above the threshold value, in particular, $T_0 >> T_{th}$, the anharmonic term is dominant. In this regime, a rough theoretical estimate yields $0 < \omega_{FPU}^H < C_0(Tk_{FPU}\beta)^{1/4}$ with $C_0 = 2\sqrt{2\pi}\Gamma(3/4)3^{1/4}/\Gamma(1/4) \approx 2.23$, where Γ is the Gamma function.

The above analysis gives energy bands of the two model in high- and low-temperature limits. At arbitrary temperature, an effective way to get the vibrational spectrum of the lattice is the discrete faster Fourier transform (DFFT) for the lattice velocity or displacement [97].

The spectra of the interface particles obtained by DFFT are shown in Fig. 2.9(a) and (b) for $\Delta > 0$ and $\Delta < 0$, respectively, and compared with the above analytical analysis (the shadow regions). In the first case, when $T_L = 0.15$ and $T_R = 0.01$, we can approximately regard the FK lattice as at high temperature limit, and the

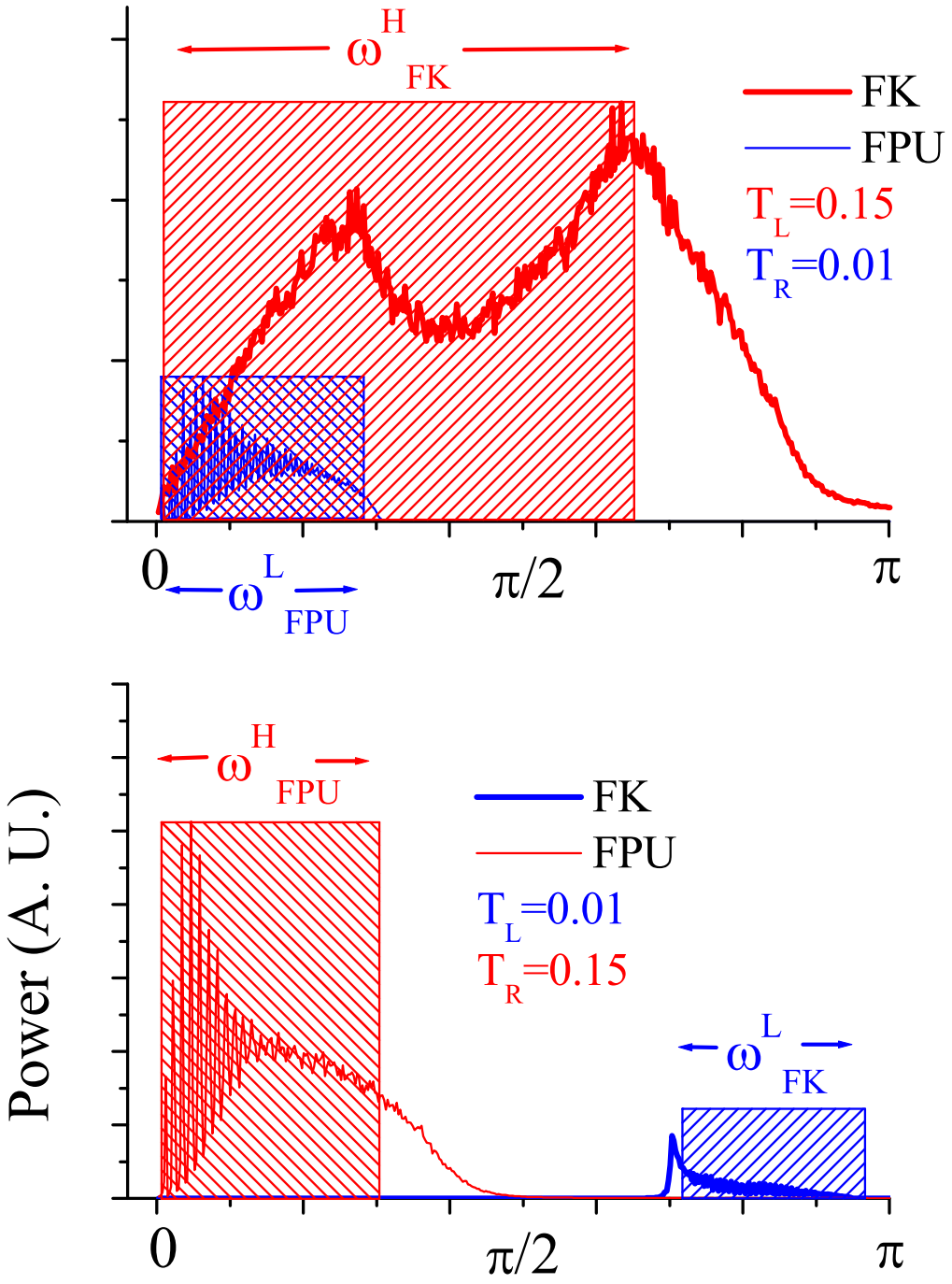

Figure 2.9: Phonon spectra of the two particles at interface and schematic phonon bands for the FK and the FPU models in two extremes. (a) $T_L = 0.15$ and $T_R = 0.01$. (b) $T_L = 0.01$ and $T_R = 0.15$. The hatched regions are the analytical estimates for the FK and FPU models. (see text for more explanation.)

FPU lattice at low temperature regime. With $k_{FK} = 1$ and $k_{FPU} = 0.2$, we have, $\omega_{FK}^{H} \in [0, 2]$, and $\omega_{FPU}^{L} \in [0, 0.89]$, which are quite close to the numerical ones.

On the other hand, when the temperatures of the two thermal baths are swapped, approximately, the FK lattice is at low temperature limit, and the FPU is at high temperature regime. In this case, according to above analysis, the effective phonon band of the FK model is $\omega_{FK}^{L} \in [2.24, 3.00]$ for $V = 5$ and $k_{FK} = 1$, and $\omega_{FPU}^{H} \in [0, 0.94]$ with $T \approx 0.15$ and $\beta = 1$ for the FPU model. They are also very close to the numerical results shown in Fig. 2.9(b).

We admit that there are some discrepancies between our analytical results and numerical ones. The main reason is that our analytical results are asymptotic ones for high and low temperature limits, while in real numerical case, temperatures used are still not in that regimes.

It is clear from Fig. 2.9 that, in the case of $T_L > T_R$, the effective phonon band of the FK lattice overlaps that one of the FPU lattice, therefore, heat can easily flow from the FK lattice to the FPU lattice as is demonstrated in Fig. 2.8 by small R_+ and large J_+. Conversely, when $T_L < T_R$, by appropriately chosen parameters, a large gap between the effective phonon bands of the FK lattice and the FPU lattice can be formed (see Fig. 2.9(b)), which inhibits heat flow from the FPU lattice to the FK lattice as is manifested by a large R_- and small J_- in Fig. 2.8. However, as T_0 increases, the gap becomes narrower and narrower, and eventually disappears when T_0 surpass a certain value. Indeed, when T_0 is large enough the two phonon bands overlap, which leads to a constant R_- as is seen in Fig. 2.8(a).

In order to quantify above asymmetric ITR, heat currents, and find the relationships with the overlap of the phonon bands of the two lattices, we introduce,

$$S_{\pm} = \frac{\int_0^\infty P_l(\omega) P_r(\omega) d\omega}{\int_0^\infty P_l(\omega) d\omega \int_0^\infty P_r(\omega) d\omega}. \tag{2.17}$$

$S_{\pm}$ correspond to the overlap for $\Delta > 0$ and $\Delta < 0$, respectively. $P_l(\omega)$ and $P_r(\omega)$ are the power spectra or density of state for the left and right part, respectively. Note that $\int_0^\infty P_{l,r} d\omega = T_{l,r}$, where $T_{l,r}$ is the temperature of the particle at left/right side of interface. In Fig. 2.10 we plot R_-/R_+ versus S_+/S_- and in the inset we show

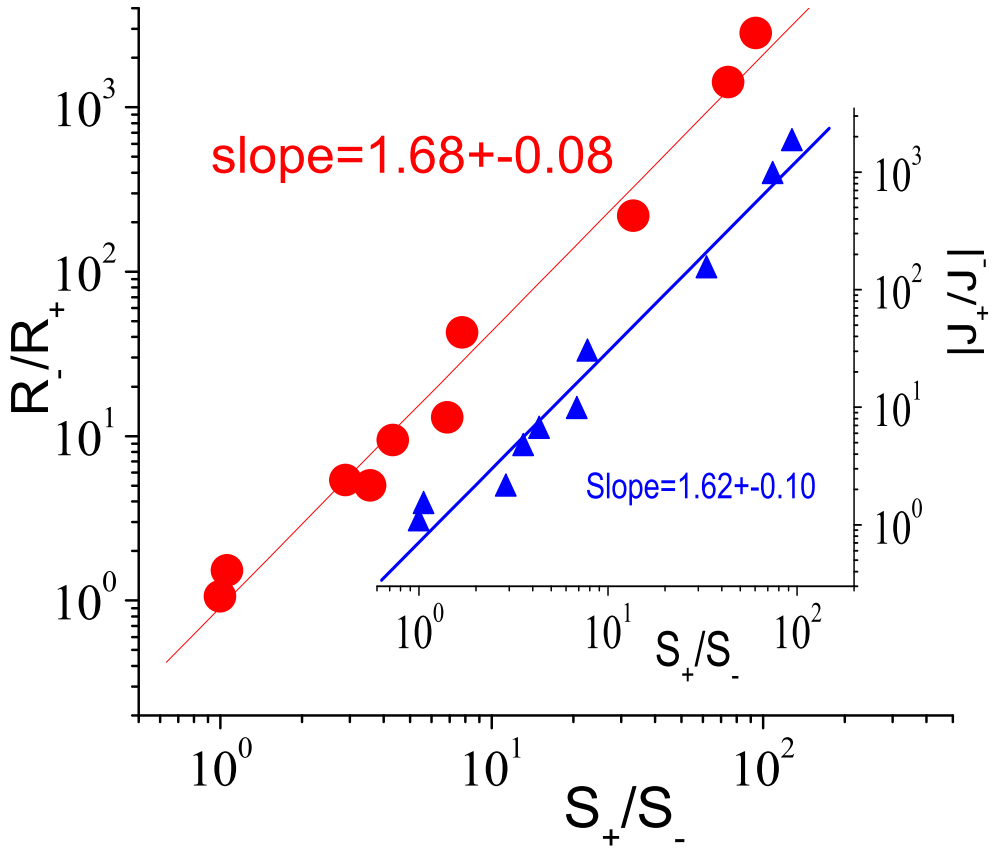

Figure 2.10: R_-/R_+ versus S_+/S_-. Inset: $|J_+/J_-|$ versus S_+/S_-.

$|J_+/J_-|$ versus S_+/S_-. Best fit gives $R_-/R_+ \sim (S_+/S_-)^{\delta_R}$ with $\delta_R = 1.68 \pm 0.08$, and $|J_+/J_-| \sim (S_+/S_-)^{\delta_J}$, with $\delta_J = 1.62 \pm 0.10$. This picture indeed illustrates that the ITR and heat current correlate strongly with the overlap of the phonon spectra of the two interface particles.

As the system contains many adjustable parameters, it is worth investigating the dependence of the ITR on these parameters. Fig. 2.11(a) is $R_\pm$ versus k_{int}. It is seen that both $R_\pm$ decreases with increasing k_{int}, namely, the strong coupling favorites the heat transport. Fig. 2.11(b) shows $R_\pm$ versus k_{FPU}, and Fig. 2.11(c) illustrates the finite size effect. The results given in Figs. 2.11(b) and (c) show that $R_\pm$ are insensitive to both k_{FPU} and the system size. The latter one might be useful for application of insulating heat flow.

As we pointed out in the Sec. 2.2.2, k_{int} should be much smaller than k_{FK} and k_{FPU} for significant rectification. Actually, we also find that the rectification will reverse ($J_+ < -J_-$)when k_int become large enough. We didn't report this finding here because the reversed rectification is very small (about 2 or 3). However, Hu's group studied the reversed thermal rectification systematically [64]. They found that the rectification will reverse when k_{int} over some values. This is because when k_{int} increases, the temperature jump in the interface will decrease. So the effective phonon bands of the particles beside the interface will change and corresponding overlap extent S_+/S_- of the bands from the two parts will also change. They also found the rectification will reverse beyond some temperature. No matter how rectification changes with k_{int} or T, you will find that $|J_+/J_-|$ always change with S_+/S_- monotonously. That means $S_+ < S_-$ when $|J_+| < |J_-|$.

In summary, we have built up an efficient thermal rectifier by coupling two dissimilar anharmonic lattices and studied the interface thermal resistance of them. The rectifying efficiency is increase to 2000, which is 1 or 3 orders larger than previous work [60, 61]. In addition, we found that the rectifying effect (asymmetric heat flow) is closely related to asymmetric interface thermal resistance (also called Kapitza resistance). Moreover, a specific relationship between the factor of heat fluxes and the overlap of the phonon spectra is demonstrated numerically. The

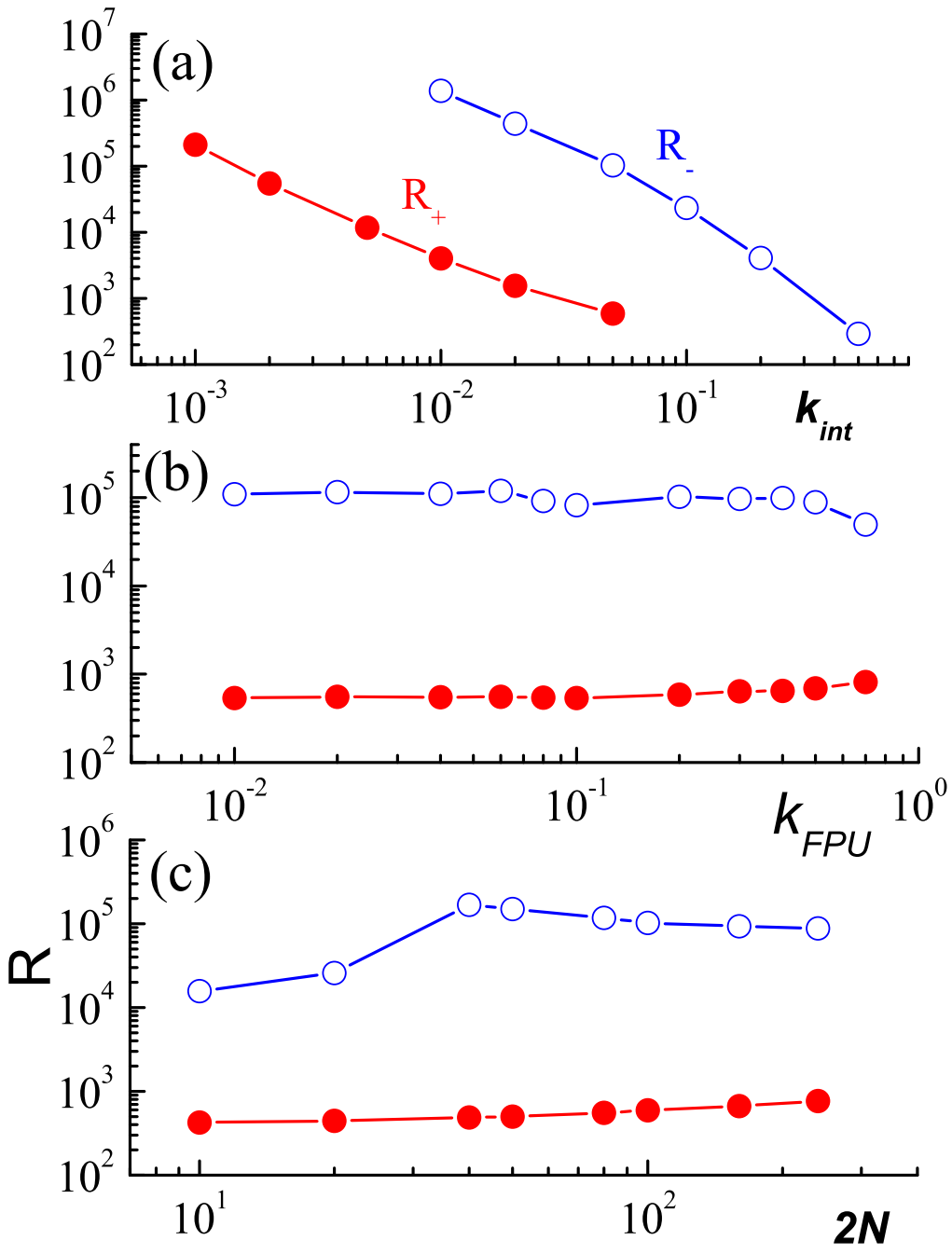

Figure 2.11: (a) $R_{\pm}$ versus the coupling constant k_{int}. (b) $R_{\pm}$ versus k_{FPU}. (c)$R_{\pm}$ versus the system size, N. For all three cases, $T_0 = 0.07$ and $|\Delta| = 0.5$. $N = 50$ for (a) and (b). $k_{int} = 0.05$ for (b) and (c).

achievement in this Chapter might be useful in heat control and management [83]. In particular, the very high ITR might find applications in building thermal insulator.

Chapter 3

Thermal Rectifying Effect in Two-dimensional Anharmonic Lattices

3.1 Introduction

In the previous Chapter, we realized thermal rectifying effect in two dissimilar lattices by tuning the anharmonicities of different parts. The thermal rectifying efficiency was increased from 100 to 2000 by connecting a FK and a FPU lattice. In addition, we find that the rectifying effect, asymmetric heat flow, is closely related to asymmetric interface thermal resistance, also called Kapitza resistance. Moreover, a specific relationship between the rectification of heat current and the overlap extent of the effective phonon spectra is demonstrated numerically.

The previous works [60–64] demonstrate the possibility to control heat current by changing structures of lattices. In fact, controlling heat current is not only a problem of scientific curiosity but also a practical application problem. It might have potential application in energy saving materials. However, almost all works so far are focused on 1D systems with finite sizes. Obviously, much progress has been achieved, but the final purpose is to put these ideas to applications. It is thus a natural step forward to seek effective thermal devices to control heat current in higher dimensions. The open questions are whether the heat control mechanism in 1D is still valid for the high dimension(s) and whether the extra dimension(s)

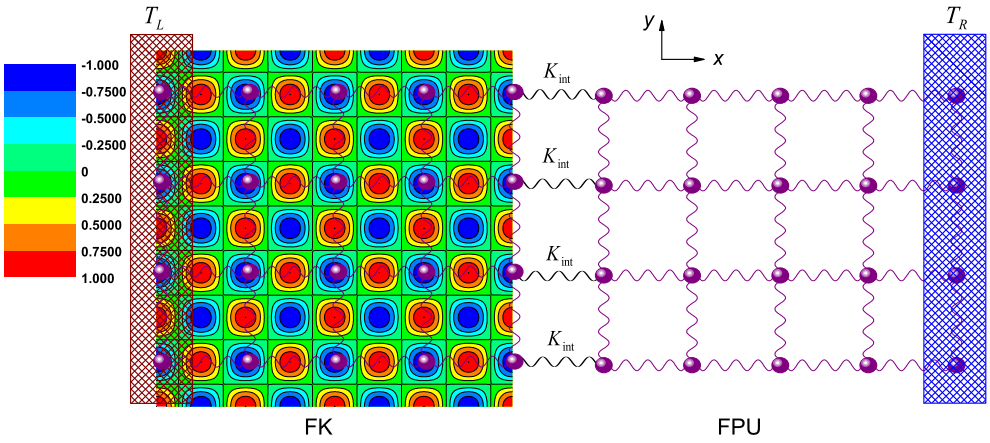

Figure 3.1: Configuration of a two dimensional (2D) thermal rectifier from the Frenkel Kotoroval and the Fermi-Pasta-Ulam lattices. The left part is a 2D FK lattice and the right one is a 2D Fermi-Pasta-Ulam lattice. The two parts are connected by harmonic springs with constant K_{int}. The left and the right ends are put into contact with heat baths of temperature T_L and T_R, respectively.

reduces the rectifying efficiency? The answer might not be trivial, as in higher dimension the lattice vibration includes not only the longitudinal one but also the transverse ones. The modes in longitudinal direction can couple to the transverse directions [45], which may affect the rectifying efficiency.

In this Chapter, we concentrate our study on a 2D rectifier which consists of 2D FK and 2D FPU lattices. We will demonstrate with numerical evidence that a 2D rectifier can be built up and it works in a very wide temperature range. The 2D thermal rectifier shows similar behaviors with the 1D thermal rectifier under similar parameters regimes. The investigation is mainly focused on the dependence of the thermal rectifying efficiency on the temperature and the temperature gradient.

3.2 Model and Methodology

In our previous work [62] we constructed a 1D thermal diode model, 1D-FK-FPU by connecting a FK lattice to a FPU lattice with a weak harmonic spring. This model

displays a very good rectifying effect. Here, we extend the 1D-FK-FPU thermal rectifier model to a 2D one denoted a 2D-FK-FPU model. The configuration of the 2D-FK-FPU model is illustrated in Fig. 3.1. The left part is a plane of harmonic oscillators on a substrate whose interaction is represented by a 2D sinusoidal on-site potential like in the 1D case. Here we plot the contour line of the 2D sinusoidal potential. For simplicity, we put one particle in each valley. The right part is an array of anharmonic oscillators represented by the 2D FPU model. The two parts are connected by weak harmonic springs in the X direction. The Hamiltonian of the system can be written as

$$H = H_{FK} + H_{FPU} + H_{int}, \tag{3.1}$$

where H_{FK}, H_{FPU}, and H_{int} are the Hamiltonian of the left part, the right part, and the interface section, respectively. They are represented in Eqs. (3.2)-(3.4), respectively.

$$\begin{aligned} H_{FK} = \textstyle\sum_{i=1}^{N_{FK}} \sum_{j=1}^{N_Y} (\frac{\vec{p}_{i,j}^2}{2} + k_{FK} V_H(|\vec{r}_{i,j;i-1,j}| - l_0) \\ + k_{FK} V_H((|\vec{r}_{i,j;i,j-1}| - l_0)) + U_{FK}(x_{i,j}, y_{i,j})), \end{aligned} \tag{3.2}$$

$$\begin{aligned} H_{FPU} = \textstyle\sum_{i=N_{FK}+1}^{N_X} \sum_{j=1}^{N_Y} (\frac{\vec{p}_{i,j}^2}{2} \\ + k_{FPU} V_{FPU}(|\vec{r}_{i+1,j;i,j}| - l_0) \\ + k_{FPU} V_{FPU}(|\vec{r}_{i,j;i,j-1}| - l_0)), \end{aligned} \tag{3.3}$$

$$H_{int} = \sum_{j=1}^{N_Y} k_{int} V_H(|\vec{r}_{N_{FK},j;N_{FK}+1,j}| - l_0), \tag{3.4}$$

where $\vec{r}_{i,j;k,l} = \vec{q}_{i,j} - \vec{q}_{k,l}$ is the relative displacement between particles, labeled as (i, j) and (k, l).

$$\begin{aligned} V_H(x) &= \frac{1}{2}x^2, \\ V_{FPU}(x) &= \frac{1}{2}x^2 + \frac{1}{4}x^4, \\ U_{FK}(x, y) &= -\frac{A}{(2\pi)^2} \cos(\frac{2\pi}{l_0}x) \cos(\frac{2\pi}{l_0}y). \end{aligned} \tag{3.5}$$

As in the 1D-FK-FPU model, the mass of the particles is uniformly 1. l_0 is the distance between nearest lattices in equilibrium. The particle at the ith column and the jth row is labeled as (i, j). The coordinates and momenta of this particle are $\vec{q}_{i,j} = (x_{i,j}, y_{i,j})$ and $\vec{p}_{i,j} = (p_{x_{i,j}}, p_{y_{i,j}})$. In order to establish a temperature gradient, the two ends of the planes are put into contact with two Nośe-Hoover heat baths [79] with temperature T_L and T_R for the left end and the right end, respectively. Particles for $i = 1, j = 1, 2, 3, ..., N_Y$ is coupled with heat bath with temperature T_L and particles for $i = N_X, j = 1, 2, 3, ..., N_Y$ are coupled with heat bath with temperature T_R. We checked in the 1D case that the result does not depend on the particular heat bath realization. A fixed boundary condition is used along temperature gradient direction, denoted as the X direction, namely, $\vec{q}_{0,j} = (0, j)$ and $\vec{q}_{N_x+1,j} = (N_x + 1, j)$. A periodic boundary condition is applied in the Y direction, namely $\vec{q}_{i,1} = \vec{q}_{i,N_Y+1}$. (see Fig. 3.1.) Under these boundary conditions, the system can be considered as a tube or a thin film expanded infinitely in the X direction. The total number of particles is $N_X \times N_Y$. All results given in this paper are obtained by averaging over $N_k \times 10^8 (N_k > 2)$ steps after a sufficient long transient time when a nonequilibrium stationary state is set up. The equations of motion of the particles are

$$\dot{\vec{q}}_{i,j} = \vec{p}_{i,j},$$

$$\dot{\vec{p}}_{i,j} = \begin{cases} -\frac{\partial H}{\partial \vec{q}_{i,j}} (i = 2, N_X - 1), \\ -\frac{\partial H}{\partial \vec{q}_{i,j}} - \xi_{i,j} \vec{p}_{i,j} (i = 1, N_X), \end{cases} \tag{3.6}$$

and the auxiliary variables $\xi_{i,j}$ are described by the equation

$$\dot{\xi}_{i,j} = \frac{1}{\mathcal{Q}} (\frac{\vec{p}^2_{i,j}}{2k_B T} - 1), \tag{3.7}$$

here, T is the temperature of the heat bath (T_L orT_R), and $\mathcal{Q}$ is the parameter of coupling between the thermal bath and the system. As in 1D case, we set $\mathcal{Q} = 1$. Our purpose is to study rectification of the 2D model and the dependence of the rectification on the system temperature and the temperature gradient, so we do not attempt to search the optimum setting of parameters. We choose the system

parameters the same as in 1D-FK-FPU model which has been tested as a good one in the 1D case, that is $k_{FK} = 1$, $A = 5$, $l_0 = 1$, $k_{FPU} = 0.2$, and $k_{int} = 0.05$. We set

$$\begin{aligned} T_L &= T_0(1+\Delta) \\ T_R &= T_0(1-\Delta) \end{aligned} \tag{3.8}$$

where $-0.8 \leq \Delta \leq 0.8$ in our simulations. So we can simply denote T_0 as the temperature added on the system and $2\Delta = (T_R - T_L)/T_0$ as the normalized temperature difference of the system.

The local temperature is defined as

$$T_{i,j} = m\langle \vec{v}_{i,j}^2 \rangle, \tag{3.9}$$

where $\langle \dots \rangle$ stands for a temporal average. The local heat flux $J_{i,j}$ is defined as the energy transfer per unit time from the particle labeled as (i, j) to the nearest particle $(i+1, j)$ along the X direction.

$$\begin{aligned} J_{i,j} &= -\vec{v}_{i+1,j} \cdot \vec{F}_{i+1,j;i,j} \\ &= -k\vec{v}_{i+1,j} \cdot \frac{\partial V(|\vec{r}_{i+1,j;i,j}| - l_0)}{\partial |\vec{q}_{i,j}|} \cdot \frac{\vec{q}_{i,j}}{|\vec{q}_{i,j}|}, \end{aligned} \tag{3.10}$$

where $k = k_{FK}, k_{FPU}$, or k_{int}, depending on the site along the X direction. For a 2D lattice, we treat only fluxes which flow along the X direction. Then we can denote the flux from the particles in the ith section to the next section in the X direction simply as J_i ($J_i = \sum_{j=1}^{N_Y} J_{i,j}$). The total current of the system is averaged over all sections,

$$J = \frac{1}{N_X} \langle \sum_{i=1}^{N_X} J_i \rangle. \tag{3.11}$$

In our simulations, the fluctuations of temporal heat fluxes through each section are all less than 5%. We use $|J_+/J_-|$ as a *rectifying efficiency* to describe quantitatively the rectifying performance of the system. J_+ is the heat current when Δ is positive (heat flows from the FK plane to the FPU plane) and J_- is the heat current when Δ is negative (heat flows from the FPU part to the FK part).

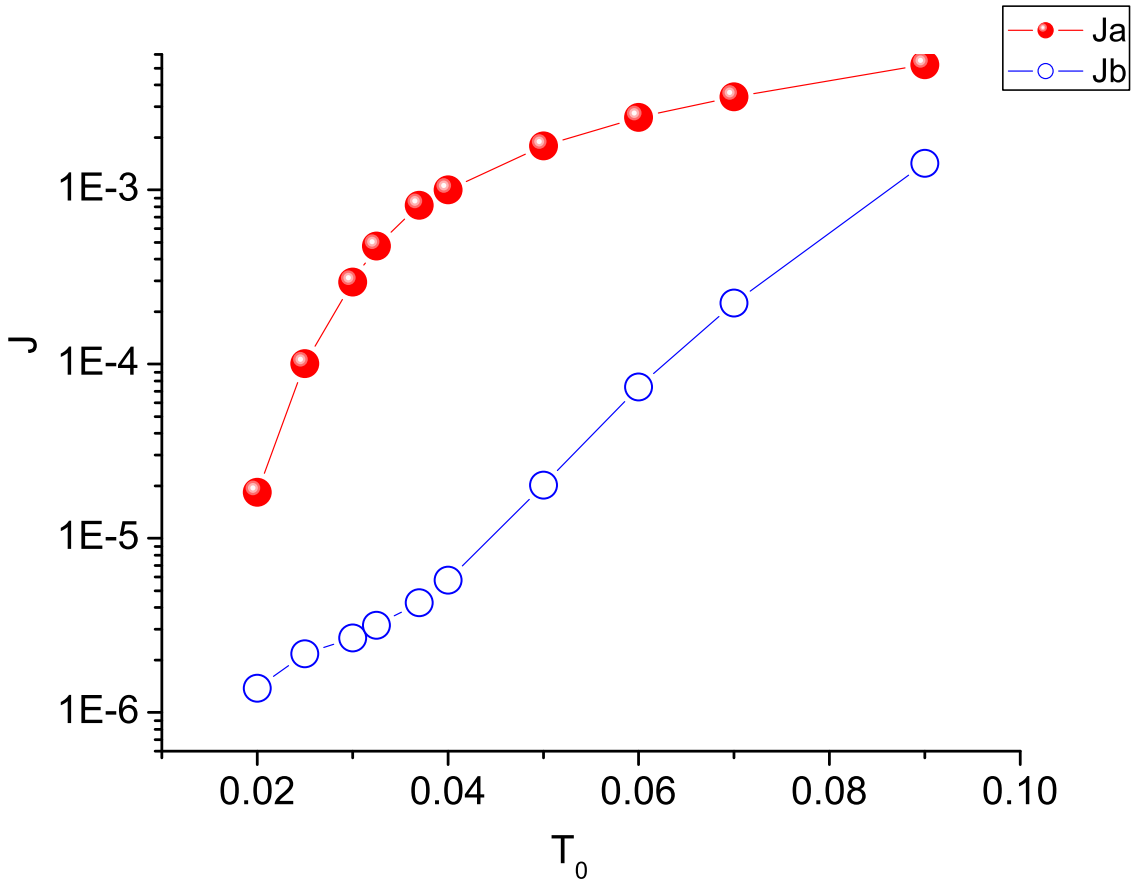

Figure 3.2: Heat current of the system with $N_Y = 4$ and $N_X = 10$ versus T_0. $|\Delta|$=0.5

The model we used is a simple extension from one dimension to two dimension, however the results in Fig. 3.2 show that it truly demonstrates good rectifying effect on heat fluxes. In Fig. 3.2, we can see the visible difference between J_+ and J_- in a very wide temperature range. The difference varies from a few times to several hundreds times.

3.3 Dependence of Rectifying Effect on Temperature and Temperature Difference

In this section, we study the dependence of the system performance on the environment temperature changes. Figure 3.3 shows the rectifying efficiency $|J_+/J_-|$ versus T_0. In Fig. 3.3(a), we can see that there exists an optimum performance (OP) of the rectifying effect when changing temperature T_0. We can define the temperature for the optimum performance as T_{OP}. In Fig. 3.3(b)-(d) we show the dependence of the ratio $|J_+/J_-|$ on temperature under different boundary conditions. We found that T_{OP} depends on the system settings along the Y direction. In Fig. 3.3(b), the number of particles along the Y direction varies from 4 to 8 and 16 while other settings are kept unchanged. We can see clearly that T_{OP} shifts to lower temperature when increasing N_Y. The value of T_{OP} is 0.04, 0.037, and 0.0325 for $N_Y = 4$, 8 and 16 respectively. T_{OP} keeps the same value when we change N_X. This is shown in Fig. 3.3(c). In Fig. 3.3(d), we change the periodic boundary condition in the Y direction to a free boundary condition. Under this condition, the system can be taken as a thin slice. T_{OP} and the optimum performance change drastically under this change. T_{OP} changes from 0.037 to 0.025 and the ratio increases almost 100%.

Quantity W_T in the figures is a variable defined as the width of the effective temperature range T_e over the half value of OP, while $\vartheta = W_T/T_{OP}$ is defined as the *quality factor*. T_e, W_T, and $\vartheta = W_T/T_{OP}$ are useful variables to estimate the temperature range in which the system has a good rectifying effect. In our investigation, T_e broadens from the center regime [0.03-0.46] to high-temperature regime or low-temperature regime. The typical value of W_T under different settings

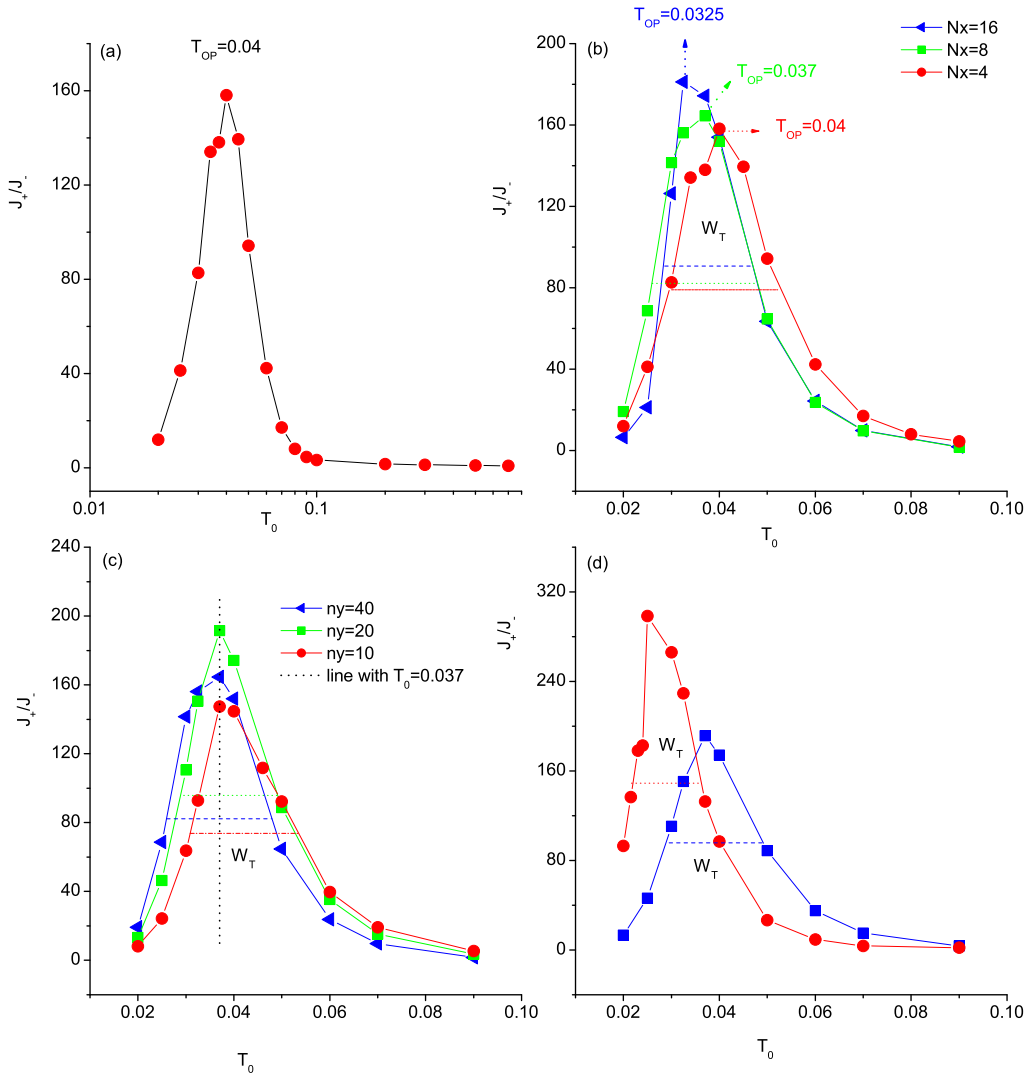

Figure 3.3: The rectifying efficiency, $|J_+/J_-|$, versus T_0 at different conditions. (a) The system with $N_Y = 4$, $N_X = 10$, and $|\Delta|$=0.5. $T_{OP} = 0.04$. (b) Comparison at three different N_Y with $N_X = 40$. $T_{OP} = 0.04$, $W_T = 0.022$, and $\vartheta = 0.55$ for the case of $N_y = 4$. When $N_Y = 8$, $T_{OP} = 0.037$, $W_T = 0.022$, and $\vartheta = 0.59$. When $N_Y = 16$, $T_{OP} = 0.0325$, $W_T = 0.018$, and $\vartheta = 0.55$.(c) Comparison at three different N_X with $N_Y = 8$. They have the same $T_{OP} = 0.037$. When $N_X = 10$, $W_T = 0.023$ and $\vartheta = 0.62$. When $N_X = 20$, $W_T = 0.020$ and $\vartheta = 0.54$. When $N_X = 40$, $W_T = 0.022$ and $\vartheta = 0.59$. (d) Comparison at different boundary conditions along the Y direction with $N_Y = 8$ and $N_X = 20$. Free boundary: The optimum performance (OP)= 298.5, $T_{OP} = 0.025$, $W_T = 0.014$, and $\vartheta = 0.56$; period boundary: OP= 191.5, $T_{OP} = 0.037$, $W_T = 0.022$, and $\vartheta = 0.59$.

is around 0.018-0.023. ϑ is always larger than 0.5. The results suggest that the system is effective in a very wide temperature range.

In Fig. 3.4, we show the heat current versus the (normalized) temperature difference, Δ, for three different T_0. Full symbols represent J_+ and empty ones $|J_-|$. We can see that J_+ increases with Δ monotonically and it is always larger than $|J_-|$, while J_- changes with Δ in different ways. One can find that there are three regions for $|J_-|$. In the first region, $|\Delta| < 0.1$, the increase of Δ leads to the increase of the heat current. However, in the second region, $0.1 < |\Delta| < 0.6$, the increase of $|\Delta|$ does not induce the increase of $|J_-|$, instead it results in a decrease of $|J_-|$. In the third region, $\Delta > 0.6$, $|J_-|$ is almost a constant independent of $|\Delta|$. In this region, the $|J_-|$ is so small that the system can be approximately considered as an insulator. The ratio $|J_+/J_-|$ becomes larger and larger when $|\Delta|$ increases. That indicates that rectifying effect increases with increasing temperature difference.

The strange behavior of $|J_-|$ observed in the second region, namely, the larger the temperature difference the smaller the heat current, is called *negative differential thermal resistance*. We will demonstrate later that this is a typical phenomenon in nonlinear lattices. It can be understood from the match and mismatch of the vibrational spectra of the interface particles.

Figure 3.5 shows $|J_+/J_-|$ versus $|\Delta|$. It is found that $|J_+/J_-|$ increases with $|\Delta|$ in an exponential way in the regime in which $|\Delta|$ is smaller than Δ_2. Approximately,

$$|J_+/J_-| \propto \exp(c|\Delta|) + \delta, \tag{3.12}$$

here c is about 9.5 under the particular parameter setting $N_Y = 8$ and $N_X = 20$ with a periodic boundary condition along the Y direction. When we change N_Y, N_X, or the boundary condition along the Y direction, c changes slightly, but it is always around 10. The variation of $|c - 10|$ is smaller than 0.5 in our investigation. δ is related with T_0 and Δ.

As in the 1D-FK-FPU model, there is also a very big temperature jump at the interfact which is dependent on temperature, temperature gradient, and the direction of the imposed temperature gradient. This is shown in Fig. 3.6.

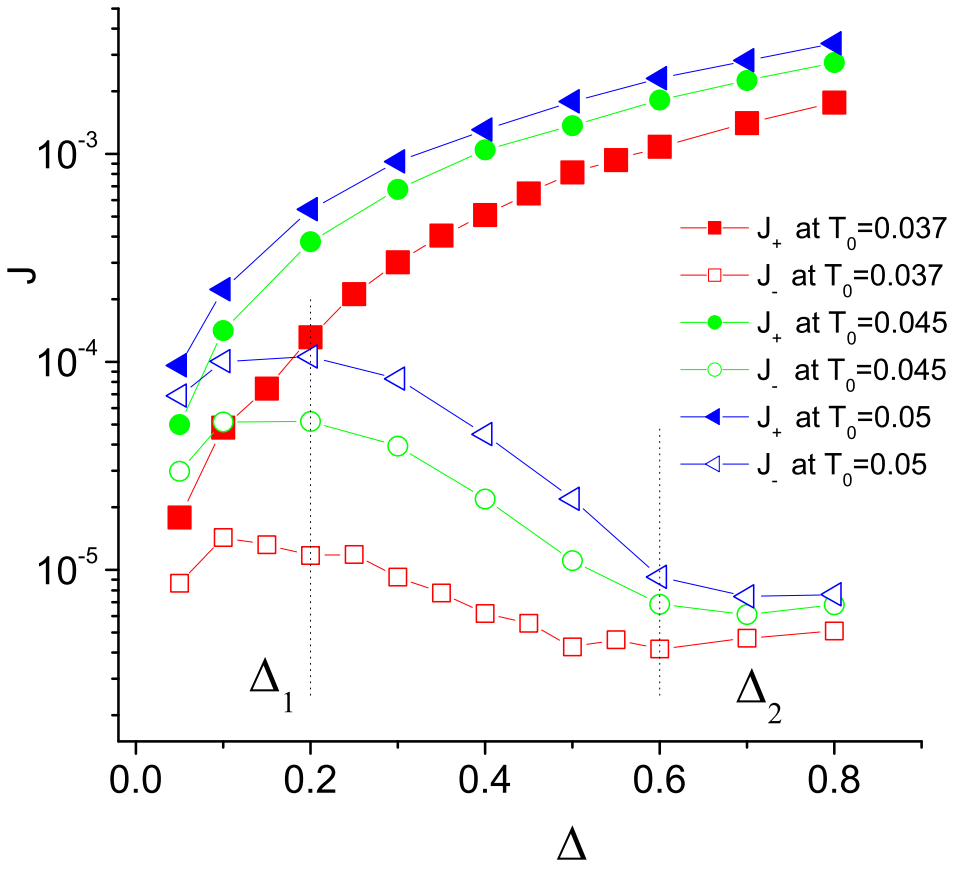

Figure 3.4: Heat fluxes of the system with $N_Y = 8, N_X = 20$ versus temperature difference at three different T_0. Note that $|J_-|$ decreases as $|\Delta|$ increases in the interval $0.2 < |\Delta| < 0.6$, this is the so-called "*negative differential thermal resistance*", see context for more explanation.

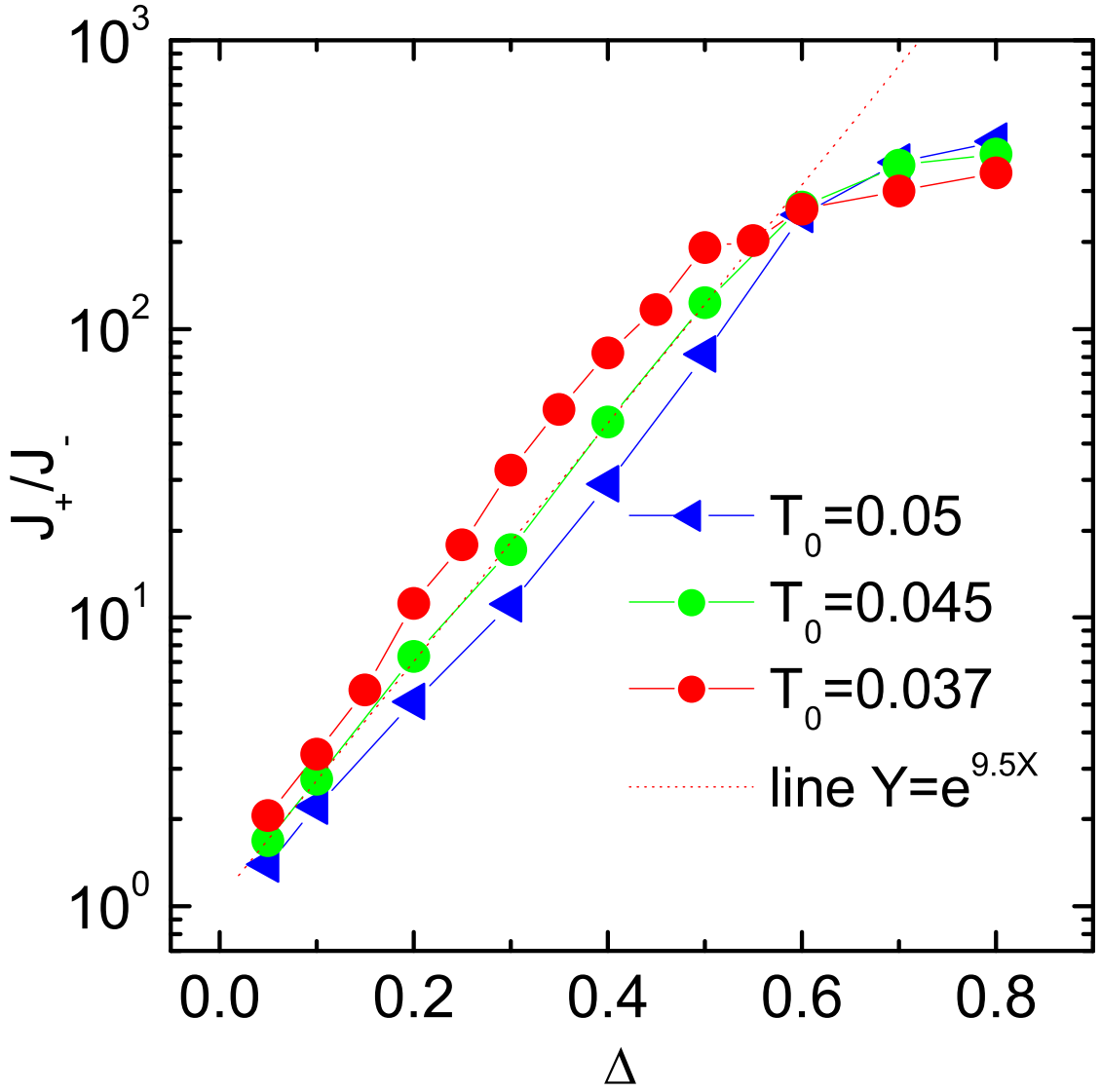

Figure 3.5: The ratio of heat current, $|J_+/J_-|$ versus half normalized temperature difference $|\Delta|$ at temperature $T_0 = 0.037, 0.045, and 0.05$. The dotted line has a slope of 9.5.

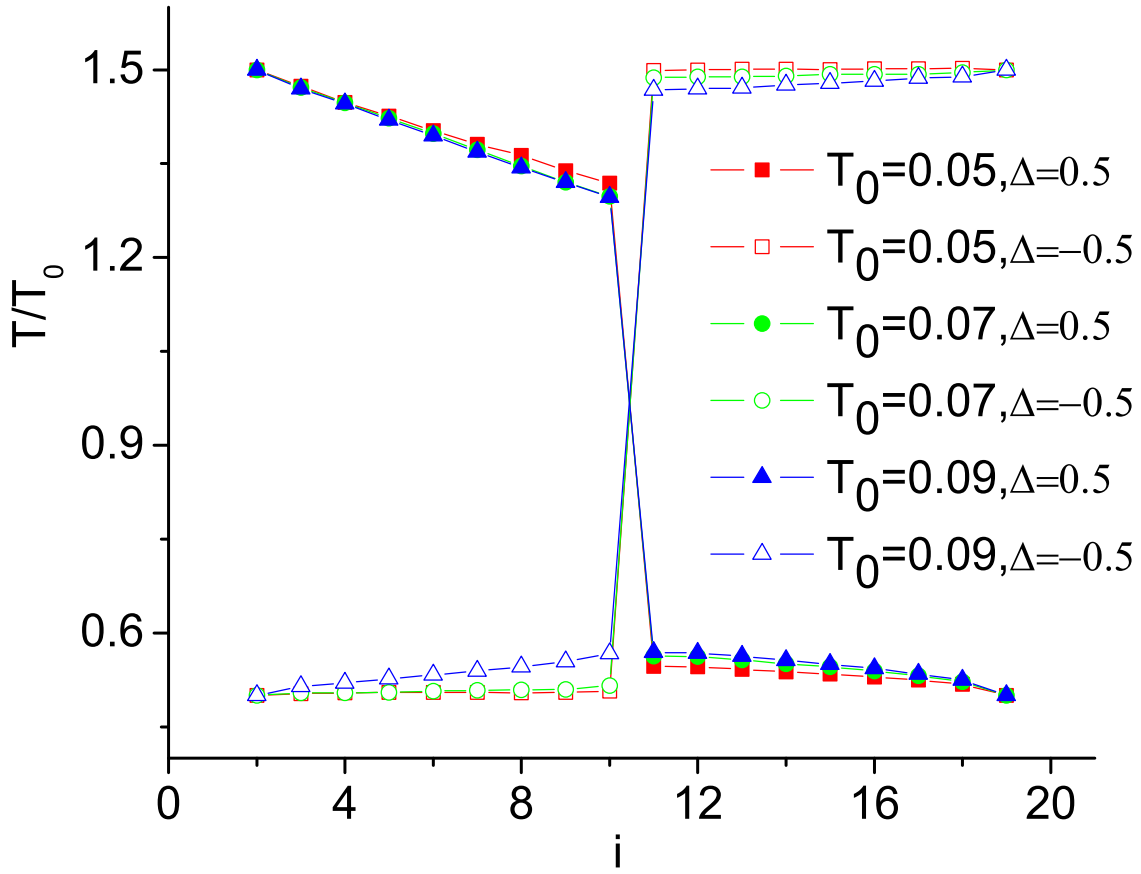

Figure 3.6: T/T_0 versus lattice site for T_0=0.05, 0.07, and 0.09. The solid symbols are for the cases of $\Delta = 0.5$ and the empty symbols are for the cases of $\Delta = -0.5$. $N_Y = 8, N_X = 20$.

3.4 Interface Thermal Resistance (ITR) - Kapitza resistance

As shown in the previous section, the temperature drops and heat fluxes are both asymmetric when the temperature gradient of the system is reversed. Here we also capture a product of ΔT and J, thermal resistance R, as in the 1D case. As in the 1D case, thermal resistance in the 2D-FK-FPU model concentrates in the interface. So here we also study ITR for the 2D thermal rectifier to see whether it answers for the asymmetric temperature jump and heat flux or not. R_+ and R_- denote the ITR for the case of $\Delta > 0$ and $\Delta < 0$, respectively.

In Figs. 3.7 and 3.8, we show the dependence of ITR on temperature T_0 and the normalized temperature difference Δ. From the two figures we can see that, generally, R_- (with larger temperature drop) is about two or three orders of magnitude larger than R_+ (with smaller temperature jump). Both R_+ and R_- decrease with T_0 until $T_0 \approx 0.2$, then both become approximately constants. In Fig. 3.7(b), we show the ratio R_-/R_+ versus temperature T_0. It is clearly seen that there exists an optimal temperature value for the ratio R_-/R_+. In Fig. 3.8, we show the resistance versus temperature difference. We can see that R_- monotonically increases with temperature difference until it reaches a maximum value, while R_+ monotonically decreases with increasing Δ. If we plot the ratio of R_- over R_+ versus temperature difference, we find that the relationship between them also obeys the exponential law like the ratio of heat current.

Comparing Figs. 3.7 and 3.8 with Figs. 3.3 and 3.5, we can find that the behaviors of the IRT and heat current through the system are very similar, both are asymmetric and both the ratio R_-/R_+ and J_+/J_- have an optimum value under different temperature and obey exponential law when changing temperature difference. The asymmetry of thermal resistance when reversing temperature gradient is the determinant factor for the rectifying effect on heat current of the system from the the definition of ITR.

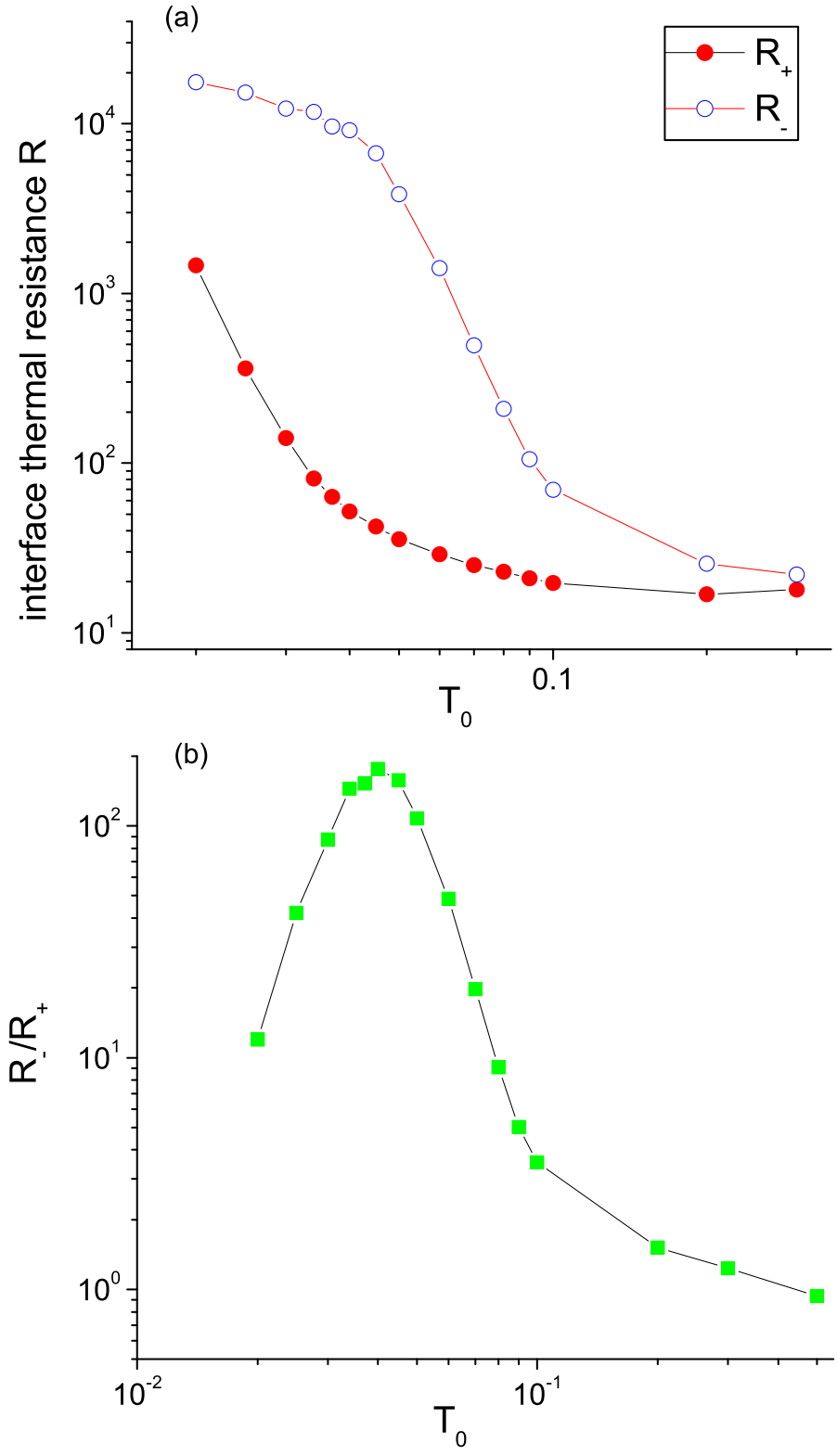

Figure 3.7: (a) Interface thermal resistance $R_{\pm}$ versus T_0. $|\Delta| = 0.5$. (b) The ratio R_-/R_+ versus T_0. $N_Y = 4, N_X = 10$.

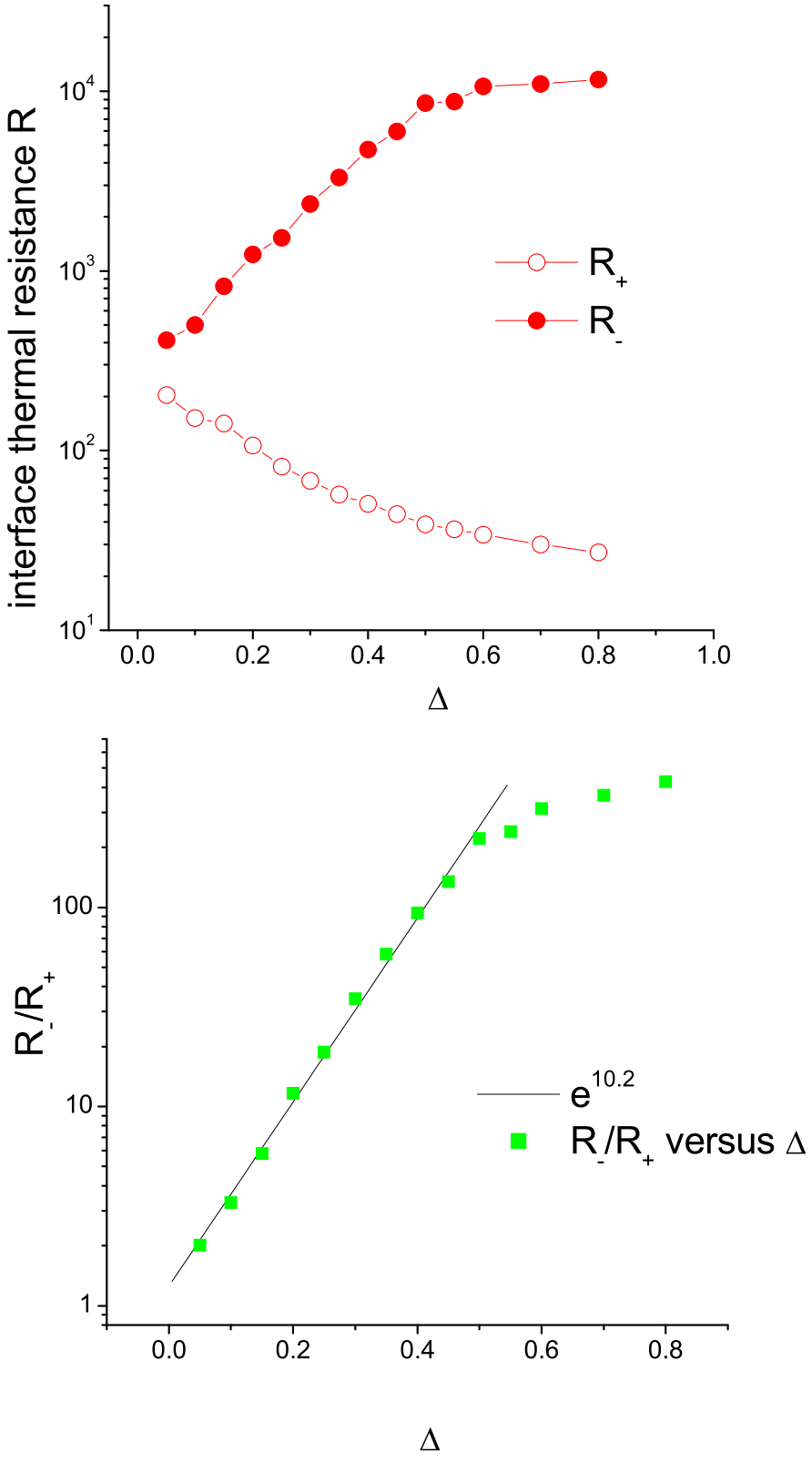

Figure 3.8: (a) $R_{\pm}$ versus the normalized temperature difference $|\Delta|$. $T_0 = 0.037$. (b) The ratio R_-/R_+ versus $|\Delta|$. $N_Y = 8, N_X = 20$.

3.5 Physical Mechanism of Rectifying Effect: An Analysis of Lattice Vibrational Spectrum

As in the 1D-FK-FPU model, we also can use energy band theory to explain the asymmetric properties observed in the 2D-FK-FPU model.

We can obtain the vibrational spectra by DFFT numerically. In the 2D FK-FPU model, the vibration has two components, v_x and v_y. Direct calculation of spectra of a vector by DFFT in 2D space will be much more complex. We can use the theorem of equipartition of energy to simplify the numerical calculation. According to the equipartition theorem, the molecules in thermal equilibrium (here we have local thermal equilibrium) have the same average energy associated with each independent degree of freedom of their motion and that energy is $k_BT/2$. For our system, we have $m\langle \mathbf{v}^2\rangle/2 = k_BT$, $m\langle v_x^2\rangle/2 = m\langle v_y^2\rangle/2 = k_BT/2$.

In our calculation, $m = 1$, $k_B = 1$. So we have $\langle v_x^2\rangle = \langle v_y^2\rangle = T$. If we do the DFFT of v_x and v_y separately, we should have

$$\begin{aligned}\sum_{i=0}^{L-1} |v_x(t)|^2 &= \Delta f \sum_{j=0}^{L/2-1} 2|P_x(j)|^2,\\ \sum_{i=0}^{L-1} |v_y(t)|^2 &= \Delta f \sum_{j=0}^{L/2-1} 2|P_y(j)|^2,\end{aligned} \tag{3.13}$$

here $P(f)$ is the Fourier transform of velocity $v(t)$. From the equipartition theorem, one has $\sum_{i=0}^{L-1} |v_x(t)|^2/L = \langle v_x^2\rangle$ and $\sum_{i=0}^{L-1} |v_y(t)|^2/L = \langle v_y^2\rangle$. From above analysis, we have

$$\begin{aligned}\Delta f \sum_{j=0}^{L/2-1} 2|P_x(j)|^2/L &= T,\\ \Delta f \sum_{j=0}^{L/2-1} 2|P_y(j)|^2/L &= T.\end{aligned} \tag{3.14}$$

The power spectra of vibration obtained from DFFT of v_x and v_y agree with the above formula very well (see Fig. 3.9). The integral of power spectra is exactly equal to the temporal average of v_x^2 and v_y^2 individually. There is a slight difference

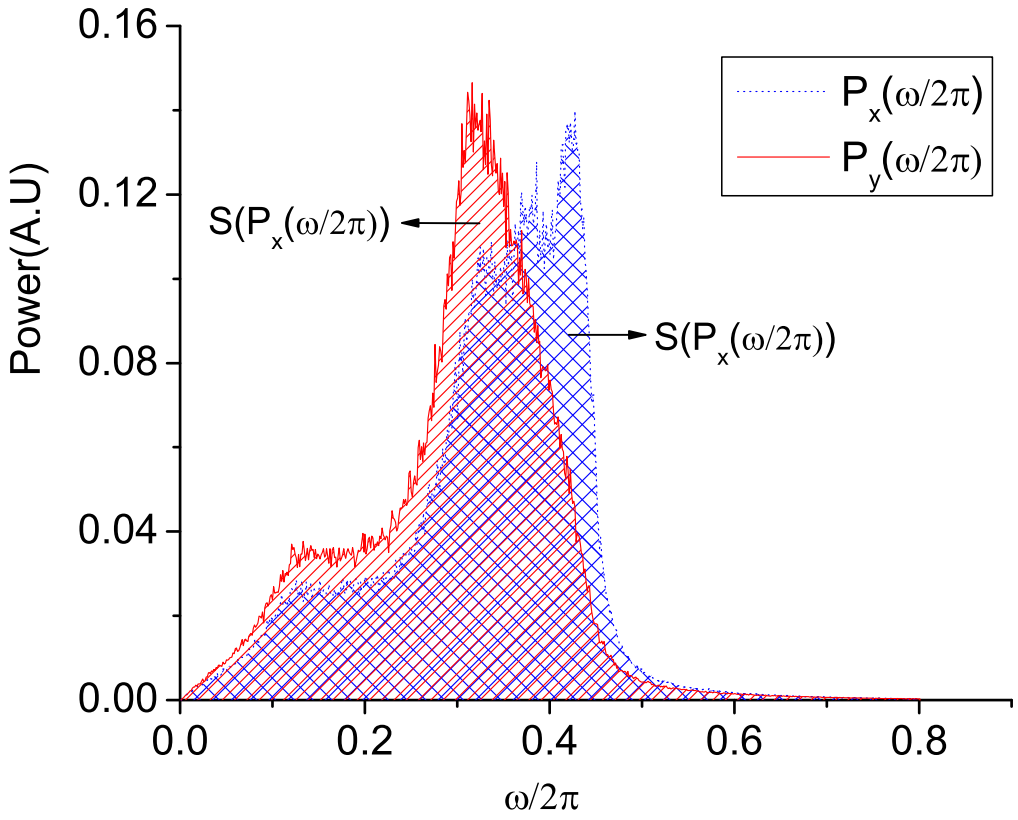

Figure 3.9: DFFT of v_x, v_y. The hatched regions represent the integral of the power spectra. $2S(P_x(\omega/2\pi)/L) = 0.05 = \langle v_x^2 \rangle \approx T$,$2S(P_y(\omega/2\pi)/L) = 0.05 = \langle v_y^2 \rangle \approx T$.

between $\langle v_x^2 \rangle$ and $\langle v_y^2 \rangle$. The difference might be caused by the number of sampled data or the different boundary conditions in the X, Y directions. In the formula, L should be infinite.

In our system, we find that the asymmetrical ITR and heat current are strongly related with the overlap of vibrational spectra of the particles at the two sides of the interface. When the vibration spectra overlap with each other, the system behaves like a thermal conductor, while the system behaves like a thermal insulator when the vibration spectra are separated.

Physically, whether an excitation of a given frequency can be transported through

a mechanical system depends on whether the system has a corresponding eigenfrequency. If the frequency matches, the energy can easily go through the system, otherwise, the excitation will be reflected. In our system, the overlap of the two spectra means that there exists common vibrational frequency in two parts of the system. The excitation (here as phonon) of such common frequency can be transported from one part to another. However, if the vibrational spectra of two parts are separated, then the excitation at any part cannot be transported to another part, because there exists no such corresponding frequency in another part. The change from overlap to separation is induced by the different temperature dependence of the vibrational spectra of the two segments, which is a general feature of any anharmonic lattice.

In Fig. 3.10, we show the vibrational spectra of the FK part and the FPU part under different temperatures. We can see that the vibrational spectra of the FK part broaden from high frequency to low frequency when increasing the system temperature. This is because at low temperature, the atoms of the FK model are confined at the valley of the on-site potential, thus the atoms oscillate in very high frequency, however, when the temperature is increased, more and more low frequency modes can be excited. In the limiting case, when the temperature is larger enough that the kinetic energy of the atom is much large than the on-site potential, then the FK model becomes a chain of harmonic oscillators which has frequency $\omega \in [0, 2\sqrt{k_{FK}}]$.

On the contrary, the vibrational spectra of the FPU part broaden from low frequency to high frequency. In fact, we have shown in previous work [62] that the highest oscillation frequency of the FPU model depends on temperature, $\omega_{FPU} \sim T^{1/4}$. Therefore, in some settings, the vibrational spectra of the FK part and the FPU part will overlap with each other, while in other temperature settings, they will separate with each other. These are shown in Fig. 3.11. The comparison of vibrational spectra of the FK part at two different temperature ranges and the FPU part at the full temperature range from 0.01 to 0.12 are shown in Fig. 3.11(a) and Fig. 3.11(b) separately. We can see that the vibrational spectra of the FK part and

the FPU part are matched with each other when the temperature of the FK part is from 0.05 to 0.12 [see Fig. 3.11(a)]. The vibrational spectra of the two parts are separated from each other when the temperature of the FK part is from 0.01 to 0.03 [see Fig. 3.11(b)]. This indicates that when the temperature of the FK part is below a certain value, which we call T_c $(0.04-0.045)$, the system will behave like a thermal insulator since the separated vibrational spectra of the interface particles make the heat conduction almost impossible. When the temperature of the FK part is above the critical point T_c, the system will be a good thermal conductor since the matched vibrational spectra allow the heat flow. Thus if we adjust T_0 and Δ appropriately to make $T_{high} \geq T_c$ and $T_{low} \leq T_c$, the system will have a good rectifying effect. If $T_{high}, T_{low} > T_c$ or $T_{high}, T_{low} < T_c$, the rectifying effect is very poor. The above analysis is based on the vibrational spectra of the system with $N_Y = 8, N_X = 20$. It is consistent with the result obtained in the previous section 3.3.

Now we look back at Fig. 3.3. The optimum point is at $T_0 = 0.037$ for $N_Y = 8, N_X = 20$, corresponding to $T_{high} = 0.0505 > T_c$ and $T_{low} = 0.0235 < T_c$. The effective temperature range T_e with $|\Delta| = 0.5$ is from 0.0261 to 0.0481. The low temperatures are all smaller than T_c and all high temperatures are larger than T_c. Both decreasing T_0 and increasing T_0 in the outside region of T_e lead the system to the two extreme cases $T_{high}, T_{low} \geq T_c$ or $T_{high}, T_{low} \leq T_c$ with poor performance. From the above analysis, we can say that the different properties of heat current under different temperature and temperature difference are determined by the temperature dependence of the vibrational spectra of the two segments.

The complex behavior of $|J_-|$ in Fig 4 can be explained in terms of the vibrational spectra of the particles in the interface. In particular, in the range from Δ_1 to Δ_2, a novel phenomenon − called the *negative differential thermal resistance* phenomenon − is observed in Ref. [61] and fully discussed in Ref. [68]. In this particular temperature interval, a larger temperature difference can induce a smaller heat current. The *negative differential thermal resistance* can be understood from the overlap and separation of the vibrational spectra of the interface particles. This phenomenon is valid for a wide range of the parameters. Moreover, in Ref. [68], Li *et al.* show that

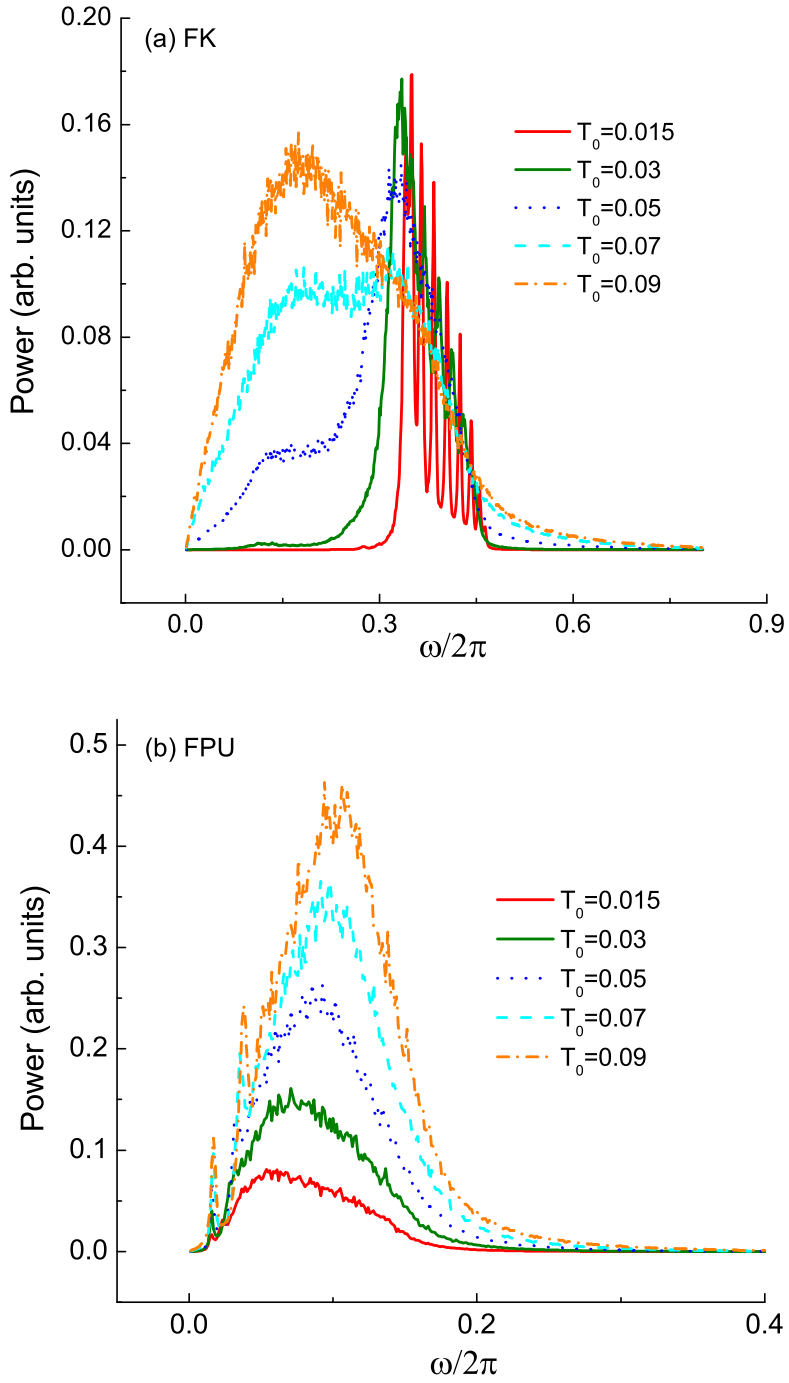

Figure 3.10: Vibrational spectra of the interface particles at different temperature. (a) The vibrational spectra of the particles in the FK segment.(b) The vibrational spectra of the particles in the FPU segment.

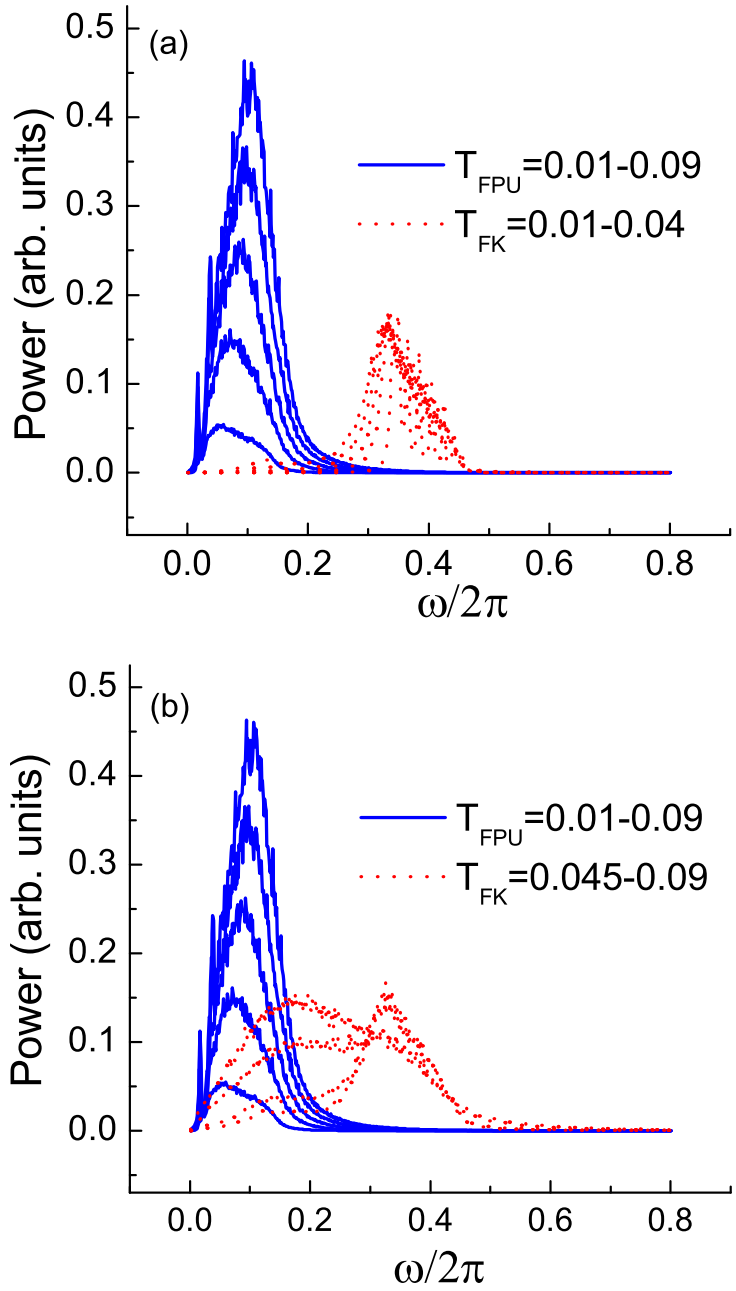

Figure 3.11: Comparison of the spectra of the FK part and the FPU part at different temperature regions. (a) The spectra of the FPU part at $T_{FPU} = 0.01 - 0.09$ (from bottom to top) and the FK part at $T_{FK} = 0.01 - 0.04$. (b) The spectra of the FPU part at $T_{FPU} = 0.01 - 0.09$ and the FK part at $T_{FK} = 0.045 - 0.09$

it is this negative differential thermal resistance property that makes the thermal transistor possible.

More importantly, we find a specific relationship between the overlap extent of the vibrational spectra of the two segments and the ratio R_-/R_+ in the interface or the ratio $|J_+/J_-|$ from two directions as in the 1D-FK-FPU. We introduce the following quantity to describe overlap of the vibrational spectra:

$$S_\pm = \frac{\int P_l^x(f)P_r^x(f)df}{\int P_l^x(f)df \int P_r^x(f)df} = \frac{\int P_l^x(f)P_r^x(f)df}{T_{int}^L T_{int}^R} \tag{3.15}$$

$S_\pm$ corresponds to the case of $\Delta > 0$ and $\Delta < 0$, respectively. In Fig. 3.12, we plot S_+/S_- versus R_-/R_+ and $|J_+/J_-|$. A very good power law was found between the ratio of resistances or heat currents and the overlap of the vibrational spectra:$|J_+/J_-| \sim R_-/R_+ \propto (S_+/S_-)^\gamma$ The best fit for the ratio of current suggests the power law constant $\gamma = 1.35 \pm 0.03$. Figures 3.11 and 3.12 give us a very clear and quantitative picture about the dependence of the rectifying effect of the system on the vibrational spectra.

Since the rectifying effect sensitively depends on the overlap of the vibrational spectra, we may find answers in Fig. 3.13 for the behavior of the 2D system responding to the temperature changes at different conditions. We can see clearly that when we change the number of particles in the Y direction, the temperature for the optimum performance will change, whereas when we change the number of particles in the X direction, the temperature for OP are kept at the same value; and the value of the temperature for the OP at different conditions found by the overlap are consistent with the value in Fig. 3.3. These results suggest that the different vibrational spectra of the two segments and the overlap between them are the determinant factors of the system complex behaviors.

3.6 Discussion and conclusions

In this Chapter, we have studied the thermal rectifying effect in a 2D anharmonic lattice. The performance of the 2D thermal rectifier under different environmental

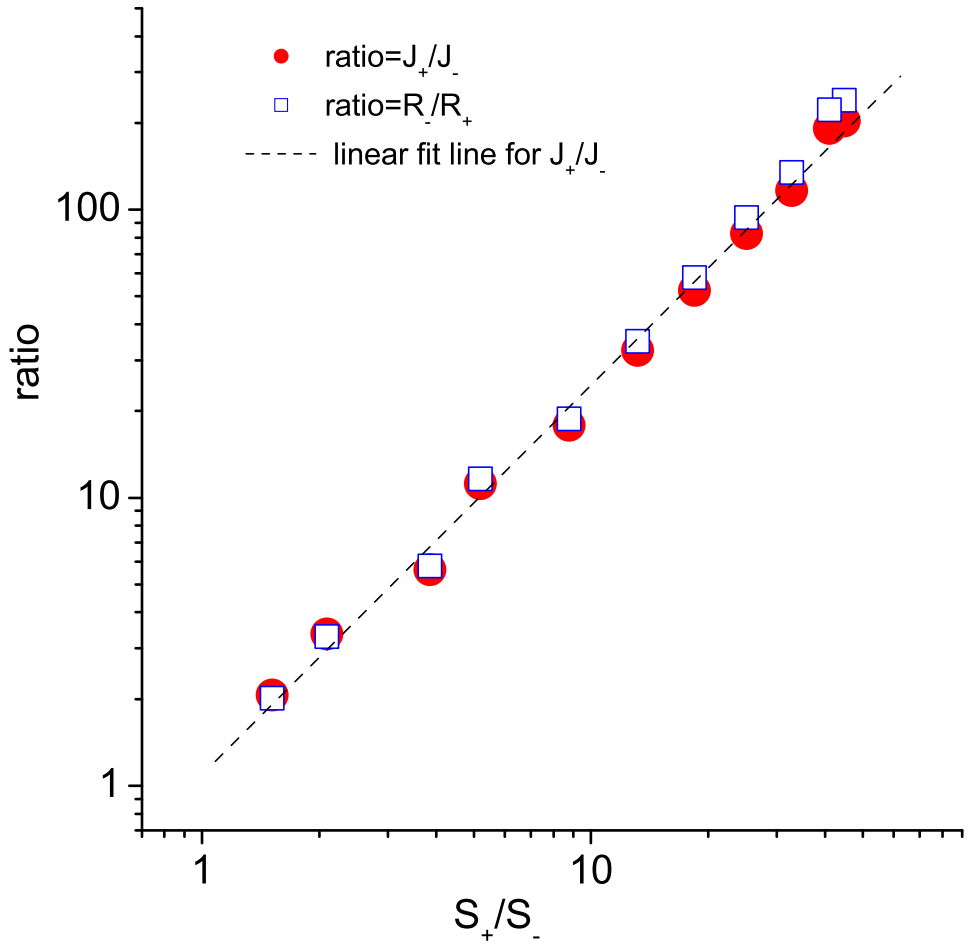

Figure 3.12: The bullet are the ratios of heat current $|J_+/J_-|$ versus S_+/S_- . Square are the ratios of the ITR R_-/R_+ versus S_+/S_-. The dotted line has a slope 1.35 ± 0.03.

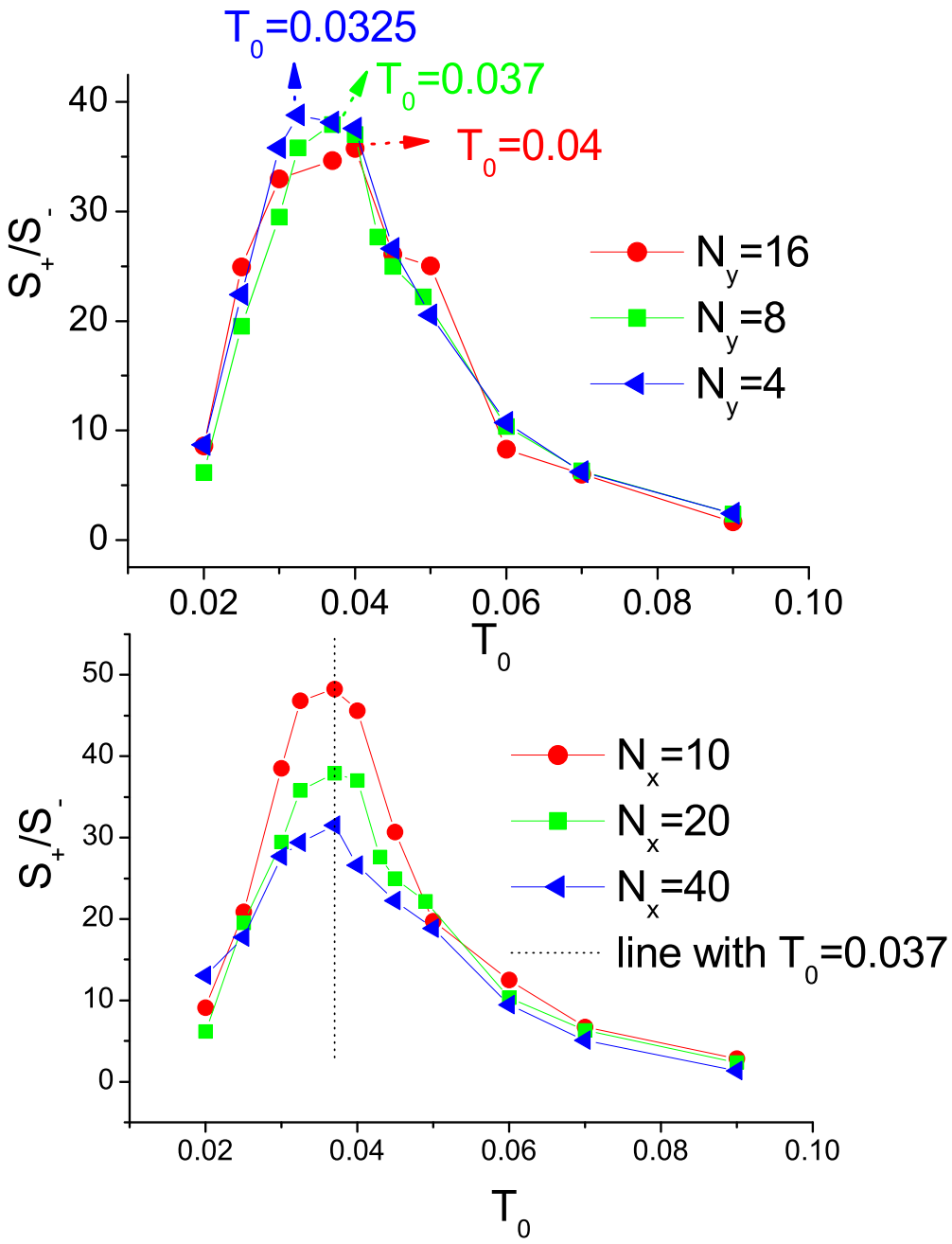

Figure 3.13: The ratio of the overlap of vibrational spectra S_+/S_- versus T_0 at different conditions. (a) Comparison at three different N_Y with $N_X = 20$.(b) Comparison at three different N_X with $N_Y = 8$.

changes, such as system temperature and the temperature difference on the two sides of the system, have been investigated systematically. We find that there exits an optimum performance (OP) for a specific thermal rectifier at certain temperature range. The OP is affected by the boundary condition and the number of particles, N_Y, along the Y direction. The OP shifts to lower temperature when increasing N_Y or changing the periodic boundary condition to the free boundary condition along the Y direction. The 2D thermal rectifier has a good rectifying efficiency in a very wide temperature range. Another important factor that affects the performance of the thermal rectifier is the temperature difference between the two ends. We find the rectifying efficiency increases approximately as an exponential law in a certain temperature range with the temperature difference. The rectifying efficiency is mainly determined by the asymmetrical ITR. The study on the ITR shows the similar behavior with heat current.

The behaviors of the ITR and heat current of the system are strongly correlated with vibrational spectra of the particles beside the interface. The asymmetry behavior of ITR and heat current is induced by the different temperature dependence of the vibrational spectra of the two parts beside the interface. We find that the vibrational spectra of the FK part broaden from high frequency to low frequency, conversely, the vibrational spectra of the FPU part broaden from low frequency to high frequency as the temperature increases. The different temperature dependence of vibrational spectra makes the system transition from a thermal conductor to an insulator possible by setting the system temperature and temperature difference properly. Moreover, a specific relationship between the performance of the system and the convolution of the vibrational spectra of the two parts is found numerically as power law.

Our study on a 2D thermal rectifier gives a very clear picture about how the system responds to the environmental changes. The results should be useful for further experimental investigation. The thermal diode constructed by a monolayer thin film or a tubelike structure might have many practical applications.

Chapter 4

Thermal Rectifier from Three-dimensional Anharmonic latties

After successful building of thermal rectifier in low-dimension systems, we are considering how to extend our study to a 3D system. But how to add a substrate to a 3D system becomes a big problem. In most theoretical approaches, a usual way is to project the effect from a substrate into a 2D surface layer or 1D chain in order to find theoretical explanations for some phenomena observed in experiments. Needless to say, the FK [50] model has been proved to be the most suitable model for the theoretical description of different nonlinear or long-range interaction phenomena on a surface [85]: commensurate-incommensurate phase transitions, charge-density-wave propagation, magnetic and ferroelectric domain walls, dislocation dynamics, and kinks structure in the adsorbed monolayers. Obviously, the 2D simplifications of substrate are more reasonable than the 1D approximations. 2D models have a lot of features in comparison with their 1D limits. Also, we should notice that when the effect from the substrate on the inner particles are considered, realistic anharmonic intermolecular potential such as the Morse potential, the Mie potential, the Gaussian decay potential and so on, are often used. Here, we want to consider a more realistic approximation of substrate. We combine these two types of approximations (low dimensional projections and intermolecular potential among inner layers. The

substrate does not only affect the atoms in the contact plane, but also affect the atoms in the direction perpendicular to the contact plane according to some attenuation, such as Morse potential, Mie potential, Gaussian decay potential, related with the distance between the substrate and layers. That is to say, our description of substrate is in real space.

The aforementioned studies on 1D [61–63] and 2D nonlinear lattices [65] tell us that the determinant factor for a thermal rectifier is the match and/or mismatch of the vibrational bands from the two segments. To this end, we need to (1) break spatial symmetry of the system; (2) introduce nonlinearity (or anharmonicity). The broken of spatial symmetry is necessary to make the heat flow asymmetric, while the introduction of the nonlinearity allows us to adjust the parameters to get match or mismatch of the vibrational spectra by reversing the temperature gradient. We know that the phonon band of a harmonic system will not change with temperature. Therefore, anharmonicity (nonlinearity) is essential to make the spectra temperature dependent.

In this Chapter, we make a step further, namely, we extend our study to a 3D model. The extension is based on two reasons: (1)a 3D or bulk material is closer to practical applications, and (2) the extension to higher dimension is scientifically more challenging, and of course more intriguing. Theoretical analysis of spectra for two representative nonlinear models and comparison of spectra with numerical result will be provided. Analytic suggestion of suitable parameter setting for an efficient thermal rectifier will be given and numerical confirmation will be demonstrated.

4.1 Model and Methodology

Like in the 1D and 2D rectifier models, our 3D model also consists of two anharmonic lattices. One is a 3D FK lattice and another is a 3D FPU lattice. In the 3D FK lattice, we allow layered particles to displace in the direction orthogonal to the substrate [99], denoted as the Z direction. The description of anharmonic decay of a layered potential along the Z direction must satisfy the following conditions: (a)

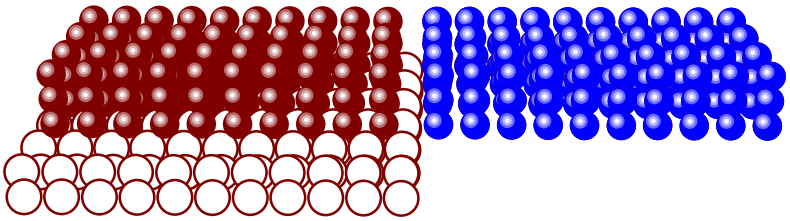

Figure 4.1: Configuration of our 3D model. The left part are harmonic oscillators. Under the harmonic oscillators is the substrate. The right part are the FPU oscillators. The left part and the right part are connected by weak couplings.

as we get further away from the minimum, it should be harder to squeeze particles together than to separate them and (b) asymptotic freedom: the particles should be free when their distance is large. There are many potential fulfilling these conditions in the literatures. We have chosen the Mie 6-12 type potential, which corresponds to the Lennard-Jones potential.

$$V(d) = \frac{A_0}{\mu - \nu}[\nu(\frac{d_0}{d})^\mu - \mu(\frac{d_0}{d})^\nu] \tag{4.1}$$

The Lennard-Jones form is $\mu = 12, \nu = 6$,

$$V(d) = A_0[(\frac{d_0}{d})^{12} - 2(\frac{d_0}{d})^6] \tag{4.2}$$

where $d = |r_{i+1} - r_i|$ is the actual distance between neighboring layered particles, d_0 is the equilibrium distance and A_0 is the potential barrier. We extend the 2D FK substrate (Eq. (2) in Ref. [65]) in the vertical Z direction with Lennard-Jones form:

$$V_s(x, y, z) = \frac{A_0}{(2\pi)^2}[(\frac{z_{eq}}{z})^{12} - (\frac{z_{eq}}{z})^6(\cos(2\pi x)\cos(2\pi y) + 1)], \tag{4.3}$$

where z_{eq} is the equilibrium position along the Z direction between the system and the substrate. In this way, the 3D substrate potential reduces to the previous 2D sinusoidal form when $z = z_{eq}$. The +1 term after the cosine function makes the average potential zero at the plane $z = z_{eq}$. When $z < z_{eq}$ the average value is positive, and it is negative when $z > z_{eq}$. The potential barrier will decrease very fast along Z direction.

The two parts are both simple cubic lattices with lattice constant a. The particle at the lth column in the X direction, the mth column in the Y direction and the nth column in the Z direction is denoted as (l, m, n). The coordinates and momenta of this particle are $\vec{q}_{l,m,n} = (x_{l,m,n}, y_{l,m,n}, z_{l,m,n})$ and $\vec{p}_{l,m,n} = (p_{x_{l,m,n}}, p_{y_{l,m,n}}, p_{z_{l,m,n}})$. The Hamiltonian of a 3D array of harmonic oscillators and the 3D FPU lattices has the following form:

$$\begin{aligned} H = \sum_{l=1}^{N_X}\sum_{m=1}^{N_Y}\sum_{n=1}^{N_Z}(\frac{\vec{p}_{l,m,n}^2}{2} &+ kV(|\vec{r}_{l+1,m,n;l,m,n}| - a) \\ &+ kV(|\vec{r}_{l,m+1,n;l,m,n}| - a) \\ &+ kV(|\vec{r}_{l,m,n+1;l,m,n}| - a)), \end{aligned} \tag{4.4}$$

where $\vec{r}_{l_1,m_1,n_1;l_2,m_2,n_2} = \vec{q}_{l_1,m_1,n_1} - \vec{q}_{l_2,m_2,n_2}$ is the relative displacement between particles (l_1, m_1, n_1) and (l_2, m_2, n_2). N_X, N_Y, and N_Z are the number of particles along the X, Y, and Z directions, respectively. So the total number of particles is $N_X \times N_Y \times N_Z$. $V = V_H(x) = \frac{1}{2}x^2$ and $k = k_H$ for the harmonic lattice. $V = V_{FPU}(x) = \frac{1}{2}x^2 + \frac{1}{4}x^4$ and $k = k_{FPU}$ for the FPU lattice. We use weak harmonic springs to connect the two parts. The Hamiltonian for the connecting springs, H_{int}, is

$$H_{int} = \sum_{m=1}^{N_Y}\sum_{n=1}^{N_Z} k_{int} V_H(|\vec{r}_{N_{FK},m,n;N_{FK}+1,m,n}| - a). \tag{4.5}$$

We put two Nośe-Hover [79] heat baths with different temperatures T_L and T_R to the left and right end of the system so as to establish heat flux along the X direction. That is, the particles with $l = 1$ and N_x, $m = 1, 2, 3, ..., N_Y, n = 1, 2, 3, ..., N_Z$

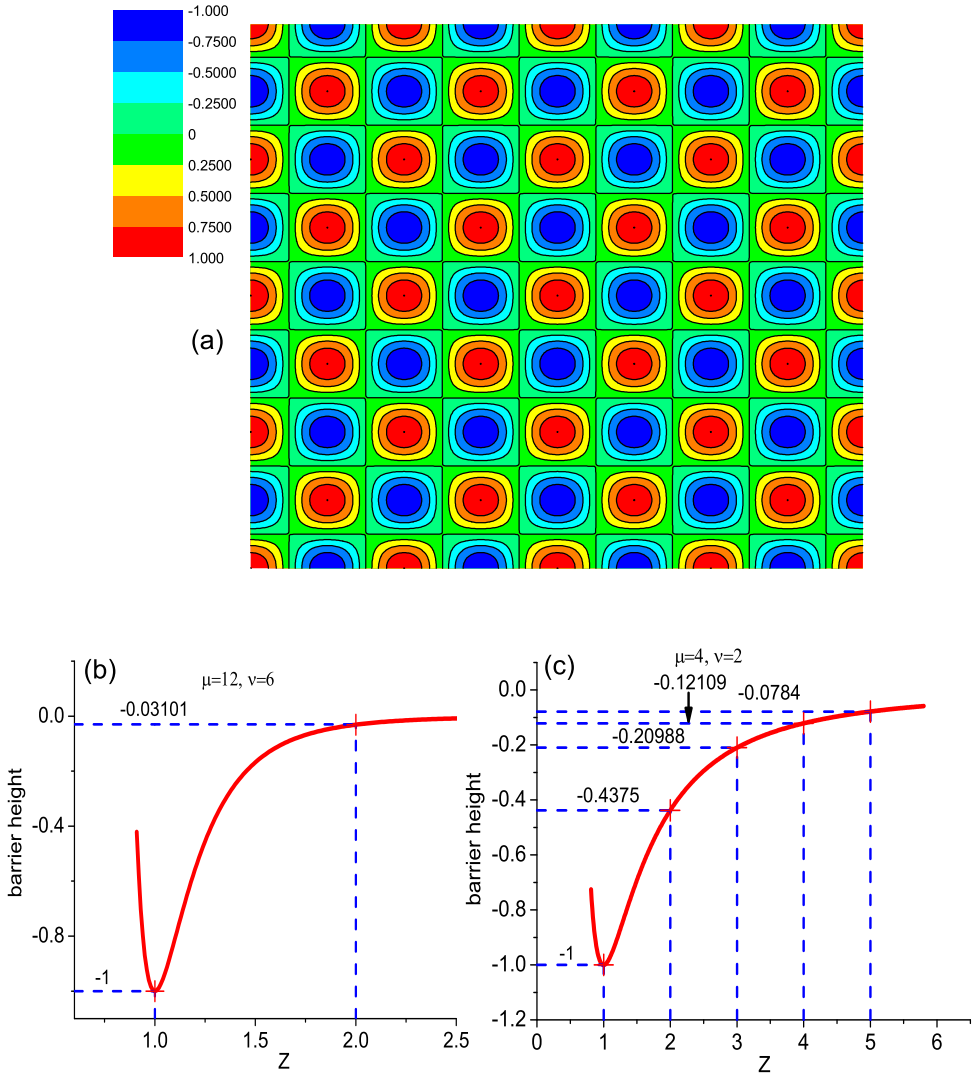

Figure 4.2: Configuration of the substrate potential. (a) Substrate potential contour in the $X-Y$ plane. (b) Barrier height changes along the Z direction with Mie 6-12 type decreasing ($\mu = 12$, $\nu = 6$). (c) Barrier height changes along the direction perpendicular to the substrate with Mie 2-4 type decreasing ($\mu = 4$, $\nu = 2$).

are coupled with Nośe-Hover heat baths at temperatures T_L and T_R, respectively. Initially, all particles are in the equilibrium position. A fixed boundary condition is used along the X direction (temperature gradient direction). A periodic boundary condition is applied in the Y direction, while there is a free boundary condition in the Z direction. Initially $\vec{q}_{0,m,n} = (0, ma, na), \vec{q}_{N_X+1,m,n} = ((N_X+1)a, ma, na)$, $\vec{q}_{l,1,n} = \vec{q}_{l,N_Y+1,n} - N_Y a\hat{y}$, $\vec{q}_{l,m,1} = (la, ma, a), \vec{q}_{l,m,N_Z} = (la, ma, N_Z a)$.

The substrate, represented by the potential V_s, is added to the 3D arrays of harmonic oscillators. We call this the 3D FK model, which has the Hamiltonian $H_{FK} = H_H + V_s$. The right segment is the 3D FPU lattice with the Hamiltonian H_{FPU} that is given in Eq. (2). The equations of motion (EOMs) of all particles are

$$\dot{\vec{q}}_{l,m,n} = \vec{p}_{l,m,n}$$

$$\dot{\vec{p}}_{l,m,n} = \begin{cases} \vec{f}_s - \dfrac{\partial H}{\partial \vec{q}_{l,m,n}} (l = 2, N_X - 1) \\ \vec{f}_s - \dfrac{\partial H}{\partial \vec{q}_{l,m,n}} - \xi_{l,m,n}\vec{p}_{l,m,n} (l = 1, N_X) \end{cases} \tag{4.6}$$

where $\vec{f}_s$ is the force from the substrate

$$\vec{f}_s = -\frac{\partial V_s}{\partial |\vec{r}|}\frac{\vec{r}}{|\vec{r}|} (l = 1, N_X/2) \tag{4.7}$$

and the auxiliary variables $\xi_{l,m,n}$ are described by the equations [79]

$$\dot{\xi}_{l,m,n} = \frac{1}{\mathcal{Q}}\left(\frac{\vec{p}^2_{l,m,n}}{3k_B T} - 1\right). \tag{4.8}$$

T is the temperature of the Nośe-Hover heat bath on the left end (T_L) or the right end (T_R) and $\mathcal{Q}$ is the coupling parameter between the thermal bath and the system. We set the same value $\mathcal{Q} = 1$ as in the 1D and 2D cases.

In our simulation, we set $z_{eq} = a_0$, which means that the equilibrium distance between substrate and lattice equals the lattice constant. In the Lennard-Jones potential (Mie 6-12 potential), the cutoff distance is about twice the equilibrium distance, $2z_{eq}$ (as shown in Fig. 4.2). This indicates that effect from substrate is neglected when $z > 2z_{eq} = 2a_0$. In Ref. [99], they studied the vertical extended FK

model on 1D lattice with Mie 2-4 type potential decreasing. The cut-off distance in their model along the vertical direction is much longer. It is about $7z_{eq}$.

The local temperature is defined as

$$\frac{3}{2}k_B T_{l,m,n} = \frac{1}{2}m\langle \vec{v}^2_{l,m,n}\rangle, \tag{4.9}$$

where k_B is the Boltzmann constant. The local heat flux $J_{l,m,n}$ along the temperature gradient is defined as the energy transfer per unit time from the particle labeled (l, m, n) to the nearest particle $(l+1, m, n)$ along the X direction.

$$\begin{aligned} J_{l,m,n} &= -\vec{v}_{l+1,m,n} \cdot \vec{F}_{l+1,m,n;l,m,n} \\ &= -k\vec{v}_{l+1,m,n} \cdot \frac{\partial V(|\vec{r}_{l+1,m,n;l,m,n}| - a)}{\partial |\vec{r}_{l+1,m,n;l,m,n}|} \frac{\vec{r}_{l+1,m,n;l,m,n}}{|\vec{r}_{l+1,m,n;l,m,n}|}, \end{aligned} \tag{4.10}$$

where $k = k_H, k_{FPU}$, or k_{int}, depending on the site along the X direction. In our study, we are concerned only with the heat flux flowing along the X direction. Then we can denote the flux from the particles in the lth section to the next section in the X direction as $J_l = \sum_{m=1}^{N_Y}\sum_{n=1}^{N_Z} J_{l,m,n}$. The total flux of the system can be written as follows:

$$J = \langle \frac{1}{N_X}\sum_{l=1}^{N_X} J_l \rangle. \tag{4.11}$$

We use J_+ to denote the heat current when the high-temperature bath is attached to the FK part and the low temperature bath is attached to the FPU part; J_- is the heat flow when the heat baths at the two ends are swapped.

4.2 Analysis of Vibrational Spectra

After some numerical studies, we found that, under the same parameter settings as in the 1D and 2D cases, rectification still exists in our 3D model, but it is very small compared with the 1D and 2D cases. The rectification is of the order 10. In order to make our model more efficient, we need to optimize the parameters. We should point out that searching for suitable parameters as in the 1D case to obtain optimum thermal rectification is not wise since we have too many parameters. On the other

hand, we already know that the rectification is determined by interface properties, such as effective phonon spectra and interface thermal resistance. Therefore, we decided to do some analytical analysis of the spectra in both segments.

4.2.1 Vibrational Spectra of the FK Part from Different Directions

In low temperature limit, we can linearize the FK model around the equilibrium position ($x^0_{l,m,n} = x^0_l = la, y^0_{l,m,n} = y^0_m = ma, z^0_{l,m,n} = z^0_n = na$). The original Hamiltonian of our 3D FK mode is

$$\begin{aligned} H_{FK} &= H + V_s \\ &= \sum_{l=1}^{N_X}\sum_{m=1}^{N_Y}\sum_{n=1}^{N_Z}[\frac{\vec{p}^2_{l,m,n}}{2} + kV_H(|\vec{r}_{l+1,m,n;l,m,n}| - a_0) \\ &+ kV_H(|\vec{r}_{l,m+1,n;l,m,n}| - a_0) + kV_H(|\vec{r}_{l,m,n+1;l,m,n}| - a_0)] \\ &+ \frac{A_0}{(2\pi)^2}[(\frac{z_{eq}}{z_n})^{12} - (\frac{z_{eq}}{z_n})^6(\cos(2\pi x_l)\cos(2\pi y_m) + 1)]. \end{aligned} \tag{4.12}$$

We can obtain a linearized version of the substrate potential by keeping the lowest nonzero terms and dropping all higher terms of Taylor expansion around equilibrium position $\vec{q}^0_{l,m,n} = (x^0_l = la, y^0_m = ma, z^0_n = na)$. This is reasonable at low temperature limit.

$$\begin{aligned} &V_s(x^0_l + \delta x_l, y^0_m + \delta y_m, z^0_n + \delta z_n) = V_s(x^0_l, y^0_m, z^0_n) + \\ &\sum_{\alpha=1}\frac{1}{\alpha!}(\delta x_l\frac{\partial}{\partial x_l} + \delta y_m\frac{\partial}{\partial y_m} + \delta z_n\frac{\partial}{\partial z_n})^\alpha V_s(x_l, y_m, z_n)|_{\vec{q}_{l,m,n}=\vec{q}^0_{l,m,n}}. \end{aligned} \tag{4.13}$$

All first order partial derivatives vanish, namely,

$$\begin{aligned} \delta x_l\frac{\partial}{\partial x_l}V_s(x_l, y_m, z_n)|_{\vec{q}_{l,m,n}=\vec{q}^0_{l,m,n}} &= 0, \\ \delta y_m\frac{\partial}{\partial y_m}V_s(x_l, y_m, z_n)|_{\vec{q}_{l,m,n}=\vec{q}^0_{l,m,n}} &= 0, \\ \delta z_n\frac{\partial}{\partial z_n}V_s(x_l, y_m, z_n)|_{\vec{q}_{l,m,n}=\vec{q}^0_{l,m,n}} &= 0. \end{aligned} \tag{4.14}$$

So all crossed terms are also zero. Nonzero terms are:

$$\begin{aligned}
&\frac{\partial^2}{\partial x_l^2} V_s(x_l, y_m, z_n)|_{\vec{q}_{l,m,n}=\vec{q}^0_{l,m,n}} = C_n^1, \\
&\frac{\partial^2}{\partial y_m^2} V_s(x_l, y_m, z_n)|_{\vec{q}_{l,m,n}=\vec{q}^0_{l,m,n}} = C_n^2, \\
&\frac{\partial^2}{\partial z_n^2} V_s(x_l, y_m, z_n)|_{\vec{q}_{l,m,n}=\vec{q}^0_{l,m,n}} = C_n^3,
\end{aligned} \tag{4.15}$$

where

$$\begin{aligned}
&C_n^1 = C_n^2 = A_0(\frac{z_{eq}}{z_n^0})^6, \\
&C_n^3 = \frac{12A_0}{(2\pi)^2}[13(\frac{z_{eq}}{z_n^0})^{14} - 7(\frac{z_{eq}}{z_n^0})^8].
\end{aligned} \tag{4.16}$$

Therefore, H_{FK} can be divided as three separated components, $H_{FK} = H_{xx} + H_{yy} + H_{zz}$; each component is related only with the freedom in its corresponding direction. We thus can obtain the EOMs of the particle (l, m, n) in three components as follows:

$$\begin{aligned}
\frac{d^2\delta x_l}{dt^2} &= -\frac{\partial H_{xx}}{\partial \delta x_l} = k(\delta x_{l+1} + \delta x_{l-1} - 2\delta x_l) - C_n^1 \delta x_l, \\
\frac{d^2\delta y_m}{dt^2} &= -\frac{\partial H_{yy}}{\partial \delta y_m} = k(\delta y_{m+1} + \delta y_{m-1} - 2\delta y_m) - C_n^2 \delta y_m, \\
\frac{d^2\delta z_n}{dt^2} &= -\frac{\partial H_{zz}}{\partial \delta z_n} = k(\delta z_{n+1} + \delta z_{n-1} - 2\delta z_n) - C_n^3 \delta z_n.
\end{aligned} \tag{4.17}$$

We now look for solutions of the plane wave $e^{-iKa-i\tilde{\omega}t}$. K is the wave vector and $\tilde{\omega}$ is the frequency. Then $d^2q/dt^2 = -\tilde{\omega}^2 q$, and we can have the dispersion relations connecting $\tilde{\omega}$ and K polarized in the X, Y and Z directions directly if we consider periodic boundary conditions along each direction,

$$\tilde{\omega}_i^2(K) = \sum_{n=1}^{N_z}(2k + C_n^i - 2k\cos(Ka))(i = 1, 2, 3). \tag{4.18}$$

The primitive translation vectors of our simple cubic lattice are taken as the following set:

$$a_1 = a_0\hat{x}, a_2 = a_0\hat{y}, a_3 = a_0\hat{z}. \tag{4.19}$$

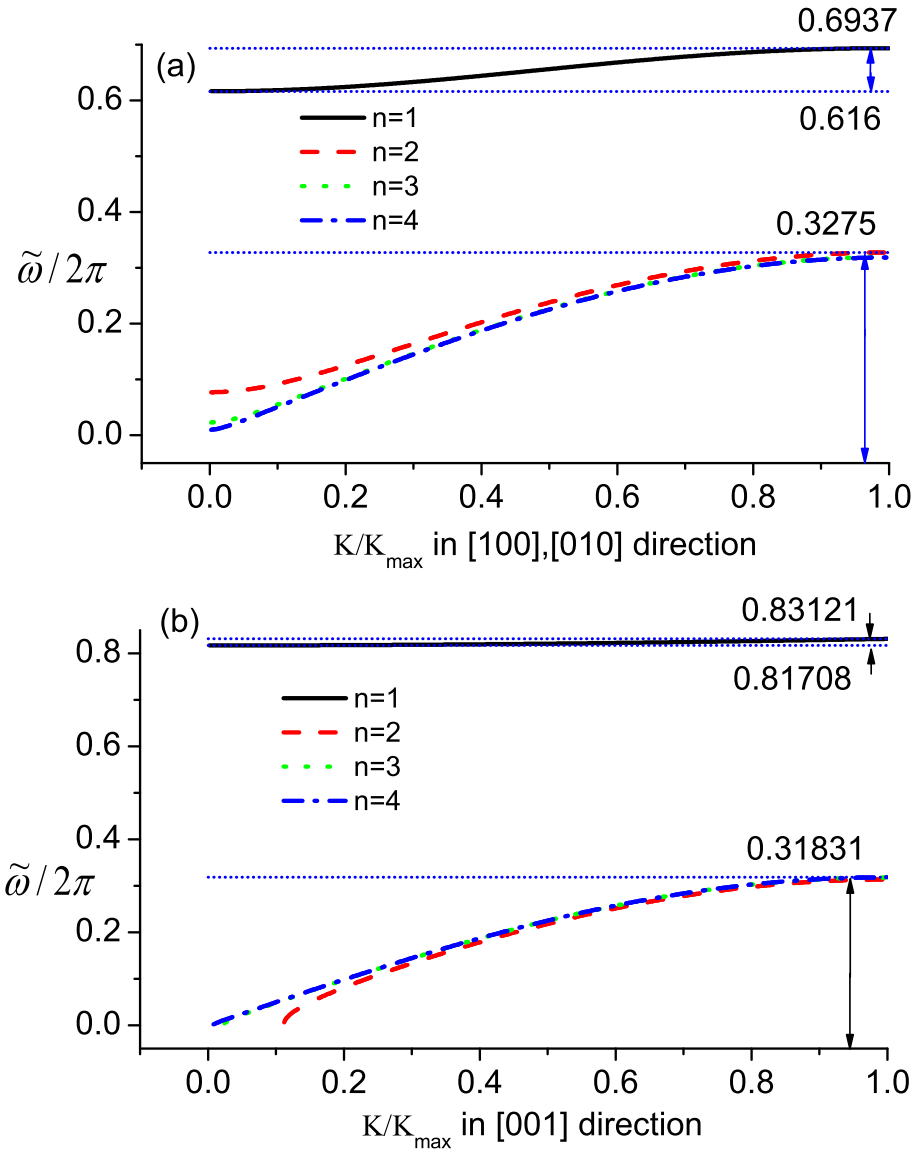

Figure 4.3: Dispersion relationship of the 3D FK model according to Eq. (4.18) when $A_0 = 15$, $K_{FK} = 1$. (a) Dispersion relationship for the polarization in the X, Y directions. (b) Dispersion relationship for the polarization in the Z direction. Horizontal lines are guidelines for the bound of different regions and numbers are the corresponding values of the lines along the vertical axis. In both (a) and (b) the curves for $n = 3$ and 4 are almost indistinguishable.

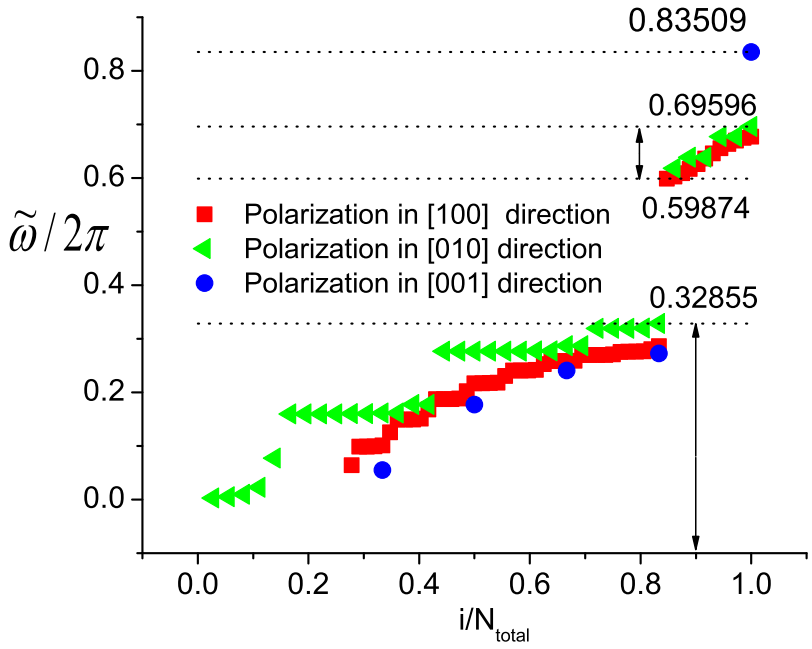

Figure 4.4: Allowed vibrational frequency obtained by numerical seeking for the solution of EOMs in the [100], [010] and [001] directions, respectively, in a finite size bulk with $A_0 = 15$, $K_{FK} = 1$ $N_x = 12$,$N_y = 6$, and $N_z = 6$. Horizontal lines are guidelines for the bound of different regions and numbers are the corresponding values of the lines along the vertical axis.

Here $\hat{x}, \hat{y}, \hat{z}$ are orthogonal vectors of unit length. The reciprocal lattice of our simple cubic lattice is itself a simple cubic lattice with lattice constant $2\pi/a$. The primitive translation vectors of the reciprocal simple cubic lattice are

$$b_1 = (2\pi/a)\hat{x}, b_2 = (2\pi/a)\hat{y}, b_3 = (2\pi/a)\hat{z}. \tag{4.20}$$

Therefore, $i = 1, 2, 3$ corresponds to the [100], [010], and [001] directions, respectively. Equation (4.18) gives the dispersion relations of the polarization in the X, Y, and Z directions.

C_n^i are gaps of all branches at zero wavenumber induced by the substrate. The effective phonon bands of the 3D FK model is $\sqrt{C_n^i} < \tilde{\omega}_n^i < \sqrt{4k_{FK} + C_n^i}(n = 1, ..., N_z$ and $i = 1, 2, 3)$. $C_n^i \propto (1/z_n^0)^\delta$, $z_n^0 = na_0$ and $\delta = 6$ for $i = 1, 2$ and $\delta = 8$ for $i = 3$) as in the Eq. (4.16); therefore C_n^i decreases to asymptotically zero very fast since it is proportional to $(1/n)^\delta$.

In Fig. 4.3, we show the dispersion relationship. We can see that the frequency has two main branches. One branch is located in the high-frequency region

$$\sqrt{C_n^i} < \tilde{\omega}_n^i < \sqrt{4k_{FK} + C_n^i}(n = 1, i = 1, 2, 3), \tag{4.21}$$

and is induced by the strongest effect of the substrate on the contact layer. Another branch is located in the low-frequency region and is induced by the weak effect of the substrate on the inner layers,

$$\sqrt{C_n^i} < \tilde{\omega}_n^i < \sqrt{4k_{FK} + C_n^i}(n > 1, i = 1, 2, 3). \tag{4.22}$$

The low-frequency region is almost overlapped with the phonon spectra of pure harmonic oscillators, $0 < \omega_n^i < \sqrt{4k_{FK}}(i = 1, 2, 3)$ [100]. Our above analysis is based on the approximation of low temperature limit. The dispersion relation for the 3D FK model in Eq. (4.18) has a similar form as in the 1D Morse model [60] or the 1D FK model [61–63]. The difference of the 3D FK and the 1D FK models is the additional low-frequency branch induced by the inner layers. We will show later that in the low-temperature limit vibrations of the 3D FK concentrate in the high-frequency branch as in low-dimensional cases, while in the high-temperature limit

vibrations concentrate in the low-frequency branch. This is because in the high-temperature limit the kinetic energy is much larger than the substrate energy. In this case particles have large enough kinetic energy to jump out of the valleys of the substrate potential and vibrate almost like harmonic oscillators with low frequency, while in the low-temperature limit, the substrate energy is much larger than the kinetic energy. In this case, particles are confined in the valleys of the substrate and oscillate with high frequency.

If we consider free boundary conditions along the Y and Z directions like shown in the Eq. (4.23), we may computationally to get the eigenvalue of the EOMs

$$\begin{aligned}\frac{d^2\delta y_m}{dt^2} =& -\frac{\partial H_{yy}}{\partial \delta y_m} = k(\delta_{1,m}(\delta y_{m+1} - \delta y_m) \\ & - \delta_{N_y,m}(\delta y_m - \delta y_{m-1})) - C_n^2 \delta z_n (m = 1, N_y) \\ \frac{d^2\delta z_n}{dt^2} =& -\frac{\partial H_{zz}}{\partial \delta z_n} = k(\delta_{1,n}(\delta z_{n+1} - \delta z_n) \\ & - \delta_{N_z,n}(\delta z_n - \delta z_{n-1})) - C_n^3 \delta z_n (n = 1, N_z),\end{aligned} \tag{4.23}$$

$\delta_{1,n}, \delta_{N_z,n}$ is $\delta_{i,j}$ function. $\delta_{i,j} = 1$ when $i = j$ and $\delta_{i,j} = 0$ when $i \neq j$.

For a specific parameter setting, such as $A_0 = 15, k_{FK} = 1$, we have $\omega/2\pi \in [0, 0.327] \cup [0.616, 0.694]$ in the [100] and [010] directions and $\omega/2\pi \in [0, 0.318] \cup [0.817, 0.831]$ in the [001] direction according to the Eq. (4.18). This is shown in the Fig. 4.3. We should point out that there is a slight difference of vibrational frequency between a system with finite size and one with infinite size. For a specific structure with $N_x = 12, N_y = 6, N_z = 6$, a periodic boundary condition along the Y direction and free boundary conditions along the X and Z directions, we obtain that $\omega/2\pi \in [0, 0.286] \cup [0.599, 0.677]$ in the [100]direction, $\omega/2\pi \in [0, 0.329] \cup [0.618, 0.696]$ in the [010] direction and $\omega/2\pi \in [0, 0.273] \cup [0.835, 0.835]$ in the [001] direction by solving the EOMs numerically. This is shown in Fig. 4.4.

If we do a DFFT (Discrete fast fourier transformation) [97] of the velocity in each direction directly, we can get the vibrational band or energy density of the vibrational frequency in each direction. A comparison of the analytic result and the numerical vibrational band by the DFFT are shown in Fig. 4.5. We compare

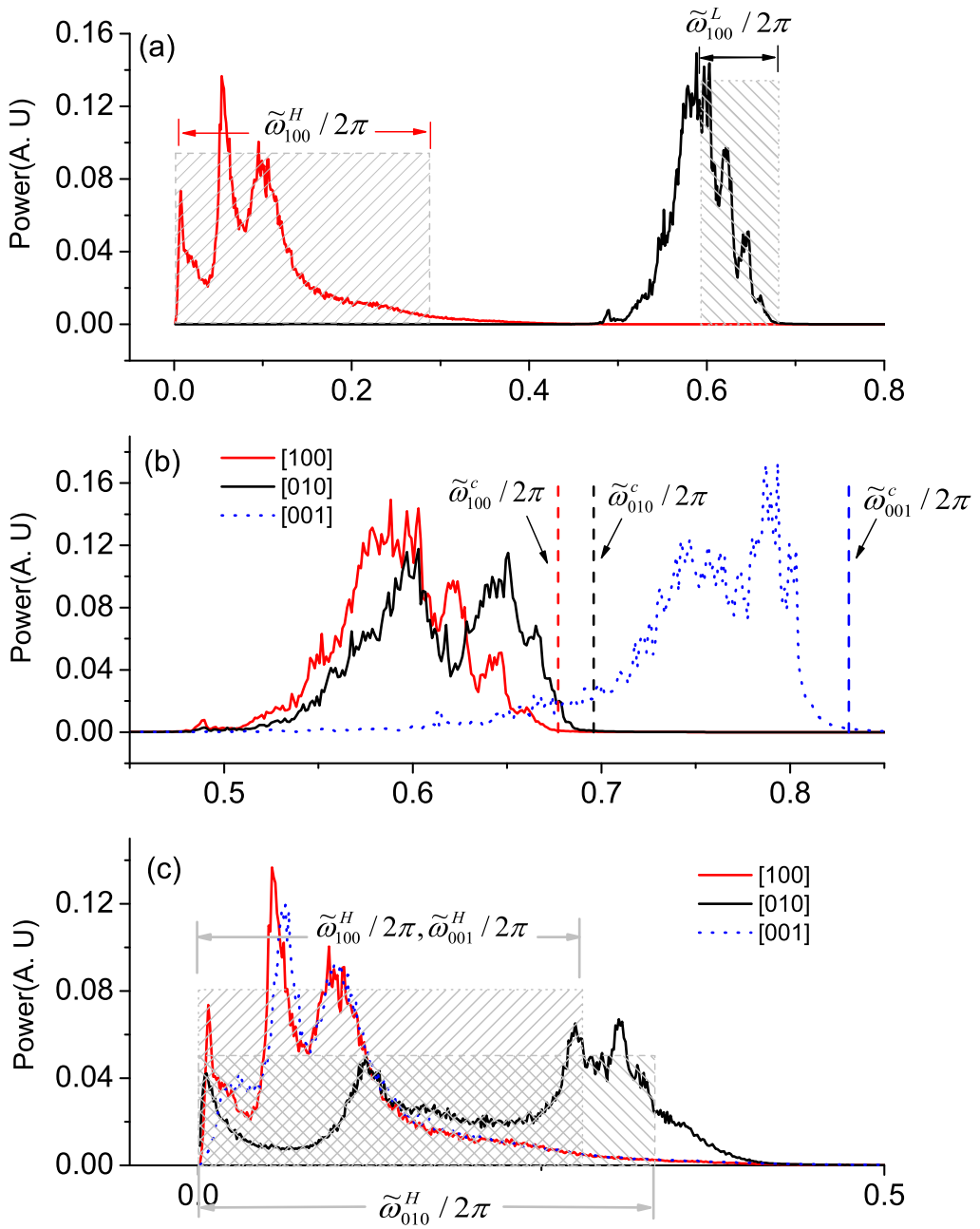

Figure 4.5: Vibrational spectra of the 3D FK model and the comparison between analytical results and numerical ones. Curves are from DFFT. Analytical ones are given by the shadow boxes. (a) Curves are the vibrational bands obtained by DFFT of velocity in the [100] direction at the low- (left curve) and high-temperature limits (right curve). (b) Vibrational band from each direction at the low-temperature limit. (c) Vibrational band from each direction at the high-temperature limit. The vertical lines in (b) are the uppers bounds of the theoretical prediction.

the analytic and numerical bands in one direction at two limits in Fig. 4.5(a). The bands in three directions at a relatively low kinetic energy are shown in Fig. 4.5(b) and at the high-temperature limit in Fig. 4.5(c). The superscript H or L of $\tilde{\omega}$ represents the vibrational band in the high and low temperature limits, respectively. The superscript c of $\tilde{\omega}$ in Fig. 4.5(b) represents the cutoff frequency predicted in the analytic approach. The subscript of $\tilde{\omega}$ means the direction of the corresponding wave vector for the vibrational band. From Fig. 4.5, we can see that our analytic predictions from the two limits (relative high and low-temperature limits) covers the numerical vibrational band very well.

4.2.2 Vibrational Spectra of the FPU part in Different Directions

In this section, we study the bands in a 3D FPU model. To be self-consistent we start from the 1D FPU. Recently, Li *et al.* [39] introduced an effective phonon band for general 1D nonlinear lattices, from which one can obtain the effective phonon frequency

$$\tilde{\omega}_K^2 = \alpha(\omega_K^2 + \gamma). \tag{4.24}$$

For the FPU model, we have

$$\begin{aligned} \alpha =& \frac{\langle \sum_{i=1}^{N} (\delta x_{i,i+1})^2 \rangle + \langle \sum_{i=1}^{N} (\delta x_{i,i+1})^4 \rangle}{\langle \sum_{i=1}^{N} (\delta x_{i,i+1})^2 \rangle} \\ =& 1 + \frac{\int_{-\infty}^{\infty} \phi^4 e^{-V/T} d\phi}{\int_{-\infty}^{\infty} \phi^2 e^{-V/T} d\phi}, \end{aligned} \tag{4.25}$$

$\gamma = 0$ for a system without on-site potential, $\omega_K = 2\sqrt{ksin(K\pi/N)}$ is the spectrum of harmonic oscillators and T is the system temperature. For the FPU model, $V = k_{FPU}(x^2/2 + x^4/4)$. In the high-temperature limit, the quartic term is dominant. We may neglect the 2th order term of the interaction when considering the second term of α and substitute $\mathbb{V} = k_{FPU}x^4/4$ into the integral of it in Eq. (4.25). We can

thus obtain an approximate expression for α,

$$\begin{aligned}\alpha &\cong 1 + \frac{\int_{-\infty}^{\infty} \phi^4 e^{-k_{FPU}\phi^4/4T} d\phi}{\int_{-\infty}^{\infty} \phi^2 e^{-k_{FPU}\phi^4/4T} d\phi} \\ &\cong 1 + \frac{\Gamma(1/4)}{2\Gamma(3/4)} (\frac{T}{k_{FPU}})^{1/2},\end{aligned} \tag{4.26}$$

where $\Gamma(1/4)/\Gamma(3/4) = 2.958 \approx 3$. So we have

$$\alpha \cong 1 + \frac{3}{2} (\frac{T}{k_{FPU}})^{1/2}. \tag{4.27}$$

Thus the effective phonon bands of the FPU model can be written as

$$\begin{aligned}\tilde{\omega}_K^2 &= \alpha \omega_K^2 \\ &\cong 4(k_{FPU} + \frac{3}{2}(T k_{FPU})^{1/2}) \sin^2(K\pi/N).\end{aligned} \tag{4.28}$$

Therefore, the effective phonon band of the 1D FPU model under different temperatures and interaction constants is

$$0 < \tilde{\omega}_{FPU} < 2\sqrt{k_{FPU} + \frac{3}{2}(T k_{FPU})^{1/2}}. \tag{4.29}$$

Even though the second term of α is obtained under the high-temperature limit and in spite of its eventually simple form, it gives a very good agreement with the numerical results at arbitrary interaction constant and temperature in our investigation, $0 < k_{FPU} < 1$, $0 < T < 0.5$, as shown in the Fig. 4.6.

If we calculate the band directly from Eq. (4.29), we obtain that $\tilde{\omega}_{FPU}^L \in [0, 1.03]$ at $T = 0.01$ and $\tilde{\omega}_{FPU}^H \in [0, 1.35]$ at $T = 0.15$. For comparison, we also draw the theoretical prediction given in our previous work [62], in which the vibrational band for the FPU model in the low-temperature limit is $\tilde{\omega}_{FPU}^L \in [0, 0.89]$, and compare with the numerical result at $T = 0.01$, while in the high-temperature limit $\tilde{\omega}_{FPU}^H \in [0, 0.94]$. A comparison among the two predictions and numerical results is shown in Fig. 4.6. The lower boxes cover the numerical curves very well. We can see that the prediction by Eq. (4.29) is much better than the prediction by the previous work [62].

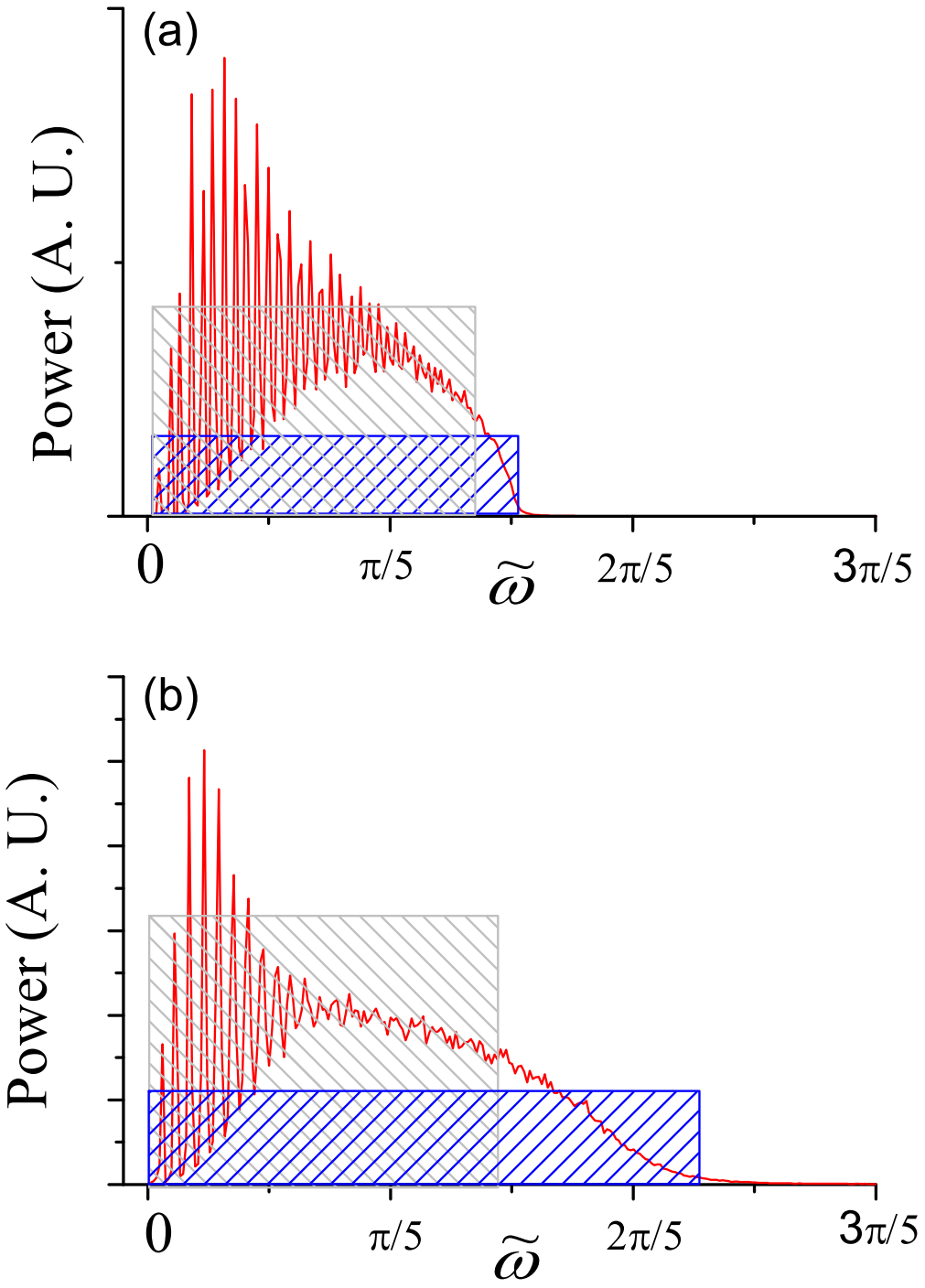

Figure 4.6: Spectra of 1D FPU model at low (a) and high temperature (b). Higher hatched boxes are spectra of the 1D FPU model given in Ref. [62]. Lower hatched boxes are spectra given in Eq.(4.28) and curves are numerical results by DFFT. $k_{FPU} = 0.2$. $T =$ (a) 0.01 and (b) 0.15. The agreement between the analytical and numerical results is very good.

The analysis of the effective phonon bands is also suitable for the 3D case. The interaction potential in the Hamiltonian of the 3D FPU in Eq. (4.4) consists of three individual parts and each part has the same form as in the 1D case when we neglect the energy interchange among different directions. We can write the Hamiltonian as:

$$\begin{aligned} H_{FPU} &= H_{100} + H_{010} + H_{001} \\ H_{100} &= \sum_{l=1}^{N_X}\sum_{m=1}^{N_Y}\sum_{n=1}^{N_Z}(\frac{(v_x)_{l,m,n}^2}{2} + kV(|\vec{r}_{l+1,m,n;l,m,n}| - a_0) \\ H_{010} &= \sum_{l=1}^{N_X}\sum_{m=1}^{N_Y}\sum_{n=1}^{N_Z}(\frac{(v_y)_{l,m,n}^2}{2} + kV(|\vec{r}_{l,m+1,n;l,m,n}| - a_0) \\ H_{001} &= \sum_{l=1}^{N_X}\sum_{m=1}^{N_Y}\sum_{n=1}^{N_Z}(\frac{(v_z)_{l,m,n}^2}{2} + kV(|\vec{r}_{l,m,n+1;l,m,n}| - a_0). \end{aligned} \tag{4.30}$$

In this way, the Hamiltonian has been divided into three parts. Each part contains the kinetic energy along one primitive axis and the interaction potential among particles originally sited on the corresponding primitive axis. Since $V(r)$ has the exact same form as $V(x)$ in one dimension, we can infer that the effective phonon band along each primitive axis is same as in the 1D case.

The effective phonon bands in the X, Y, and Z directions from numerical results and the theoretical predictions are plotted in Fig. 4.7. We can see that the theoretical predictions by Eq. (4.28) agree with the numerical results very well in the 3D case. The slight difference might come from the different boundary conditions.

4.2.3 Match and Mismatch of Bands of Two Parts

From the above analysis, we see that the vibrational bands of the 3D FPU lattice always concentrate in the low-frequency region as in low-dimensional cases. In contrast, the 3D FK lattice has two main branches, which correspond to low and high-temperature limits, respectively, and the two regions separate from each other when the parameters are chosen appropriately. Therefore, by choosing suitable parameters, it is possible to match and mismatch the bands of the two parts when

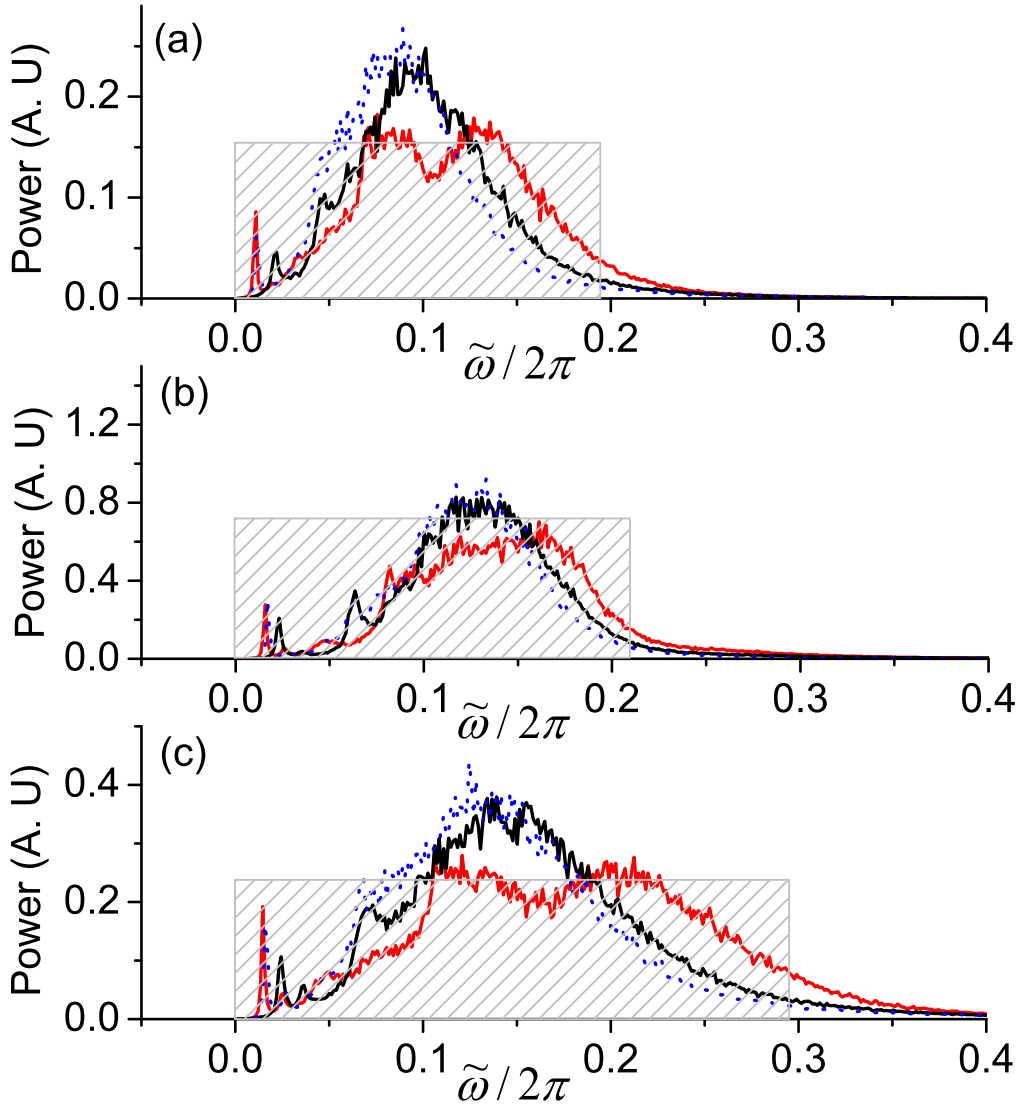

Figure 4.7: Spectra of 3D FPU model with different parameters. (a) $T = 0.04$ and $k_{FPU} = 0.2$. (b) $T = 0.15$ and $k_{FPU} = 0.2$. (c) $T = 0.1$ and $k_{FPU} = 0.5$. Boxes are spectra of the 3D FPU model given by theoretical prediction in Eq. (4.28) and curves are numerical results by DFFT.

swapping the temperature at the two ends, thus leading to good thermal rectification. In this section, we show how to select suitable parameters of the system and suitable temperatures on the system to obtain the best rectification.

In Fig. 4.8, we show how the bands of the FK and FPU lattices change with the system parameters. In Figs. 4.8(b) and 4.8(c), we can see that the width and position of the vibrational band of the FK part change with the barrier height of the substrate potential and system temperature. In Fig. 4.8(b), the spectra broaden from the low to the high-frequency region when the barrier height increases. However, in Fig. 4.8(c), the spectra shift from the high to the low-frequency region when the temperature is increased. The physical mechanism here is clear. When A_0 is small, the particles have large enough kinetic energies to jump out of the potential valleys. The substrate potential becomes negligible. The FK lattice degenerates to a harmonic one. When we increase the barrier height A_0, the substrate becomes dominant and the particles are confined in the valley of the substrate potential. Thus the atoms oscillate at very high frequency. In Fig. 4.8(c), we fix the barrier height and change temperature. At low temperature the substrate is dominant; thus the particles are confined in the valley of the substrate. When we increase the temperature, the kinetic energy of the particles becomes larger and larger. It eventually becomes dominant compared with the effect from the substrate. So, when the temperature is increased, the main part of the spectrum shifts from high frequency (substrate is dominant) to low frequency (kinetic energy is dominant).

In Figs 4.8(d)-4.8(f), we show the spectra of the FPU lattice. In Fig. 4.8(d), the slight difference among the bands from each direction should come from the different boundary condition in each direction, as we analyzed previously. In Figs. 4.8(e) and 4.8(f), we show how the bands change with temperature and interaction constant. We can see that the band becomes broader and broader as the temperature and interaction constant are increased. This result is consistent with our theoretical analysis.

From the above analysis, we can write the effective phonon band of the FK part in one formula as $\sqrt{C} < \tilde{\omega}^i < \sqrt{4k_{FK} + C}$, where $C = C_n^i$ $(n > 1)$ in the

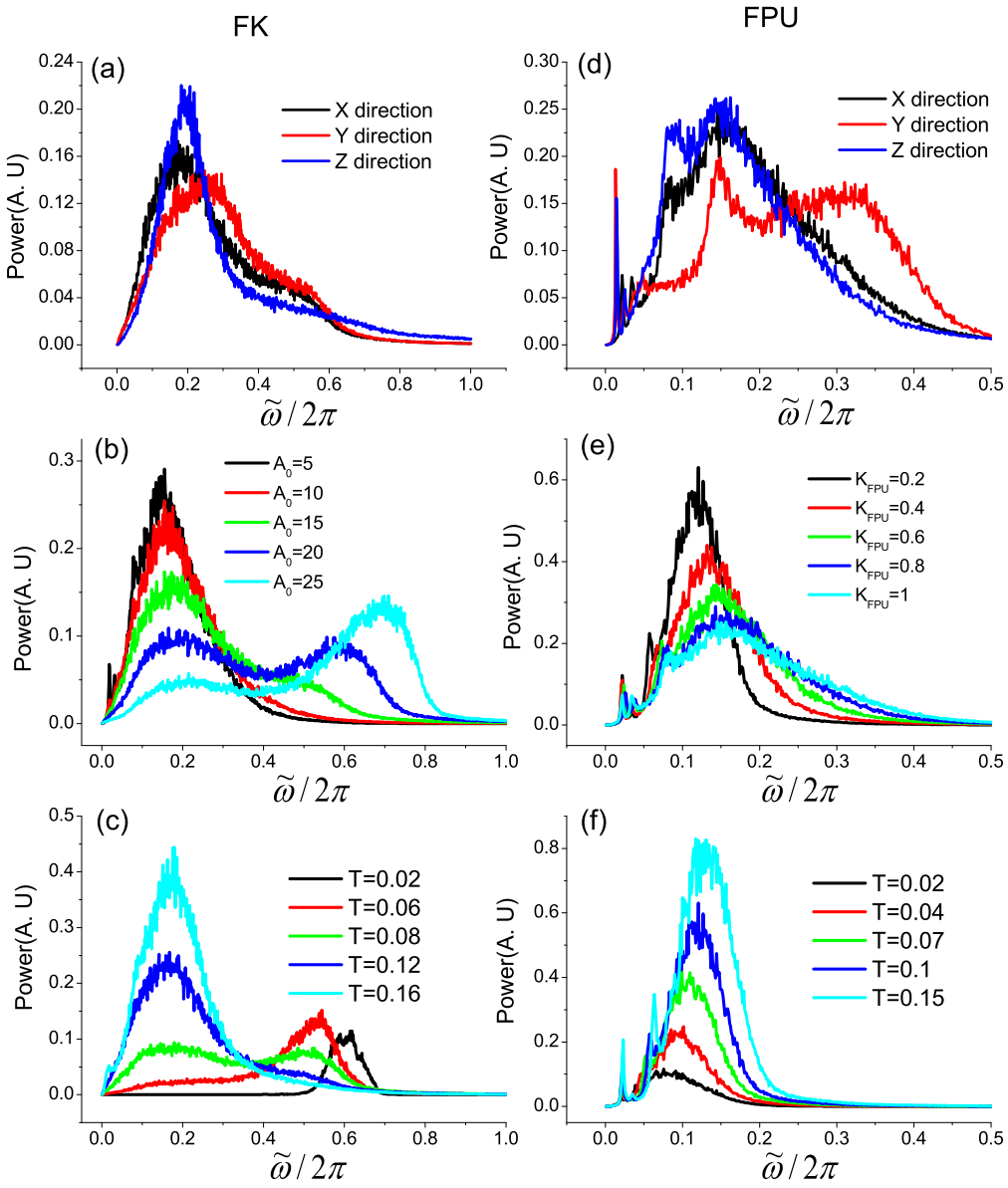

Figure 4.8: (a),(b),(c) Vibrational spectra of the 3D FK lattice under different conditions. (d),(e),(f) Spectra of the 3D FPU lattice under different conditions. (a) and (d) are vibrational spectra in the X, Y, Z directions with $T = 0.1$, $A_0 = 15$, $K_{FPU} = 1$. (b) and (e) are vibrational spectra along the X direction with different parameters such as A_0, K_{FPU}, with fixed temperature $T = 0.1$. (c) and (f) are vibrational spectra along the X direction at different temperatures with fixed parameters $A_0 = 15$, $K_{FPU} = 0.2$.

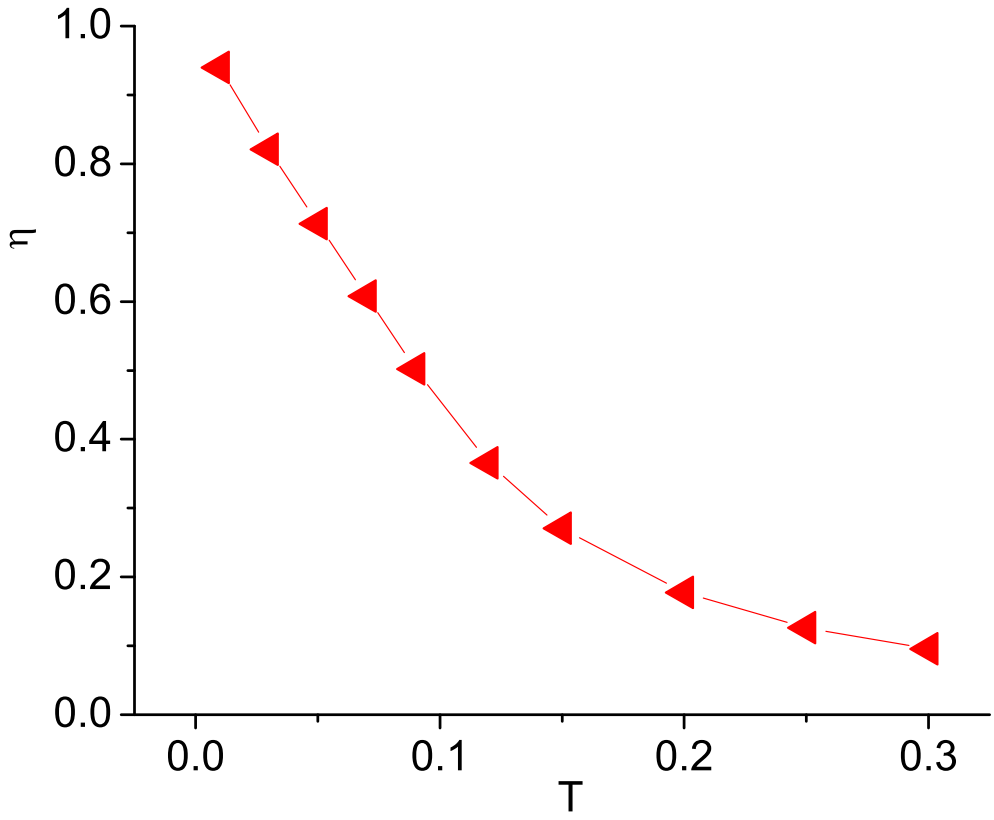

Figure 4.9: Nonlinearity parameter η [refer to Eq. (4.31) for definition] versus temperature.

high-temperature limit and $C = C_1^i$ (a finite value only related with barrier height) in the low-temperature limit. C_n^i decreases to zero asymptotically very fast. For example, $C_3^i \approx 0.00137 C_1^i$ and $C_2^i \approx 0.0156 C_1^i$. From these two limits, we can see that C is temperature dependent. We will show that it decreases with increasing temperature. This is consistent with previous studies [60] of the 1D model.

Figures. 4.8(b) and 4.8(c) tell us that the gap C depends on temperature and barrier height. Therefore, we may write it as $C(T, A_0)$. The upper limit of $C(T, A_0)$ is determined by A_0 through Eq. (4.18), and $C(T, A_0)$ decreases monotonically to

zero with temperature. Following a similar concept introduced in Ref. [40], we define a quantity η to describe the nonlinearity due to the substrate,

$$\begin{aligned} \eta &= \frac{\varepsilon_s}{\varepsilon_s + T} \\ \mathfrak{C}(T) &= \eta C_{up}(A_0), \end{aligned} \tag{4.31}$$

where $\varepsilon_s = \langle V_s \rangle$ is the temporal average of the substrate potential, which has different values at different temperatures, and $C_{up}(A_0)$ is the upper limit of the gap. In this way, the quantity $\mathfrak{C}(T)$ has the same behavior as the gap $C(T, A_0)$ as temperature changes, and they have exact the same values in the two limits (high- and low-temperature limits). The behavior of η with temperature is shown in Fig. 4.9. It decreases from a finite value to 0 asymptotically as temperature increases. Thus we may use $\mathfrak{C}(T)$ to approximate the gap $C(T, A_0)$. We can then obtain the effective phonon band of the FK model under different temperatures and parameters,

$$\sqrt{\mathfrak{C}(T)} < \tilde{\omega}_{FK} < \sqrt{4k_{FK} + \mathfrak{C}(T)}, \tag{4.32}$$

where $\mathfrak{C}(T)$ is determined by Eq. (4.31). In Fig. 4.10, we show the spectra from Eq. (4.32) at two limits and the numerical one obtained by DFFT.

For the FK lattice, the spectra in the low- and high-temperature limits separate from each other, while in the FPU lattice, the spectrum always concentrates at low frequency. So when the left part is at high temperature and the right part is at low temperature, the vibrational bands of the two parts are matched with each other as shown in Fig. 4.11(a). When swapping the temperatures of the two parts, the bands of the two parts are mismatched with each other as shown in Fig. 4.11(b). In terms of the match or mismatch of the bands when changing temperature under suitable parameters, the system should have strong rectification since matched bands indicates a large heat flux along the system and mismatched bands inhibits heat flux along it. In the following part, we will give numerical evidence to support the above analysis.

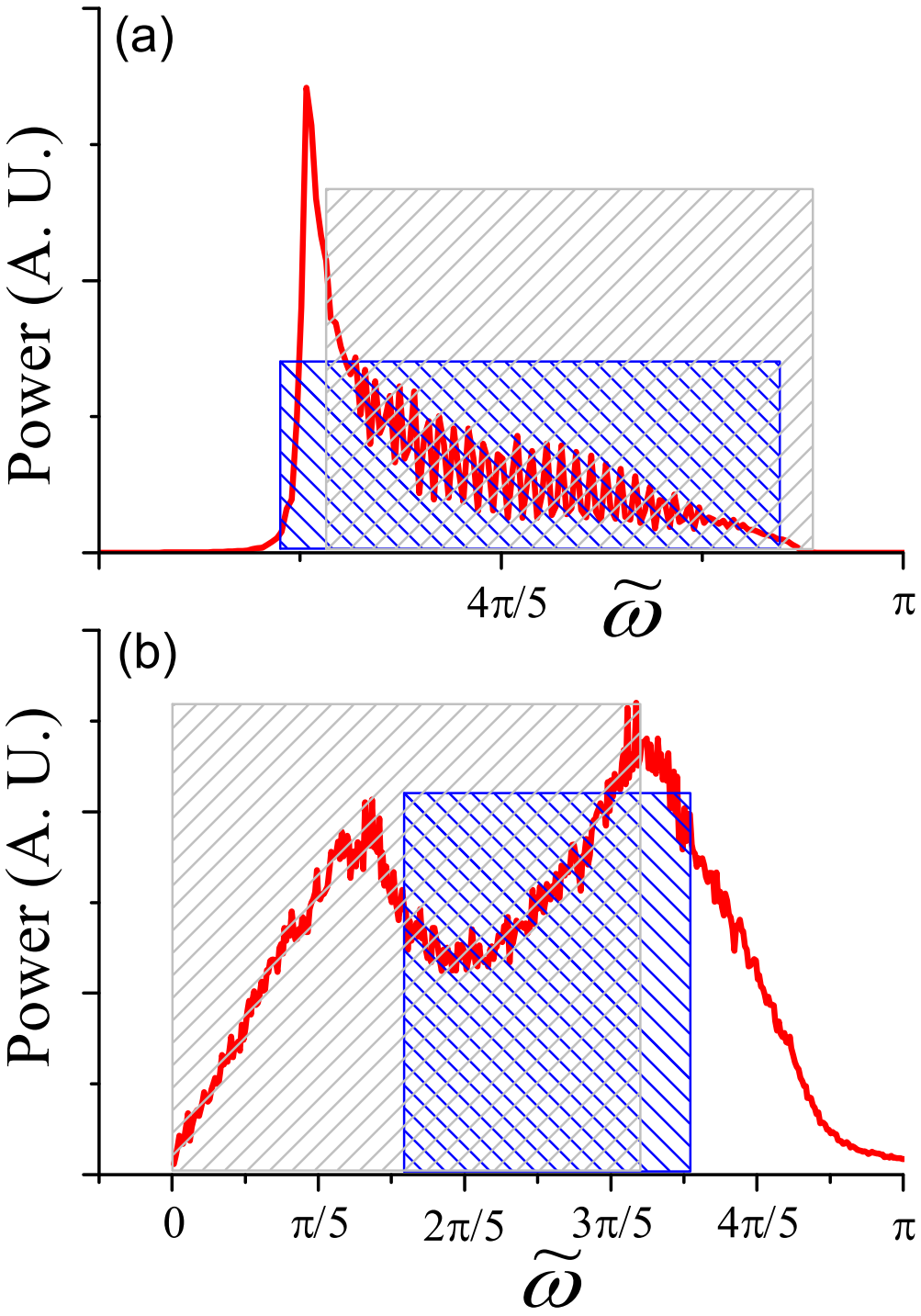

Figure 4.10: Spectra of 1D FK model at different temperatures. T =(a) 0.01 and (b) 0.15. High hatched boxes are spectra given in Ref. [62] at the low- and high-temperature limits. Lower hatched boxes are spectra given by Eq. (4.31) and curves are numerical results by DFFT.

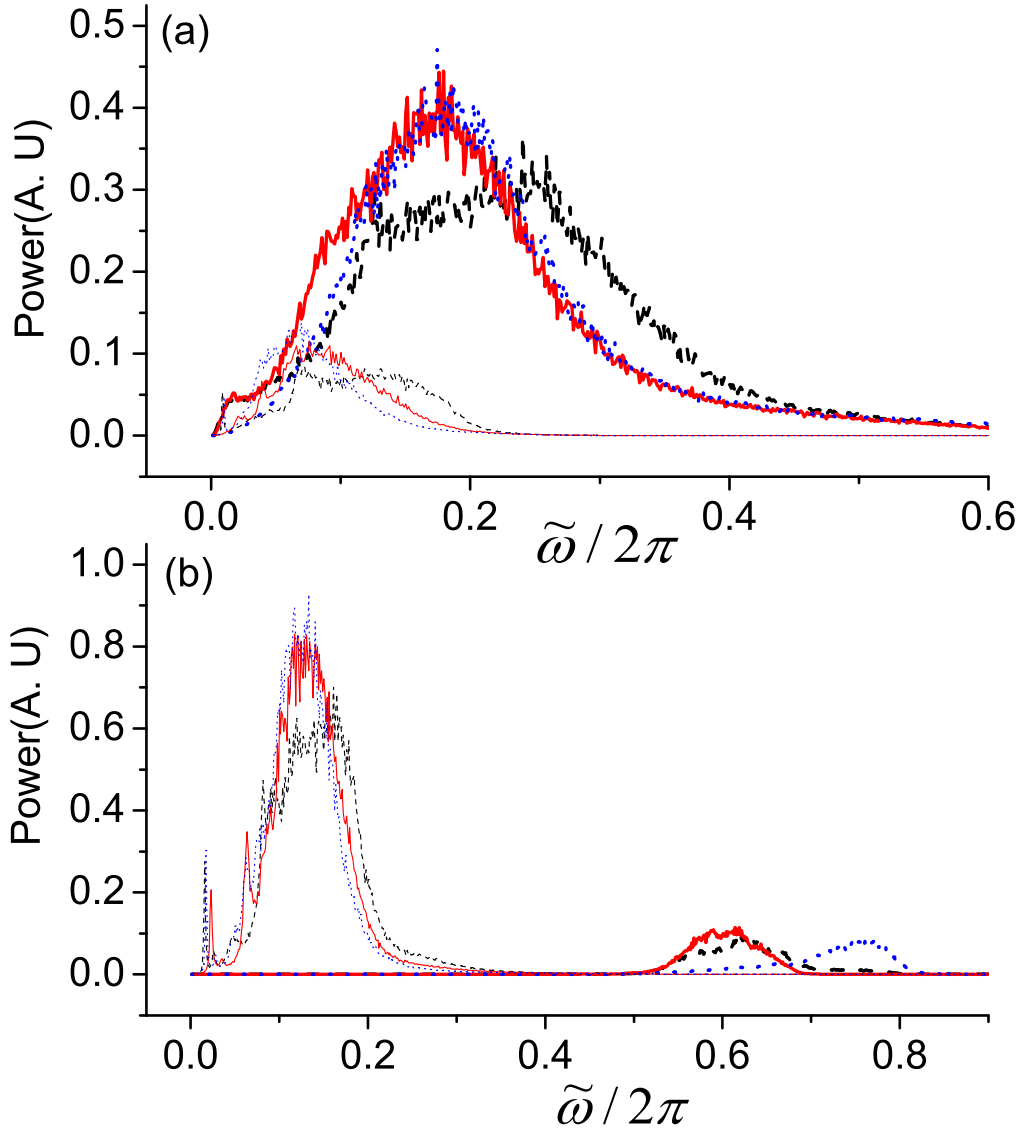

Figure 4.11: Matched (a) and mismatched (b) vibrational spectra in the X, Y, Z directions of the two parts with different parameters $A_0 = 15$, $K_{FPU} = 0.2$. (a) T_L=0.15, $T_R = 0.02$ and (b) T_L=0.02, $T_R = 0.15$. In (a) the upper three curves are for the FK model, the lower three curves are for the FPU. In (b), the left three curves are for the FPU and the right three curves are for the FK model. Thick curves are for the FK part and the thin curves for the FPU part. Black, red and blue curves are for the X, Y, and Z directions, respectively.

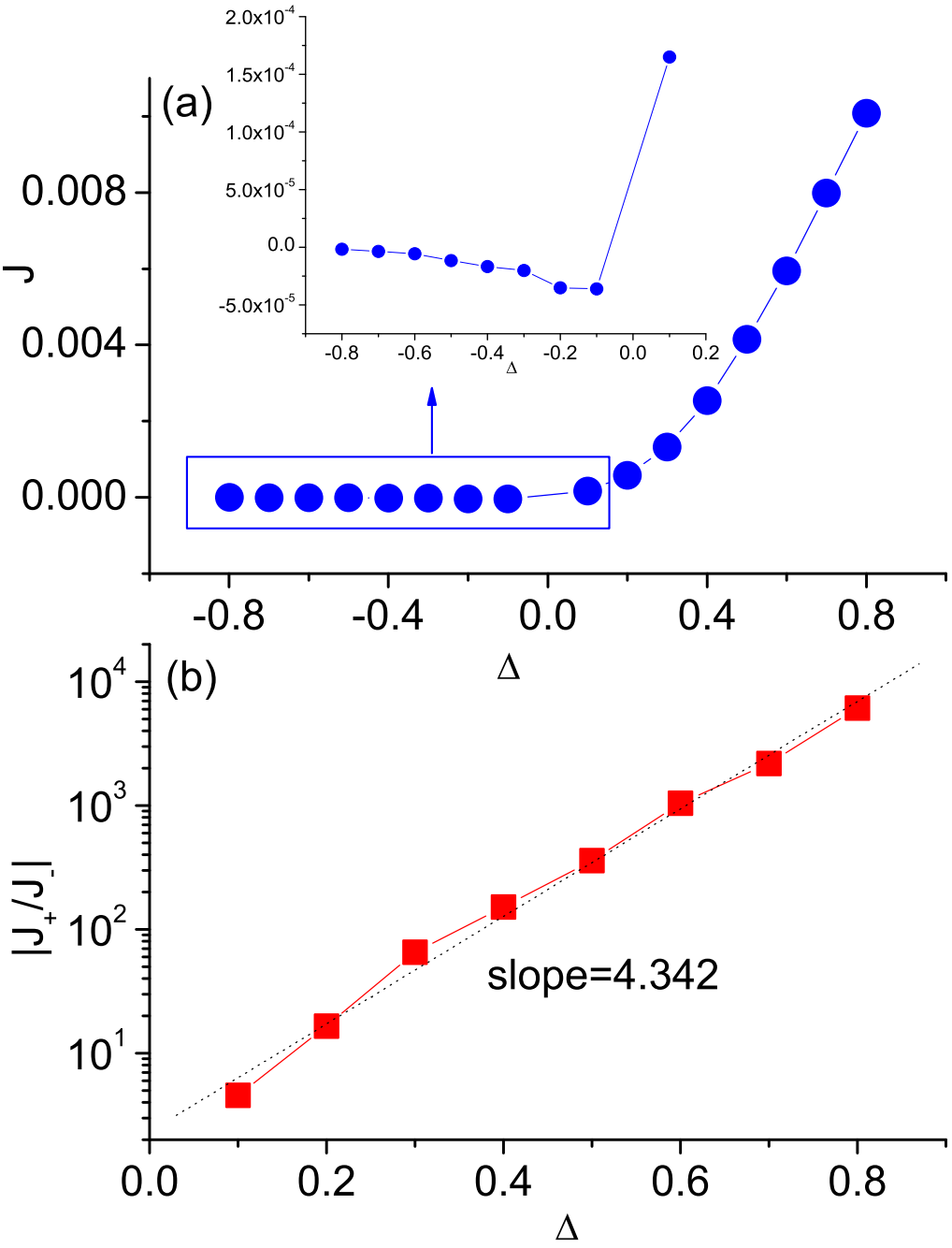

Figure 4.12: (a) Heat current J versus the dimensionless temperature difference Δ at temperature $T_0 = 0.06$. (b) Rectification $|J_+/J_-|$, versus dimensionless temperature difference. The dotted line has a slope of 4.342. In our numerical simulation, $N_X = 12, N_Y = 6$, and $N_Z = 3$.

4.3 Rectifying effect in 3DFK-FPU model

After theoretical analysis of the vibrational spectra, we select $A_0 = 15$, $k_{FK} = 1$, and $k_{FPU} = 0.2$. We denote the temperature as $T_L = T_0(1-\Delta)$, $T_R = T_0(1+\Delta)$. So T_0 is the system average temperature and Δ is the normalized temperature difference.

In Fig. 4.12, we show the heat flux and rectification versus Δ. The ratio of heat fluxes, $|J_+/J_-|$ the rectification, can be as much as several thousands. Some properties observed in 1D and 2D are still observable in the 3D case. The exponential dependence of the rectification on the normal temperature is also true. For negative Δ, we clearly see the decrease of $|J_-|$ as $|\Delta|$ increases. This interesting phenomenon, so-called *negative differential thermal resistance*, is a typical phenomenon in nonlinear lattices. It is very essential for the design of thermal transistor [68]. Therefore, one also expects that the 1D thermal transistor model can be extended to higher dimensions.

The exponential dependence of rectification on Δ obeys the following formula:

$$|J_+/J_-| \propto \exp(c\Delta), \tag{4.33}$$

where $c = 4.342$ is different from the coefficient found in the 2D case [65].

In Fig. 4.13, we show how the rectification changes with the system temperature. As in the low-dimensional case, there exists an optimum temperature under which the system has the largest rectification. Away from the optimum temperature, the rectification decreases. But the effective temperature region is very broad. W_T is the quantity defined as the width of the effective temperature range T_e over half the value of the largest rectifying efficiency. It is about 0.04 in this case.

In Fig. 4.13(b), we keep the absolute temperature difference as a constant $|T_L - T_R| = 0.06$ and change the system temperature $T_0 = (T_L + T_R)/2$. From this figure, we can see that with this kind of temperature difference, the system works very well at low temperature.

Finally, we show the dependence of rectification on the system size. We change the number of particles along the direction perpendicular to the temperature gradient, the Y direction, and the Z direction (perpendicular to the contact plane

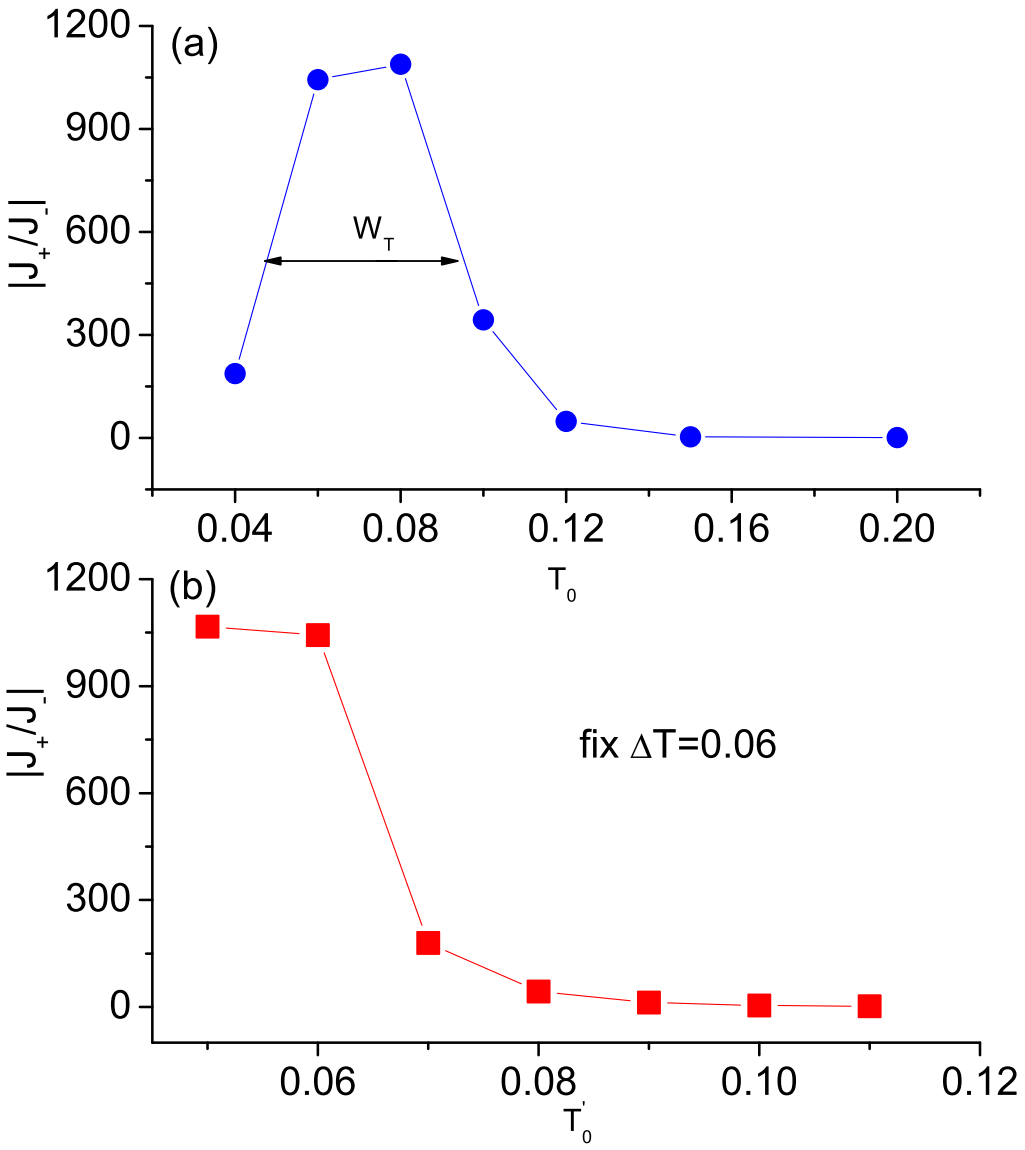

Figure 4.13: (a) Rectification versus temperature T_0 when fixed $\Delta = 0.5$. (b) Rectification versus system temperature T_0 by fixing the temperature difference $T_L - T_R = 0.06$. $T_0 = (T_L + T_R)/2$, $\Delta = (T_L - T_R)/(2T_0)$. In our numerical simulation, $N_X = 12, N_Y = 6$, and $N_Z = 3$.

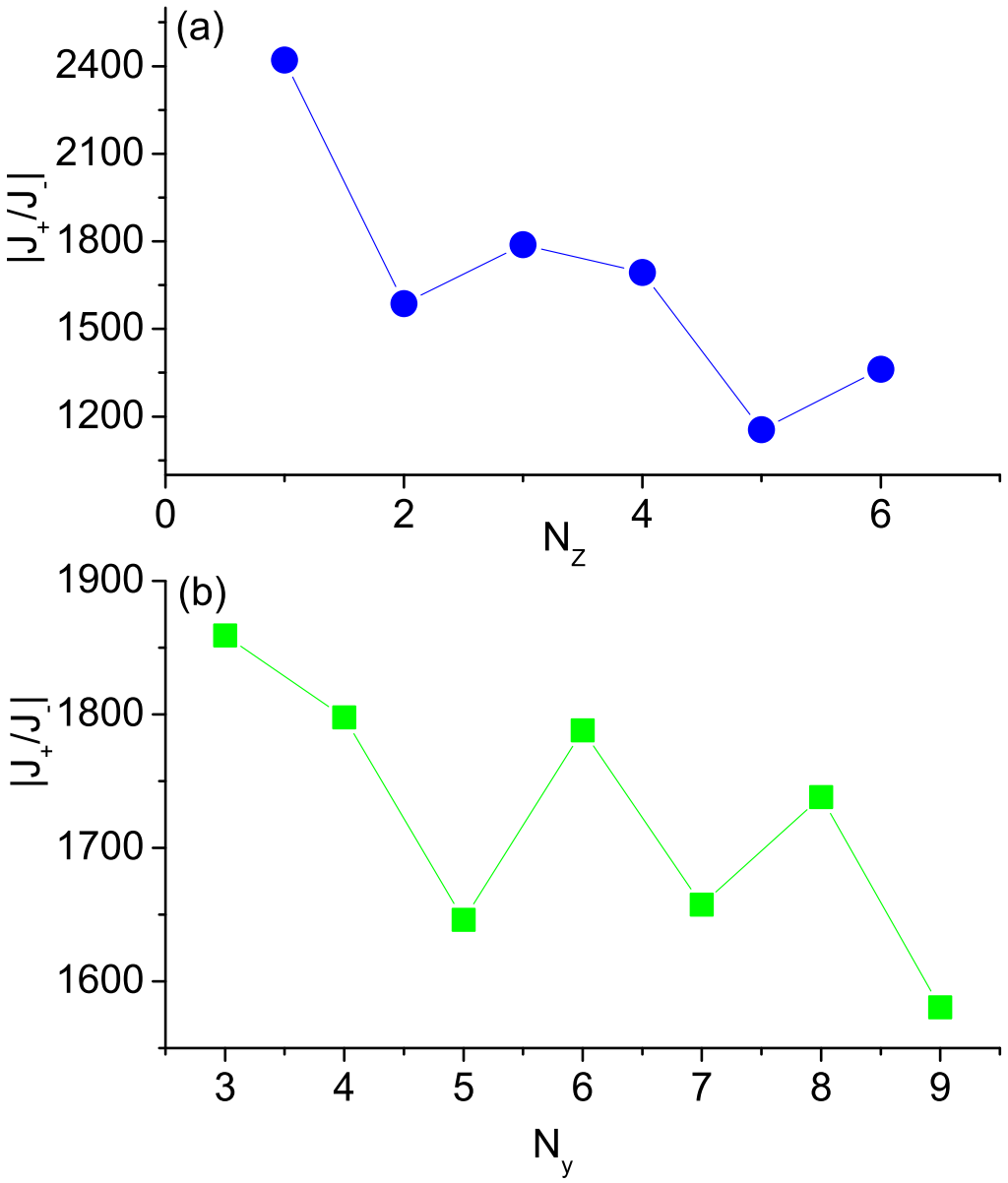

Figure 4.14: (a)Thermal rectification versus the number of particles along the Z direction. $N_X = 12, N_Y = 6$. (b)Thermal rectification versus the number of particles along the Y direction. $N_X = 12, N_Z = 3$.

with substrate). In Fig. 4.14, the rectification decreases slowly as the system size increases. From the phonon bands theory and the relationship between the rectification and the convolution of bands from the two parts, which was obtained in our previous work [62,65], the decreasing trend should stop at a certain system size since the increase of the system size along the direction perpendicular to temperature gradient will not change the temperature jump at the interface. The vibrational bands of the two parts will tend to the theoretical prediction as the system size increases. We should point out that the oscillation of the rectification in our results is due to the fluctuation of J_{-}, because its amplitude is too small.

4.4 Conclusion

In this Chapter, we have proposed a 3D efficient thermal diode which consists of layered harmonic oscillators coupled with the substrate, namely, a 3D FK lattice, and the other part is the 3D FPU model. First of all, we have studied analytically and numerically the vibrational spectra for both the 3D FK and 3D FPU models. For the FK model, the band is concentrated in the high-frequency region, which is mainly induced by the substrate in the low-temperature limit, and shifts to the low-frequency region on increasing temperature; while for the FPU model, the band broadens from a harmonic band slowly as the temperature increases.

The different temperature dependence of the bands makes the transition from matched band to mismatched band possible when swapping temperature at the two ends and consequently makes it possible to realize thermal rectification.

From energy band theory we know whether an excitation of a given frequency can be transported through a mechanical system depends on whether the system has a corresponding eigenfrequency. If the frequency matches, the energy can be easily go through the system, otherwise, the excitation will be reflected. From our analysis, we know the role of substrate is to induce a gap at zero wave-number. That makes it possible for the transition from the matched band to mismatched band in each direction when considering the substrate in real space. However if

we only consider the substrate in lower dimension the transition of the match and mismatch of bands can only occurs along directions coupled with substrate while in the direction without substrate the energy can always go through fluently. This is because particles without on-site potential always oscillate with low frequency. The fluent flowing of heat energy in one or two directions will make it very difficult to increase thermal efficiency.

Chapter 5

Discussion and Conclusions

The main objective of this thesis is to build up an efficient thermal rectifier by coupling two dissimilar ahharmonic lattices and to generalize it from a 1D to 3D system. We show that, because of anharmonic terms, the width and position of an "effective" phonon band depend on temperature. By tuning the anharmonicities of two different coupled chains it is possible to control the effective overlap between the phonon bands of the two chains. In particular, the extent of this overlap can be made to depend on the sign of the imposed thermal gradient, thus leading to thermal rectification.

The components of our models are two representative anharmonic lattices: the Frenkel-Kontorova lattice and the Fermi-Pasta-Ulam lattice. The FPU model is a representative anharmonic lattice without on-site potential and the FK model is the one with on-site potential. Both models have been widely used to study different problems in condensed matter physics and nonlinear dynamics [84, 85].

The underlying mechanism in our two-segment model is summarized in Fig. 5.1. The transition from matched bands to mismatched bands is due to different temperature dependence of different segments. As shown in Fig. 5.1, the left part has a broad band in high-temperature limit and shifts to a narrow high-frequency region at low-temperature limit; while the band of the right part broadens slowly as temperature increases. So when the high temperature is added at the left part and low temperature is added at the right part, the broad band of the left part

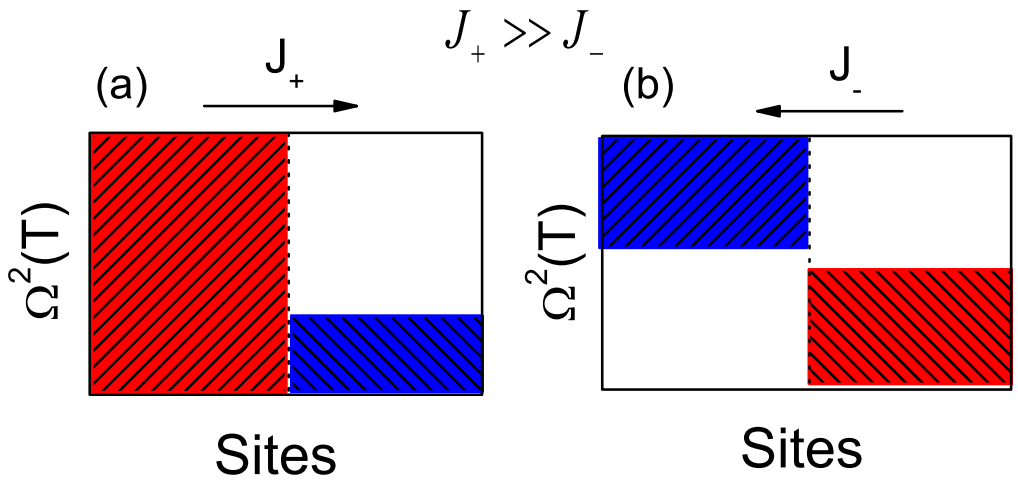

Figure 5.1: Schematic picture of the phonon bands in our work [62, 65, 66]. The bands in the left and right anharmonic regions change with temperature. (a)When high temperature is added on the left end, the spectra of the two regions matched with each other. (b) when high temperature is added on the right end, the spectra of the regions separate with each other.

matches the one from the right part as shown in Fig. 5.1(a). In this situation, heat flux can go through the system fluently with a large value. However when reversing the temperature at the two parts, the band of the left band will contract to a high-frequency region and the band of the right band broadens but still concentrates in a low-frequency region. The total effect is the separation of the two bands as shown in Fig. 5.1(b). In this situation, heat flux was inhibited by the mismatched bands with a very small value.

Here, we should point out that the asymmetric phenomenon we observed in this Ph.D project is very general in system with asymmetric geometries. The rectifying effect in available rectifiers [60–65, 67]comes from asymmetry between different segments. In our two-segment model, the sensitive dependence of vibrational bands on temperature and the big temperature jump at the interface make the strong rectifying effect possible. The rectification is general from few hundreds to few thousands.

In the first part of the study, we establish strong rectifying effect in the 1D model [62]. By replacing one segment with a Fermi-Pasta-Ulam (FPU) lattice, the

rectification can be improved to 2,000, namely one order of magnitude better than the two-segment FK model [61]. We found that the rectification, or asymmetric heat flow, results from an asymmetric thermal interface resistance - Kapitza resistance. By investigation the thermal resistance in the interface, we found that Kapitza resistance also demonstrates strong directional effect and Kapitza thermal resistance (interface thermal resistance) has the major contribution to the total thermal resistance. So we may say that the strong rectifying effect on heat flux in our model is mainly determined by strong asymmetric Kapitza thermal resistance in the interface.

In order to understand the physical mechanism of this asymmetric phenomenon, we studied vibrational bands of the two segments at different temperature numerically. We found that the bands of the two segments sensitively depend on temperature. So when we swap the temperature at the two ends, the bands of the two segments change from matched bands to mismatched bands and the corresponding amplitude of the heat flux changes from a large value to a small value. That means matched bands indicates a large heat flux or small thermal resistance along the system and mismatched bands indicates a small heat flux. So the underlying mechanism for asymmetric heat flux or Kapitza resistance we observed is that the extent of overlap of bands from the two segments is temperature dependent. That makes the transition in our model possible from a thermal conductor to a thermal insulator when we swap temperature gradient.

In the second part of this thesis, a 2D thermal rectifier was extended directly from the 1D model [65]. The performance of the 2D thermal rectifier under different environment changes, such as the system temperature and the temperature difference on the two sides of the system, have been investigated systematically. We find that there exits an optimum performance (OP) for a specific thermal rectifier at certain temperature range. The OP is affected by the boundary condition and the number of particles, N_Y, along the direction vertical to the imposed temperature gradient. The OP shifts to the lower temperature when increasing N_Y or changing the periodic boundary condition to the free boundary condition along the Y direction. The rectification of the 2D thermal rectifier is general several hundreds with

the same parameter settings as in the 1D case.

Another important factor that affects the performance of the thermal rectifier is the temperature difference between the two ends. We find the rectifying efficiency increases approximately as an exponential law in certain temperature range with the temperature difference. The study on the interface thermal resistance shows the similar asymmetric behavior with heat current. The asymmetry behavior of interface thermal resistance and heat current is also found to be induced by the different temperature dependence of the vibrational spectra of the two parts beside the interface. A power law with a different power constant from the one of the 1D thermal rectifier is also found in the 2D rectifier between the rectification and the convolution of the vibrational spectra of the two segments.

In the third part of this thesis, we make a step further, namely, to extend our study to a three-dimensional (3D) model [66]. The 2D FK substrate in our previous work [65] is extended in the vertical direction. The substrate does not only affect the atoms in the contact plane, but also affect the atoms in the direction perpendicular to the contact plane according to Lennard-Jones's attenuation. We provide theoretical analyses of spectra for two representative nonlinear lattices, the 3D FK and the 3D FPU lattices, and make a comparison of spectra with numerical results. We make it clear that the high-frequency vibration induced by the substrate in the FK model is dominant in low-temperature limit and the low-frequency vibration is dominant in high-temperature limit; while the band of the FPU model broadens from a harmonic band slowly as temperature increases. And we provide an effective way to estimate the effect of nonlinearity on the position and width of vibrational band at different temperatures in the FK model. Predictions of suitable parameter settings for an efficient thermal rectifier is given and numerical confirmation is provided.

From our works to control heat current, we know that the success for a thermal rectifier lies on two factors: The first one is the asymmetry of the system; The second one is nonlinearity of the system. The broken of the spatial symmetry is necessary to make the heat flow asymmetric, while the introduction of the nonlinearity allows

us to adjust the parameters to get the vibrational spectra match or mismatch by reverse the temperature gradient.

We make it clear that nonlinearity will modify spectra and induce the dependence of the spectra on the temperature. The modification of nonlinearity from molecular interaction on a vibrational band is a broadening from a harmonic one with temperature as ($0 < \tilde{\omega}_{FPU} < 2\sqrt{k_{FPU} + 3(Tk_{FPU})^{1/2}/2}$). However the modification of nonlinearity from a on-site potential is a shift or a gap at zero wavenumber ($\sqrt{C} < \tilde{\omega}_{FK} < \sqrt{4k_{FK} + C}$) and the width and position of the shifted band depends on the strength of on-site potential (C is temperature dependent). So asymmetric nonlinearity of the system will induce asymmetry dependence of spectra on temperature. This makes it possible to realize rectifying effect by tuning the nonlinearities of different parts.

Moreover we connected the rectifying efficiency with the overlap extent of bands from the two parts by giving an explicit numerical finding (J_+/J_- or $R_-/R_+ \sim (S_+/S_-)^{\delta}$). $S_\pm$ is the normalized convolution of bands from the two parts. The information of asymmetry properties is included in this product.

So far, our numerical investigations and theoretical predictions about rectifying effect are consistent with each other very well. We should point out that our theoretical analysis is general valid for nonlinear models. Our study on thermal rectifying effect in the two dissimilar anharmonic lattices has general meaning since the two anharmonic lattices are two representative ones widely studied in different fields of physics. The FPU model can be regarded as the approximation of molecular interaction at equilibrium of an ideal crystal, while the FK model is to describe the crystal coupled with substrate. Most physical systems can be divided into our two representative models: one with on-site potential and another without on-site potential. We believe our systematical study on thermal rectifier based on these two representative models can provide useful guidance and meaningful suggestion when designing thermal rectifier with other different materials or with different structures.

Our theoretical framework is also suitable to give reliable reference for experimental set-ups of thermal rectifier. For example, a connection of our theoretical

work with a recent - the world first - experimental work on solid-state thermal rectifier is possible. Zettl's group at Berkeley realized the thermal rectification by using carbon nanotubes (CNTs) and boron nitride nanotubes (BNNTs) [101]. The experiment is a basically a two-segment thermal rectifier as we proposed [61, 62]. They introduced the asymmetry by depositing $C_9H_{16}Pt$ on the half part of nanotube with non-uniform mass-loading. The loaded $C_9H_{16}Pt$ can be regarded as substrate. So the loaded part is a segment coupled with substrate and the suspended part is a segment without substrate. Previous studies have demonstrated that the thermal conductivity of 1D CNTs and BNNTs is dominated by phonons [102, 103]. So we can use our theoretical method of phonons to analyze the energy transport in CNTs and BNTs qualitatively.

The experiment can be linked with our theoretical model through $\mathfrak{C}(T) \propto \eta(T)\varepsilon_s/M$ as Eq. (4.31) for the loaded half part, ε_s is the coupling between deposit and tube and M is the mass of the deposit. For the suspended part $k \propto \varepsilon_{ke}/m$, ε_{ke} is the kinetic energy of atoms and m is the corresponding mass. In the experiment, $\varepsilon_s < \varepsilon_{ke}$ and $M > m$, while $\eta(T)$ is a value from 0 to 1. So the total effect is that $\mathfrak{C}(T)$ is much smaller than k. From our previous investigation, we know the directional effect is mainly induced by the drastic change of $\mathfrak{C}(T)$. If we substitute the small $\mathfrak{C}(T)$ and relatively large k into Eq. (4.32), we can see clearly that it is very hard to result in the significant difference of spectra of the loaded part when swapping heat baths on the two ends. The above two main fundamental drawbacks make it difficult to realize significant rectifying effect. In the experiment, the rectification is less than 10%.

Possible realization of our current 3D model might be the half suspend nanowire and/or nanorod. We can put the nanowire/nanorod on a substrate of semiconductor which will induce an on-site substantial, while another half of the nanowire/rod is suspend in the vacuum [104].

Bibliography

[1] H. C. Von Baeyer, *Warmth Disperses and Time Passes C the History of Heat*, (New York: The Modern Library, 1998).

[2] E. Mendoza, *Reflections on the Motive Power of Fire*(1988) C E. Clapeyron and R. Clausius, other Papers on the Second Law of Thermodynamics. (New York: Dover Publications, Inc.).

[3] S. R. De Groot and P. Mazur, *Non-Equilibrium Thermodynamics*, (Dover, New York, 1984); *Mathematical physics*, (Imperial College, London, 2000).

[4] F. Bonetto, J. Lebowitz, and L. Rey-Bellet, in *Mathematical Physics 2000*, edited by A. Fokas, A. Grigoryan, T. Kibble and B. Zegarlinski (Eds.). (Imperial College Press, London, 2000), p.128.

[5] H. Matsuda and K. Ishii, Suppl. Prog. Theor. Phys. **45**, 56 (1970)

[6] A. Casher and J. L. Lebowitz, J. Math. Phys. **12**, 1701 (1971).

[7] R. J. Rubin and W. L. Greer, J. Math. Phys. **12**, 1686 (1971).

[8] A. J. O'Conner and J. L. Lebowitz, J. Math. Phys. **15**, 692 (1974).

[9] H. Spohn and J. L. Lebowitz, Commun. Math. Phys. **54**, 97 (1977).

[10] M. Toda, Phys. Rep. **18C**, 1 (1975).

[11] M. Toda, Phys. Scr. **20**, 424 (1979).

[12] M. Toda, *Theory of Nonlinear Lattices*, Springer Series in Solid-State Sciences **20** (Springer, Berlin, 1981).

[13] Z. Rieder, J. L. Lebowitz, and E. Lieb, J. Math. Phys. **8**, 1073 (1967).

[14] R. E. Peierls, *Quantum theory of solid* (Oxford University Press, London, 1955).

[15] E. Fermi, J. Pasta, and S. Ulam, in collected papers of E. Fermi, University of Chicago Press, Chicago, **2**, 78 (1965)

[16] G. Casati, J. Ford, F. Vivaldi, and W. M. Visscher, Phys. Rev. Lett. **52**, 1864 (1984).

[17] T. Prosen and M.Robnik, J. Phys. A **25**, 3449 (1992).

[18] H. Kaburaki and M. Machida, Phys. Lett. A **181**, 85 (1993).

[19] A. Fillipov, B. Hu, B. Li, and A. Zeltser, J. Phys. A **31**, 7719 (1998).

[20] K. Aoki and D. Kusnezov, Phys. Rev. Lett. **86**, 4029 (2001).

[21] S. Lepri, R. Livi, and A. Politi, Phys. Rev. Lett. **78**, 1896 (1997).

[22] S. Lepri, R. Livi, and A. Politi, Europhys. Lett. **43**, 271 (1998).

[23] S. Lepri, Phys. Rev. E **58**, 7165 (1998).

[24] S. Lepri, R. Livi, and A. Politi, Phys. Rev. E **68**, 067102 (2003).

[25] B. Hu, B. Li, and H. Zhao, Phys. Rev. E **57**, 2992 (1998).

[26] B. Hu, B. Li, and H. Zhao, Phys. Rev. E **61**,3828 (2000).

[27] C. Giardin'a, R. Livi, A Politi, and M. Vasalli, Phys. Rev. Lett. **84**, 2144 (2000).

[28] O. V. Gendelman and A. V. Salvin, Phys. Rev. Lett. **84**, 2381 (2000).

[29] G. Casati and T. Prosen, Phys. Rev. E **67**, 015203(R) (2000).

[30] T. Prosen and D. K. Campbell, Phys. Rev. Lett. **84**, 2857 (2000).

[31] R. Kubo, M. Toda, and N. Hashitsume, *Statistical Physics II*; Springer Series in Solid State Sciences **31**, Springer, Berlin (1991).

[32] Y. Pomeau, R. Résibois, Phys. Rep. **19**, 63 (1975).

[33] B. Li, L. Wang, and B. Hu, Phys. Rev. Lett. **88**, 223901 (2002).

[34] D. Alonso, A. Ruiz, and I. de. Vega, Phys. Rev. E **66**, 066131 (2002).

[35] B. Li, G. Casati, and J. Wang, Phys. Rev. E **67**, 021204 (2003).

[36] A. Pereverzev, Phys. Rev. E **68**, 056124 (2003).

[37] B. Li and J. Wang, Phys. Rev. Lett. **91**, 044301 (2003); **92**, 089402 (2004).

[38] B. Li, G. Casati, J.Wang, and T. Prosen, Phys. Rev. Lett. **92**, 254301 (2004).

[39] N. Li, P.-Q. Tong, and B. Li, Europhys. Lett. **75**, 49 (2006).

[40] N. Li and B. Li, Europhys. Lett. **78**, 34001 (2007).

[41] T. Hatano, Phys. Rev. E **59**, R1 (1999).

[42] P. Grassberger, W. Nadler, and L. Yang, Phys. Rev. Lett. **89**, 180601 (2002).

[43] J. M. Deutsch and O. Narayan, Phys. Rev. E **68**, 010201 (R) (2003); **68**, 041203 (2003).

[44] P. Cipriano, S. Denisov, and A. Politi, Phys. Rev. Lett. **94**, 244301 (2005).

[45] J.-S. Wang and B Li, Phys. Rev. Lett. **92**, 074301 (2004), Phys. Rev. E **71**, 066203 (2005).

[46] A. Dhar, Phys. Rev. Lett. 86, 5882 (2001).

[47] O. Narayan and S. Ramaswamy, Phys. Rev. Lett. 89, 200601 (2002).

[48] S. Lepri, R. Livi, and A. Politi, Phys. Rep. **377**, 1 (2003).

[49] G. Basile, C. Bernardin, and S. Olla, Phys. Rev. Lett. **96**, 204303 (2006)

[50] Y. Frenkel and T. Kontorova, Zh. Eksp. Teor. Fiz. **8**, 89 (1938).

[51] D. Alonso, R. Artuso, G. Casati, and I. Guarneri, Phys. Rev. E **82**, 1859 (1999).

[52] S. Denisov, J. Klafter, and M. Urbakh, Phys. Rev. Lett. **91**, 194301 (2003).

[53] P. Cipriani, S. Denisov, and A. Politi, Phys. Rev. Lett. **94**, 244301 (2005).

[54] T. Mai and O. Narayan, Phys. Rev. Lett. **73**, 061202 (2006).

[55] H. Zhao, Phys. Rev. Lett. 96, 140602 (2006)

[56] A. Williams, Ph.D thesis, Manchester University (1966).

[57] G. Y. Eastman, Sci. Am. **218**, 38 (1968).

[58] T. R. Thomas and S. D. Probert, Int. J. Heat Mass Transfer **12**, 789 (1970).

[59] P. W. O'Callaghan, S. D. Probert, and A. Jones, J. Phys. D **3**, 1352 (1970).

[60] M. Terraneo, M. Peyrard, and G. Casati, Phys. Rev. Lett. **88**, 094302 (2002).

[61] B. Li, L. Wang, and G. Casati, Phys. Rev. Lett. **93**, 184301 (2004).

[62] B. Li, J. Lan, and L. Wang, Phys. Rev. Lett. **95**, 104302 (2005).

[63] B. Hu and L. Yang, Chaos **15**, 015119 (2005).

[64] B. Hu, L. Yang, and Y. Zhang, Phys. Rev. Lett. **97**, 124302 (2006).

[65] J. Lan and B. Li, Phys. Rev. B **74**, 214305 (2006).

[66] J. Lan and B. Li, Accepted for publication in Phys. Rev. B (2007).

[67] J. P. Eckmann and C. Mejía-Monasterio, Phys. Rev. Lett. **97**, 094301 (2006)

[68] B. Li, L. Wang, and G. Casati, Appl. Phys. Lett **88**, 143501 (2006).

[69] D. Segal and A. Nitzan, Phys. Rev. Lett. **94**, 034301 (2005)

[70] D. Segal, A. Nitzan, P. Hänggi, and J. Chem. Phys. **119**, 6840 (2003).

[71] J. Lebowitz, J. K. Percus, and L. Verlet, Phys. Rev. Lett. **153**, 250 (1967)

[72] R. A. MacDonald and D. H. Tsai, Phys. Rep. **46**, 1 (1978).

[73] J. P. Eckmann, C. A. Pillet, and L. Rey-Bellet, Commun. Math. Phys. **201**, 657 (1999).

[74] D. N. Payton, M. Rich, and W. M. Visscher, Phys. Rev. **160**, 706 (1967).

[75] R. I. Mclachlan, P. Atela, Nonlinearity **5**, 541 (1992).

[76] L. Casetti, Phys. Scr. **51**, 29 (1995)

[77] R. Tehver, F. Toigo, J. Koplik, and J. R. Banavar, Phys. Rev. E **57**, R17 (1998).

[78] D. J. Evans, G. P. Morriss Statistical Mechanics of Nonequilibrium Liquids, (Academic Press, San Diego, 1990).

[79] S. Nośe, J. Chem. Phys. **81**, 511 (1984); W. G. Hoover, Phys. Rev. A **31**, 1695 (1985).

[80] Focus issue on "Chaos and irreversibility", CHAOS **8** (2) (1998).

[81] N. Chernov, J. L. Lebowitz, J. Stat. Phys. **86**, 953 (1997).

[82] P. L. Garrido, P. I. Hurtado, and B. Nadrowski, Phys. Rev. Lett. **86**, 5486 (2001).

[83] D. G. Cahill et al. J. App. Phys. **93**, 793 (2003).

[84] Focus Issue on "50th anniversary of Fermi-Pasta-Ualam model", edited by D. K. Campbell, P. Rosenau, and G. Zaslavsky, Chaos **15**, 015101 (2005).

[85] O. M. Braun and Yu. S. Kivshar, "The Frenkel-Kontorova Model: Concepts, Methods, and Applications" (Springer-Verlag, Berlin, 2003).

[86] M. L. James, G. M. Smith, and J. C. Wolford, *Applied Numerical Methods for Digital Computation* (Harper Collins College Publishers, New York) (1993), 4th ed.

[87] P. Bak, Rep. Prog. Phys. **45**, 587 (1982), and references therein.

[88] W. Selke, *Phase Transitions and Critical Phenomena*, edited by C. Domb and J. L. Lebowitz (Academic Press, London, 1992), Vol. **15**.

[89] S. Aubry, in Solitons and Condensed Matter Physics, edited by A. R. Bishop and T. Schneider (Springer-Verlag, Berlin, 1978); J. Phys. (France) **44**, 147 (1983); M. Peyrard and S. Aubry, J. Phys. C **16**, 1593 (1983); S. Aubry, Physica D **7**, 240 (1983).

[90] H. Kinder and K. Weiss, J. Phys.: Condens. Matter **5**, 2063 (1993).

[91] T. Nakayama, in Progress in Low Temperature Physics, edited by D. F. Brewer, p. 115. (North-Holland, Amsterdam, 1989).

[92] P. L. Kapitza, J. Phys. (Moscow) **4**, 181 (1941).

[93] I. M. Khalatnikov, Zh. Resp. Teor. Fiz. **22**, 687 (1952).

[94] E. T. Swartz and R. O. Pohl, Rev. Mod. Phys. **61**, 605 (1989).

[95] E. T. Swartz and R. O. Pohl, Appl. Phys. Lett. **51**, 26 (1987).

[96] W. A. Little, " The transport of heat between dissimilar solids at low temperatures", Can. J. Phys. **37**, 334 (1959).

[97] H. P. William *et al.*, *Numerical recipes*, (Cambridge University Press, Cambridge, U.K., 1992).

[98] T. Dauxois, M. Peyrard, and A. R. Bishop, Phys. Rev. E **47**, 684 (1993).

[99] J. Rodríguez-Laguna and S. N. Santalla, Phys. Rev. B **72**, 214305 (2005).

[100] C. Kittel, *Introduction to Solid State Physics*, 7th ed. (John Wiley and Sons, New York, 1996).

[101] C. W. Chang, D. Okawa, A. Majumdar, and A. Zettl, Science **314**, 1121 (2006).

[102] C. W. Chang, W. Q. Han, and A. Zettl, J. Vac. Sci. Technol. B **23**, 1883 (2005).

[103] J. Hone, M. Whitney, C. Piskoti, and A. Zettl, Phys. Rev. B **59**, R2514 (1999).

[104] E. Pop et al, Phys. Rev. Lett, **95**, 155505 (2005).

Appendix A

Publication list

1. Giuluo Casati , Tomaz Prosen, Jinghua Lan, and Baowen Li, "Universal Decay of the Classical Loschmidt Echo of Neutrally Stable Mixing Dynamics ", Phys. Rev. Lett. 94, 114101 (2005)

2. Baowen Li, Jinghua Lan, and Lei Wang, "Interface Thermal Resistance between Dissimilar Anharmonic Lattices", Phys. Rev. Lett. 95, 104302 (2005).

3. Jinghua Lan and Baowen Li, "Thermal Rectifying Effect in Two-dimensional Anharmonic Lattices", Phys. Rev. B 74, 214305 (2006).

4. Jinghua Lan and Baowen Li, "Vibrational Spectra and Thermal Rectification in Three-dimensional Anharmonic Lattices", accepted for publication in Phys. Rev. B (2007).